JAIST Repository
https://dspace.jaist.ac.jp/

Title	人工クモ糸の劣化機構の解明とその安定化技術の開発
Author(s)	中山, 超
Citation	
Issue Date	2020-03
Type	Thesis or Dissertation
Text version	ETD
URL	http://hdl.handle.net/10119/16666
Rights	
Description	Supervisor:谷池　俊明, 先端科学技術研究科, 博士

JAIST
JAPAN
ADVANCED INSTITUTE OF
SCIENCE AND TECHNOLOGY

Japan Advanced Institute of Science and Technology

Elucidation of Degradation Mechanism of Recombinant Spider Silk and Its Stabilization

Koyuru NAKAYAMA

Japan Advanced Institute of Science and Technology

Doctoral Dissertation

Elucidation of Degradation Mechanism of Recombinant Spider Silk and Its Stabilization

Koyuru NAKAYAMA

Supervisor: Associate Professor Dr. Toshiaki Taniike

Graduate School of Advanced Science and Technology

Japan Advanced Institute of Science and Technology

[Materials Science]

March 2020

Referee-in-chief: **Associate Professor Dr. Toshiaki Taniike**
Japan Advanced Institute of Science and Technology

Referees: **Associate Professor Dr. Kazuaki Matsumura**
Japan Advanced Institute of Science and Technology

Associate Professor Dr. Eijiro Miyako
Japan Advanced Institute of Science and Technology

Associate Professor Dr. Ken-ichi Shinohara
Japan Advanced Institute of Science and Technology

Group Leader Dr. Junji Mizukado
National Institute of Advanced Industrial Science and Technology

Contents

Preface

The present dissertation is the result of the studies under the direction of Associate Professor Dr. Toshiaki Taniike during 2017-2020. The purpose of this dissertation is to elucidate degradation mechanism of recombinant spider silk and develop stabilization technology of recombinant spider silk. The first chapter is a general introduction according to the object of this research. Chapter 2 describes elucidation of thermo-oxidative and photo degradation mechanism of recombinant spider silk. Chapter 3 describes stabilization of recombinant spider silk in thermo-oxidative and photo degradation. Chapter 4 describes development of recombinant spider silk/clay nanocomposites. Chapter 5 describes the conclusion of this dissertation.

Koyuru Nakayama

Taniike Laboratory,

Graduate School of Advanced Science and Technology,

Japan Advanced Institute of Technology

March 2020

Chapter 1

General Introduction

1.1 Polymer

Polymer

The concept of polymer was established in the 1920s by Prof. Dr. Staudinger, who proposed that the word of polymer was composed of the repeating units connected by a covalent bond. Thermoset resins such as urea resin and phenol resin were initial examples of the polymer at that time, which were produced from coal, and then the new synthetic polymers had been developed.

The linear polymers prepared from oil such as polyester, polyamide and polyolefin were then synthesized. Their production had rapidly been enlarged in order to replace the traditional materials, e.g., metal, because of their excellent properties. Polymer materials are mainly classified into commodity plastics, engineering plastics and super engineering plastics. The commodity plastics can be represented by polyethylene (PE), polypropylene (PP), polyvinyl chloride and polystyrene, which are widely used for various applications due to advantages such as the low production costs, balanced mechanical properties, good processability, etc. In the case of polymers with high strength and heat resistance, these are called engineering plastics, i.e., including polyamide, polycarbonate, polyacetal, polybutylene terephthalate and desaturated polyphenylene ether. Super engineering plastics are mostly for extreme usage conditions, especially at high temperature or pressure.

With the rapid growth of the polymer industry, the new material design using renewable resources has become an important trend and requirement to sustain the global environment and society [1–3]. A type of natural polymer produced by microorganisms becomes an attractive way to synthesize all the biological polymer and proteins [4,5]. It is expected to be used as a tailor-made polymer capable of designing a primary structure, including and as subsequent biomass [6,7].

Biopolymer

A biopolymer is a naturally produced polymer, for instance, carbohydrate and protein [8–10]. Although the small percentage of this biopolymer being produced is currently used comparing to the synthetic polymer, it can be significantly useful on the decrease in the production of polymer. Nowadays, many studies on a new material design giving high performance and properties of this biopolymer have been paid attention [11–14]. A rapid progress of the development of biopolymer material is based on a decent knowledge background on biological structures with the aid of both analytical and synthetic technology. The application of biological principals for the technical challenging is referred to as biomimetic or biomechanics. This topic is intentionally studied to understand assembly-formation, structure-performance correlation, and molecular biology. A biopolymer produced by microorganisms has sophisticated structure and sequence, in other words, is remarkable of self-assembly with complex structure possessing the extraordinary function, which is difficult to be achieved by synthetic polymers.

However, the challenging to apply the biomimetic on a big scale in the polymer industry is limited due to the technological operation (comparing to the general synthetic polymer with easier structure) and economic decision/investment (that is higher than commodity plastics).

Protein

Protein can be classified into two groups, which are functional protein and structural protein. The structural protein is an essential building block of life in terms of motion, elasticity, scaffold [15,16], anatomy [17,18], skin [19], protection [20], and stabilization [21]. The protein is generated from the relatively small domain of only common monomer building block as known as 20 types of amino acids, which possess

various chemical properties (aliphatic, acidic, basic, polar, non-polar, etc.) for a tremendous potential and multiple applications.

A difference in a primary sequence leads to the numerous diversities of structure, properties, and biological functions. Polypeptide chains form different secondary structure conformations (as α-helix or β-sheets), in which their formation and stabilization are based on relatively weak non-covalent interactions (e.g., electrostatic, Van der Waals force, hydrophobic effects, thermodynamic preference process-driven of binding hydrogen) and/or covalent interactions (e.g., disulfide bridges).

Silk

Silk, a type of fiber material produced from insect, is an attractive structural protein having the function on lifeline protection, web, traps, wrapping, and offspring [22–25]. Commercial silk has been used in the textile industry for thousands of years of daily human life due to its superior natural texture and ability to mix with dyes. On top of this general success, silk is intensively applied for decades to use in advanced biomedical applications and tissue engineering from its unique biocompatibility and biodegradable at fixed conditions [26–30].

In general, silkworm silk fiber composed of two fibroin monofilaments, which secreted from the posterior part of the silk gland [31–34], wrapped in a proteinaceous sericin coat [35,36]. The almost circular to elliptical fibroin has an average diameter in a range of 7 to 16 μm and consists of a core-shell structure. This core-shell structure is typically constituted of three protein components: 1) heavy chain fibroin (H chain, about 350 kDa), 2) light chain fibroin (L chain, about 25 kDa) and 3) the fiber Axis-glycoprotein (P25, approximately 30 kDa) [35,37–42]. The H chain and L chain are linked by a disulfide bond, and this structure is preferentially aligned as a bundle of nanofibrils

through non-covalent interaction with a typical molar ratio of H: L: P25 for 6:6:1 [43]. The fibroins have a high content of typical primary structure characterized by alternating blocks of hydrophobic and hydrophilic domains. The random coil and amorphous structure of fibroin, namely Silk I conformation, can be adopted in a solution and formed a structure rich in hydrogen-bonded antiparallel β-sheet, called as Silk II in spinning process.

Spider Silk

After the evolution for 400 million years, there are 48296 species, 4149 genera, and 120 families of spider as reported by taxonomist in 2019 (World Spider Catalog in 8th of October 2019) [44]. **Figure 1.1** expressed the different types of glands produced by a spider, where the obtained dragline silk in a major ampullate gland has attracted a significant attention in view of mechanical properties as shown in **Table 1.1**.

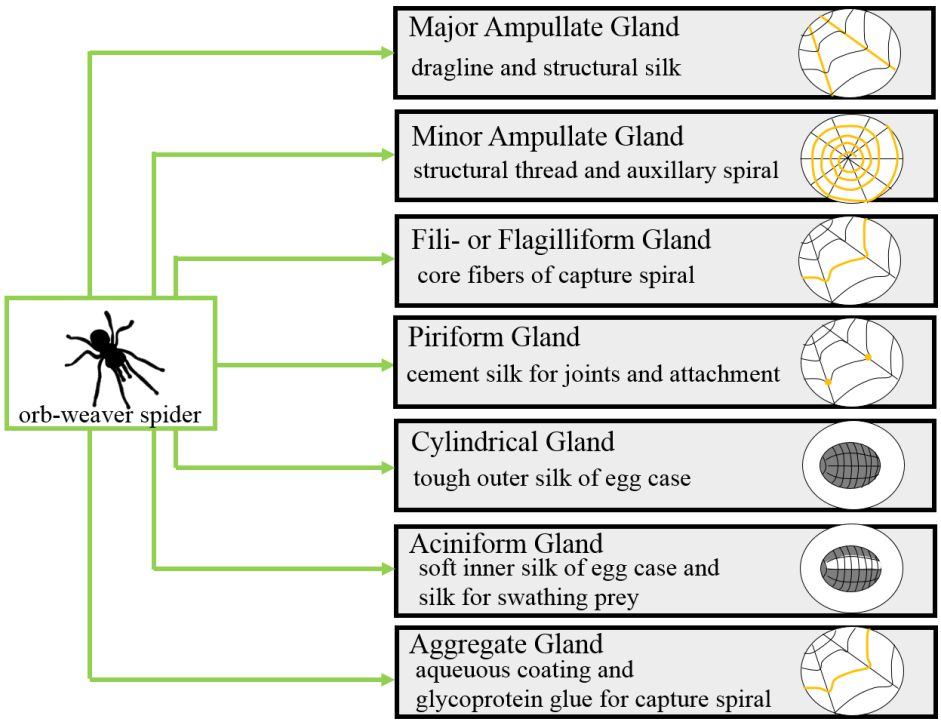

Figure 1.1. Summary of different types of glands.

Table 1.1. Comparison of mechanical properties between typical fiber materials [45]

Material	Young's modulus (GPa)	Strength (GPa)	Elongation at break (%)	Toughness (MJm^{-3})
Spider silk	10	1.1	27	160
Bombyx mori cocoon silk	7	0.6	18	70
Synthetic rubber	0.001	0.05	850	100
Nylon fibre	5	0.95	18	80
Kevlar 49 fibre	130	3.6	3	50
Carbon fibre	300	4	1	25
High-tensile steel	200	1.5	1	6

As compared with carbon fiber and aramid fiber (Kevlar 49™), the spider dragline silk possesses similar tensile strength and higher toughness, which has five and three times stronger than those of iron and Kevler 49™, respectively [45,46]. Due to the outstanding mechanical properties, spider silk has been considered for various applications, which are a parachute, composite material in transportation equipment, bulletproof vest, medical material, drug delivery, and scaffolds. Nowadays, the spider fibroin (spidroin) of dragline spider silk from *Nephila clavipes* (*N. clavipes*) [47–50] and *Araneus diadematus* (*A. diadematus*) [51–53] species are widely studied as a benchmark. The dragline spider silk of *A. diadematus*, called as *A. diadematus* fibroin (ADF) of ADF-3 and ADF-4, are composed of major ampullate spidroin 1 (MaSp1) and 2 (MaSp2). The MaSp1 and MaSp2 consists of approximately 3500 amino acid residues, corresponding to 250-320 kD [54–56].

Spidroin preserved of about 50% (w/v) protein liquid solution, namely as dope, based on water in the gland [57]. Dope can be formed to fiber shape structure from liquid crystalline polymer state by applying minimal force on extrusion molding process. The conformation of spidroin in dope are mostly composed of helical and strand or random coil, which is influenced by the several factors, i.e. the ion composition, pH, shear stress,

and water removal during spinning process [58,59]. The preliminary arrangement without reorientation of uncontrolled molecular of dope can be affected to the liquid crystalline formation. As the spidroin is crystallized along the aggregation, the crystal region will become hydrophobic during phase transition.

Supercontraction of Spider Silk

The remarkable properties of spider dragline silk are made during spinning at ambient temperature and low-pressure at aqueous solution. Apart from excellent mechanical properties, contact with water or relative humidity above 60% causes the dragline thread to begin to expand radially. This led to an increase in diameter with a contraction of about 50% of the length, that is a distinct feature call "supercontraction" [60–62]. It is believed that this feature is made by the entropy-driven reorientation of silk molecules, especially in relation to the breakdown of hydrogen bonds between spider silk proteins during water intake [45,63]. It can be said that the most prominent aspect of supercontraction of spider silk occurs at a ambient temperature, whereas it is generally requires temperature or harsh solvent conditions for artificial fibers. Thus, controlling supercontraction can be used as a mechanism to adjust properties for various applications. However, the ultra-shrinkage poses a major drawback to the creation and application of biomaterials, for example, the bulletproof vest.

Recombinant Spider Silk

The cultivation of spiders is difficult due to their high territoriality and carnivorous feature. Besides, there is also an unsatisfied amount of spidroin taken from a spider in the industrial viewpoint. Therefore, the production of recombinant spider silk becomes ta target of researches [64]. A heterologous host including bacteria [65–67], yeast [68,69], mammal cell [70], transgenic plant [71,72], animal [73,74] and insect [75–77] has been widely studied to develop for being a platform of spidroin producers. The

ability to produce spider silk protein in sufficient quantities at reasonable cost effectiveness is essential for the consumption of spider silk in high-performance materials. The enzymatic polymerization is used to achieve spider silk-like polypeptides having the specific domain sequences of $(Ala)_n$ and Gly-rich regions. This technique has been significantly paid attention as new material designs, although the mechanical properties and molecular weight are still in a completely inferior to those of native and recombinant spider silk. *Escherichia coli* (*E. coli*) has been widely used to produce protein due to the ease of genetic manipulation, short time of cultivation, and low-cost, while spidroin fragments obtained from *N. clavipes* and *A. diadematus* are mostly employed. Moreover, partial spidroin, 4RepCT derived from MaSp1, was produced using *E. coli* [78]. 4RepCT consisted of $(Ala)_4$ and native C-terminus of spider silk possessing approximately 100 mer amino acid residues. However, there is some complication during expression of spidroin using E. coli. Gene including GC (guanine and cytidine)-rich part have a problem of the structural stability of mRNA. It causes a premature termination of translation. The mass of 43 kD of recombinant spidroin using *E. coli* was reported in 1998 [79]. Recently, native-size recombinant spidroin of 285 kDa was expressed using *E. coli*, in which the recombinant spider silk was developed by modification using bioinformatics techniques [65].

1.2 Polymer Degradation and its Stability

Polymer Degradation

A service lifetime of polymer materials is limited by their degradation. The degradation is caused by various environmental factors, e.g., temperature, light, humidity, pressure, impurity, mechanical load, etc. The degradation accompanies modification in chemical and physical properties such as molecular weight, mechanical strength, shock resistance, color changing, etc. Understanding the degradation of polymer is generally complicated due to their diffusion process, a tiny amount of chemical changes, heterogeneous induction/propagation. The oxidation is noted to be one of the most important degradation processes from the exposure to oxygen in molding and service. The first reports wad made in the early 19th century, which demonstrated that the degradation of natural elastomer was associated with the adsorption of oxygen. Since then, the oxidative degradation has been widely studied for many polymer materials.

Mechanism of Oxidation of Polymer

The auto-oxidation mechanism is widely accepted to describe the reaction between oxygen molecule, and organic materials based on a free radical process, which is initiated by thermal, photochemical, and mechanical factors [80–82]. Factors such as impurities, sterically encumber some branches, and unsaturated functional groups can significantly increase the rate of oxidation.

Figure 1.2 illustrates the mechanism of auto-oxidation which is described by initiation, propagation, chain branching, and termination. In the early 1940's, Balland, Gee, and Bateman proposed a free radical chain mechanism from the study of oxidation of hydrocarbon in a liquid state, which provided the basis of the auto-oxidation mechanism.

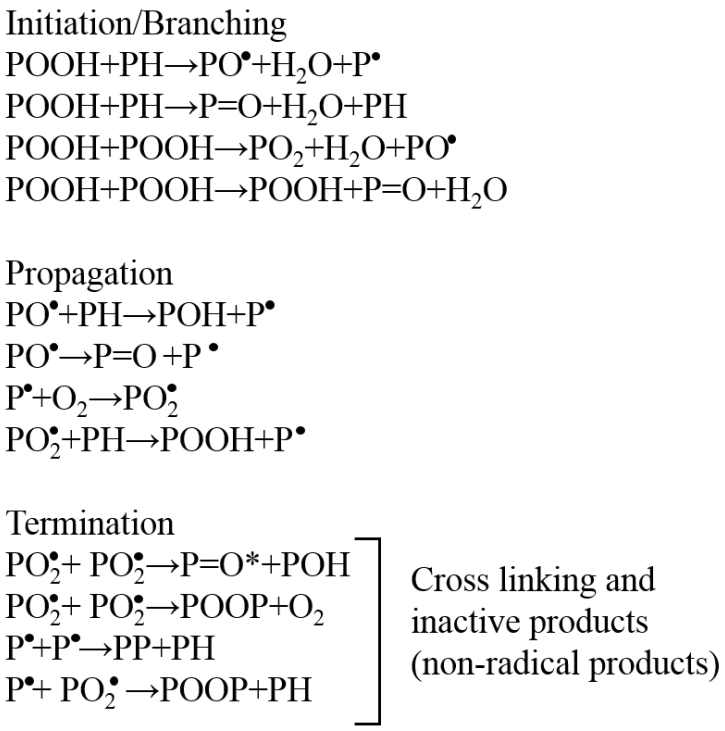

Figure 1.2. Fundamental auto-oxidation mechanism derived from free radical chain reaction in liquid-state.

Figure 1.3 shows the modified free radical chain reaction mechanism for polymer, in which the direction reaction between polymer and oxygen molecule is unlikely in thermodynamic and kinetic viewpoints. The transition metal, radical initiator, and impurities, and UV light can remove a hydrogen molecule at a certain position in the polymer chain, forming an alkyl radical and then hydroperoxide. At the last, the formed hydroperoxide decomposes to generate a free radical. Studies on the oxidative degradation of polymer using electron spin resonance (ESR) showed that the alkyl radical is immediately reacted to oxygen molecule to form peroxy radical [83,84]. The rate of hydrogen subtraction increases in the order of tertiary C-H < secondary C-H < primary C-H. In the other words, these radicals are formed by the subtraction of hydrogen from

the polymer chain leading to the chain branching formation. Moreover, these radicals formation from hydroperoxide during thermolysis can cause the chain branching.

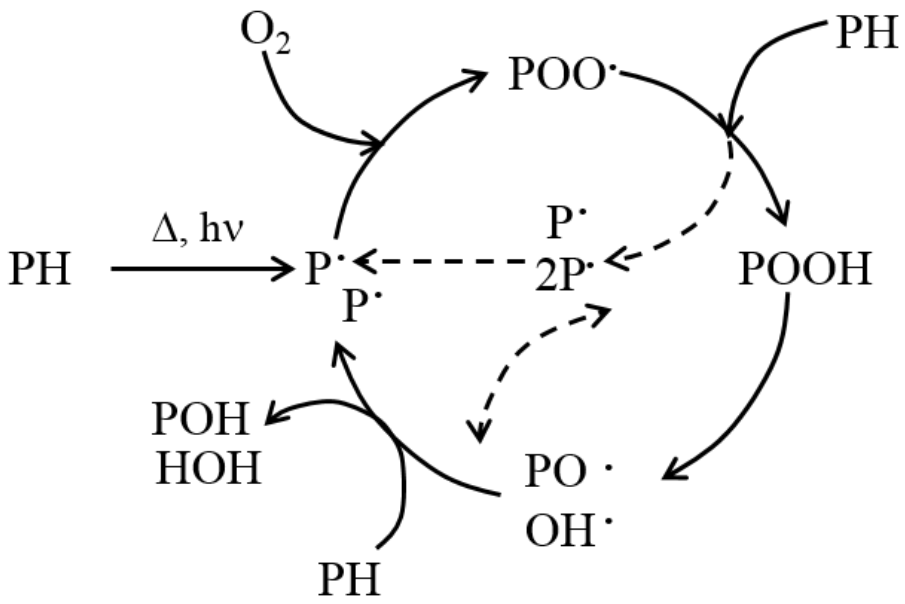

Figure 1.3. Auto-oxidation mechanism.

The binding energy of O-O bond in hydroperoxide and peroxide is approximately 200 kJ·mol^{-1} and less than that, in which this bond is readily cleavage and formed alkoxy and hydroxyl radicals [85,86]. The initial oxidative reaction of polymer is still contentious with many factors contributing for the first alkyl group formation. The propagation reaction demonstrated the rapid formation of alkyl peroxide from those of alkyl radical and oxygen molecule. Following this reaction, the hydroperoxide formation can occur due to the subtraction of hydrogen. The intermediate forms into inactive products as the same time as initiation reaction is continuously renewed. Finally, the oxidative degradation causes the decay of polymer properties, in

which the termination reaction depends on the molecular structure and degradation conditions.

Oxidation of Protein

The oxidation of protein is widely studied in pathology and physiology fields because the oxidative stress can be associated with aging and disease such as Alzheimer dementia. In this research, the preparation of protein under moderate condition in solution for the oxidation triggered by H_2O_2 will be used [87,88]. Up to date, the study of free radical formation from protein in microorganism, control of free radical and oxidation of DNA through the repairing pathway with enzyme have been carried out [89]. However, these studies are proved in various way with the fact that solid protein can be degraded at high temperature as well as the denaturation of protein needs to seriously consider.

Recently, there are few studies on the thermal degradation of solid protein such as silkworm silk, collagen, and keratin. Primarily, using silkworm silk is expected to provide the useful information on the degradation for the recombinant spider silk. Koperska et.al expressed the thermos-oxidative degradation of silkworm silk using IR technique [90–92]. It was found that the formation of carbonyl group was detected with the help of humidity as accelerator. Vassileva et. al have used the titration and chromatography to investigate the photooxidation of silkworm silk, in which the yellow color referring to α-keto acid of silkworm silk was identified [93–95]. However, the results were provided only for partial degradation mechanism, which is assured to refer the complicate degradation of protein due to the consisting of multiple monomers.

Stabilization of Polymer

Most of polymers require stabilization for long-term lifetime against the adverse effects to prevent, or at least reduce the degradation caused by the environmental factors

such as light, air and heat. That is why the stability of polymers is one of the most important considerations for application.

A variety of stabilizers have been developed and more or less commercially available for each type of polymer and its application. However, if one aims at enormous stabilization beyond average, only the way is to explore stabilizers and their combination specific to the polymer and application of interests, otherwise, it is inevitable to merely increase the amount of the addition in cost of concomitant drawbacks. The problem lies in the difficulty to accumulate systematic knowledge on detailed structure–activity relationships of stabilizers and their combination.

The polymer stability can be acquired through the addition of special chemicals, mainly called stabilizers that have to be adjusted to the nature of the polymer and the specific application considered. The stabilization of polymer involved the retardation or elimination of chemical process in polymers that occur during heating or light irradiation. The following stabilizing systems have been developed which depend on the action of stabilizer: (a) peroxide decomposers, (b) radical scavengers, (c) excited state quenchers, (d) light screeners and (e) UV absorbers. Of these, it is believed that peroxide decomposers, and radical scavengers is quite effective. A radical scavenger traps radical in polymer chain, and peroxide decomposer suppresses to generate new peroxide. Typical stabilization mechanism is shown in **Scheme 1.1**.

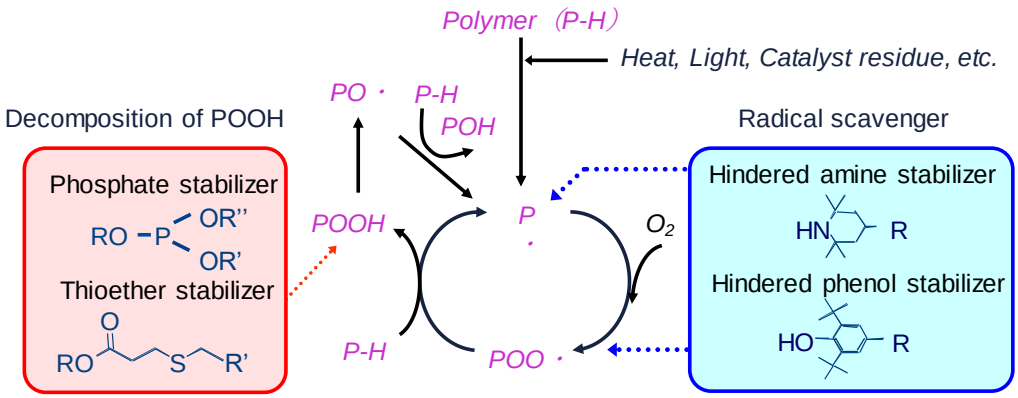

Scheme 1.1. Typical stabilization mechanism of polymer.

For commercial needs, other requirements become necessary not only to maintain the properties of polymers but also to extend its service life. Much more developments of high-performance of the polymer materials are highly required, which addresses more stringent or new requirements such as more severe processing and use conditions and/or environmental concerns.

There are limited publications in literature dealing with the stabilization of protein. The stabilization of polyamide (PA), which has amide bond with analogy to protein, can be an inspiration for protein stabilization.

1.3 Polymer Nanocomposites

Polymer Nanocomposites

Nanotechnology has attracted immense interests since 1959 by a famous lecture R.P. Feynman [96]. It was suggested that the control and manipulation on the nano structure can possibly provide new physical, biological, and chemical properties at a very fine scale. From the early 1990 until now, the attention to polymer nanocomposites has continuously been grown into numerous innovations. The definition of polymer nanocomposites is the combination of polymer and particles where at least one of the diameters of the reinforcing phase is in the nanometer scale.

We divide each approach into the types and dimensions of the controlled nano - objects within the polymer, i.e., zero-dimensional (0D) nanoparticles, one-dimensional (1D) nanotubes, and Two-dimensional (2D) nanosheets. In a 0D nanocomposites, all three dimensions of the filler are of the order of 1–100 nm (metal and metal-oxide nanoparticles, silicate oxide nanoparticles, quantum dots, detonation nano diamonds etc.) [97–99]. 1D nanocomposite filler particles whose two dimensions are nano sized (fibers, whiskers or nanotubes) [100–102]. 2D nanocomposites refer to plate-shaped fillers (graphite, layered silicates etc.) [103–105]. Nanocomposites can be divided into two types based on their applications, which are structural and functional. In the case of nanocomposites for structural purposes, the introduction of filler particles is aimed to enhance their inflammability, durability, barrier properties and mechanical properties. For functional use, nano-sized fillers can greatly impact to properties, e.g. electric conductivity[106] or biocidal properties [107,108]. For the fabrication of nanocomposites, it is necessary to create stable mixtures, in which inorganic nanoparticles are well dispersed throughout the bulk of a polymer matrix without agglomeration. Besides, orientation control is important when anisotropic particles are selected. In the case of

functional purposes, the role of filler particles is much more significant, since the magnetic, optical and electric properties of materials substantially depend on the characteristics of nanoparticles. The interaction between the polymer matrix and filler at the molecular level is of great significance because it leads to a synergy of organic and inorganic components.

Preparation of Polymer Nanocomposites

Several processing techniques have been developed to disperse nano-sized particles into the polymer matrix including in-situ method, melt compounding and solution processing. The in-situ preparation can be divided into two routes: in-situ polymerization in the presence of nanoparticles and in-situ synthesis of nanoparticles in the polymer matrix. In the first case, the particles are first dispersed in-situ in the monomer(s) followed by the polymerization. Okada et al. at Toyota Central Research and Development Labs. has reported this method for the preparation of poly (amide-6) /silica nanocomposites [109–111]. Firstly, the silica particles were mixed with ε-caproamide followed by addition of the appropriate polymerization initiator. The mixture was then polymerized at elevated temperature under a nitrogen atmosphere. Well dispersed particles with a particle size of ~50 nm was obtained, but aggregation occurred when using particle sizes of ~12 nm. The aggregation of silica particles was explained to be originated from the increase of surface energy of smaller particles.

The melt compounding is the most useful method approaching industrial applications, in which the current compounding and processing techniques are compatible due to no use of solvents. Herrera et al. prepared polylactic acid (PLA) nanocomposites with cellulose or chitin nanocrystal using a twin-screw extruder [112]. The addition of nanocrystals shows the improvement on optical, thermal and mechanical properties.

Another frequently used technique for the dispersion of nanoparticles is solution processing. Wilkie et al. dissolved PVC and clay particles in a polar solvent for several hours, then the mixture was casted and the solvent was perfectly evaporate [113]. This process yielded well-dispersed PVC-organophilic clay nanocomposites. Bansal et al. achieved the excellent dispersion of untreated or polystyrene (PS)-grafted silica nanoparticles in PS based on casting from a toluene solution [114]. It was shown that the dispersion of nanoparticles was strongly affected by the choice of solvents.

The majority of biopolymer can be prepared via solution processing, which is dependent upon the thermal instability of biopolymer. The solution casting method has been the most used method for the nanocomposites preparation based on polyhedral oligomeric silsesquioxanes (POSS) [115], silica [116], graphene [117], layered-double hydroxides (LDH) [118] and clays [119–121] were reported. However, only a few studies have been reported on using protein for these nanocomposites at the best of my knowledge. This is because protein can dissolve in kinds of limited solvents, where the dispersion of nanoparticles can be difficult.

Dispersion State

Advantages of nanocomposites through several properties can be attained if the dispersion of nanoparticles is well controlled. In some cases, a perfectly homogenous dispersion is needed, while this is not always. For example, in depending on properties of interest, carbon nanotubes filled polymer systems for electric conduction. A percolation network is necessary by appropriate control of aggregation of nano tubes. Mediocre performance of nanocomposites can be attributed to several factors, such as poor dispersion, poor alignment, poor interfacial load transfer, process related deficiencies, and so on.

The filler geometry is an important factor that can influence the state of dispersion of nanoparticles. In general, lower 1D and 2D fillers are more difficult to be dispersed than 0D fillers. The difference arises from the fact that 1D fillers can have a contact along the full length of the cylinder, which can increase the particle-particle interaction, whereas 0D fillers only exhibit the point to point contact. In the case of 2D sheets with larger contact areas, the increase in the particle contact area and interaction makes homogeneous dispersion even more difficult. Considering these factors, 3-dimensional fillers such as spherical particles are significantly noted to easier disperse than either rods or sheets.

1.4 Objectives

With the rapid growth of the polymer industry, the new material design using renewable resources has become an important trend and requirement to sustain the global environment and society. Stabilization technology was designed based on the degradation mechanism. A variety of stabilizers have been developed and more or less commercially available for each type of polymer and its application. However, if one aims at enormous stabilization beyond average, only the way is to explore stabilizers and their combination specific to the polymer and application of interests.

In this work, I focus on the elucidation of degradation of recombinant spider silk and development of stabilization including the stabilizer screening and nanocomposite technology. Chapter 1 describes general introduction. Chapter 2 describes elucidation of thermo-oxidative and photo degradation mechanism of recombinant spider silk. Chapter 3 describes stabilization of recombinant spider silk in thermo-oxidative and photo degradation. Chapter 4 describes development of recombinant spider silk/clay nmanocomposites.

Reference

[1] J.M. Raquez, M. Deléglise, M.F. Lacrampe, P. Krawczak, Thermosetting (bio)materials derived from renewable resources: A critical review, Prog. Polym. Sci. 35 (2010) 487–509.

[2] M. Okada, Chemical syntheses of biodegradable polymers, Prog. Polym. Sci. 27 (2002) 87–133.

[3] L. Yu, K. Dean, L. Li, Polymer blends and composites from renewable resources, Prog. Polym. Sci. 31 (2006) 576–602.

[4] A. Steinbüchel, B. Füchtenbusch, Bacterial and other biological systems for polyester production, Trends Biotechnol. 16 (1998) 419–427.

[5] B.H.A. Rehm, Bacterial polymers: Biosynthesis, modifications and applications, Nat. Rev. Microbiol. 8 (2010) 578–592.

[6] A.A. Garforth, S. Ali, J. Hernández-Martínez, A. Akah, Feedstock recycling of polymer wastes, Curr. Opin. Solid State Mater. Sci. 8 (2004) 419–425.

[7] R. Kumar, S. Singh, O. V. Singh, Bioconversion of lignocellulosic biomass: Biochemical and molecular perspectives, J. Ind. Microbiol. Biotechnol. 35 (2008) 377–391.

[8] P. Cazón, G. Velazquez, J.A. Ramírez, M. Vázquez, Polysaccharide-based films and coatings for food packaging: A review, Food Hydrocoll. 68 (2017) 136–148.

[9] M. Wihodo, C.I. Moraru, Physical and chemical methods used to enhance the structure and mechanical properties of protein films: A review, J. Food Eng. 114 (2013) 292–302.

[10] M.G.A. Vieira, M.A. Da Silva, L.O. Dos Santos, M.M. Beppu, Natural-based plasticizers and biopolymer films: A review, Eur. Polym. J. 47 (2011) 254–263.

[11] B. Khan, M. Bilal Khan Niazi, G. Samin, Z. Jahan, Thermoplastic Starch: A Possible Biodegradable Food Packaging Material-A Review, J. Food Process Eng. 40 (2017) e12447.

[12] R. Muthuraj, M. Misra, A.K. Mohanty, Biodegradable compatibilized polymer blends for packaging applications: A literature review, J. Appl. Polym. Sci. 135 (2018) 45726.

[13] V. Balan, L. Verestiuc, Strategies to improve chitosan hemocompatibility: A review, Eur. Polym. J. 53 (2014) 171–188.

[14] B. Imre, B. Pukánszky, Compatibilization in bio-based and biodegradable polymer blends, Eur. Polym. J. 49 (2013) 1215–1233.

[15] H.J. Kim, U.J. Kim, G. Vunjak-Novakovic, B.H. Min, D.L. Kaplan, Influence of macroporous protein scaffolds on bone tissue engineering from bone marrow stem cells, Biomaterials. 26 (2005) 4442–4452.

[16] J.E. Dueber, G.C. Wu, G.R. Malmirchegini, T.S. Moon, C.J. Petzold, A. V. Ullal, K.L.J. Prather, J.D. Keasling, Synthetic protein scaffolds provide modular control over metabolic flux, Nat. Biotechnol. 27 (2009) 753–759.

[17] J.S. Richardson, The anatomy and taxonomy of protein structure, Adv. Protein Chem. 34 (1981) 167–339.

[18] A.A. Bogan, K.S. Thorn, Anatomy of hot spots in protein interfaces, J. Mol. Biol. 280 (1998) 1–9.

[19] S. Shuster, M.M. Black, E. McVitie, The influence of age and sex on skin thickness, skin collagen and density, Br. J. Dermatol. 93 (1975) 639–643.

[20] F. Wild, P. Giraudon, D. Spehner, R. Drillien, J. Pierre Lecocq, Fowlpox virus recombinant encoding the measles virus fusion protein: protection of mice

against fatal measles encephalitis, Vaccine. 8 (1990) 441–442.

[21] D.L. Brasaemle, The perilipin family of structural lipid droplet proteins: Stabilization of lipid droplets and control of lipolysis, J. Lipid Res. 48 (2007) 2547–2559.

[22] T.D. Sutherland, J.H. Young, S. Weisman, C.Y. Hayashi, D.J. Merritt, Insect Silk: One Name, Many Materials, Annu. Rev. Entomol. 55 (2010) 171–188.

[23] D. Jones, The endocrine basis for developmentally stationary prepupae in larvae of Trichoplusia ni pseudoparasitized by Chelonus insularis, J. Comp. Physiol. B. 155 (1985) 235–240.

[24] C.D. Johnson, J. Romero, E. Raimúndez-Urrutia, Ecology of AMBLYCERUS CRASSIPUNCTATUS Ribeiro-Costa (Coleoptera: Bruchidae) in Seeds of Humiriaceae, a New Host Family for Bruchids, with an Ecological Comparision to Other Species of AMBLYCERUS , Coleopt. Bull. 55 (2001) 37–48.

[25] P.W. Geier, The life history of codling moth, Cydia pomonella (L.) (Lepidoptera: Tortricidae), in the Australian capital territory, Aust. J. Zool. 11 (1963) 323–367.

[26] Y. Wang, H.J. Kim, G. Vunjak-Novakovic, D.L. Kaplan, Stem cell-based tissue engineering with silk biomaterials, Biomaterials. 27 (2006) 6064–6082.

[27] Y. Cao, B. Wang, Biodegradation of Silk Biomaterials, Int. J. Mol. Sci. 10 (2009) 1514–1524.

[28] U.J. Kim, J. Park, H. Joo Kim, M. Wada, D.L. Kaplan, Three-dimensional aqueous-derived biomaterial scaffolds from silk fibroin, Biomaterials. 26 (2005) 2775–2785.

[29] C. Vepari, D.L. Kaplan, Silk as a biomaterial, Prog. Polym. Sci. 32 (2007) 991–1007.

[30] G.H. Altman, F. Diaz, C. Jakuba, T. Calabro, R.L. Horan, J. Chen, H. Lu, J. Richmond, D.L. Kaplan, Silk-based biomaterials, Biomaterials. 24 (2003) 401–416.

[31] P. Couble, A. Moine, A. Garel, J.C. Prudhomme, Developmental variations of a nonfibroin mRNA of Bombyx mori silkgland, encoding for a low-molecular-weight silk protein, Dev. Biol. 97 (1983) 398–407.

[32] K.U. Sprague, Bombyx mori silk proteins. Characterization of large polypeptides, Biochemistry. 14 (1975) 925–931.

[33] J.-C. PRUDHOMME, P. COUBLE, J.-P. GAREL, J. DAILLIE, Silk Synthesis, in: Biochemistry, Elsevier, 1985: pp. 571–594.

[34] H. Sinohara, Y. Asano, A. Fukui, Glycopeptides from silk fibroin of Bombyx mori, BBA - Gen. Subj. 237 (1971) 273–279.

[35] T. Gamo, T. Inokuchi, H. Laufer, Polypeptides of fibroin and sericin secreted from the different sections of the silk gland in Bombyx mori, Insect Biochem. 7 (1977) 285–295.

[36] J.J. Michaille, P. Couble, J.C. Prudhomme, A. Garel, A single gene produces multiple sericin messenger RNAS in the silk gland of Bombyx mori, Biochimie. 68 (1986) 1165–1173.

[37] M. Chevillard, P. Couble, J.C. Prudhomme, Complete nucleotide sequence of the gene encoding the Bombyx mori silk protein P25 and predicted amino acid sequence of the protein, Nucleic Acids Res. 14 (1986) 6341–6342.

[38] K. SHIMURA, A. KIKUCHI, K. OHTOMO, Y. KATAGATA, A. HYODO, Studies on Silk Fibroin of Bombyx mori. I. Fractionation of Fibroin Prepared from the Posterior Silk Gland, J. Biochem. 80 (1976) 693–702.

[39] K. Shimura, A. Kikuchi, Y. Katagata, K. Ohotomo, The Occurrence of Small Component Proteins in the Cocoon Fibroin of Bombyx mori, J. Sericultural Sci. Japan. 51 (1982) 20–26.

[40] P. Couble, M. Chevillard, A. Moine, P. Revel-Chapuis, P. Jean-Claude, Structural organization of the P_{25} gene of *Bombyx mori* and comparative analysis of its 5′ flanking DNA with that of the fibroin gene, Nucleic Acids Res. 13 (1985) 1801–1814.

[41] Y. Kikuchi, K. Mori, S. Suzuki, K. Yamaguchi, S. Mizuno, Structure of the Bombyx mori fibroin light-chain-encoding gene: upstream sequence elements common to the light and heavy chain, Gene. 110 (1992) 151–158.

[42] C.-Z. Zhou, Fine organization of Bombyx mori fibroin heavy chain gene, Nucleic Acids Res. 28 (2000) 2413–2419.

[43] S. Inoue, K. Tanaka, F. Arisaka, S. Kimura, K. Ohtomo, S. Mizuno, Silk fibroin of Bombyx mori is secreted, assembling a high molecular mass elementary unit consisting of H-chain, L-chain, and P25, with a 6:6:1 molar ratio, J. Biol. Chem. 275 (2000) 40517–40528.

[44] N.H.M. of Bern, World Spider Catalog, (n.d.). https://wsc.nmbe.ch/.

[45] Y. Liu, Z. Shao, F. Vollrath, Relationships between supercontraction and mechanical properties of spider silk., Nat. Mater. 4 (2005) 901–905.

[46] P.M. Cunniff, S.A. Fossey, M.A. Auerbach, J.W. Song, D.L. Kaplan, W.W. Adams, R.K. Eby, D. Mahoney, D.L. Vezie, Mechanical and thermal properties of dragline silk from the spider Nephila clavipes, Polym. Adv. Technol. 5 (1994) 401–410.

[47] M.-E. Rousseau, D. Hernández Cruz, M.M. West, A.P. Hitchcock, M. Pézolet,

Nephila clavipes Spider Dragline Silk Microstructure Studied by Scanning Transmission X-ray Microscopy, J. Am. Chem. Soc. 129 (2007) 3897–3905.

[48] D.H. Hijirida, K.G. Do, C. Michal, S. Wong, D. Zax, L.W. Jelinski, 13C NMR of Nephila clavipes major ampullate silk gland, Biophys. J. 71 (1996) 3442–3447.

[49] J.E. Jenkins, M.S. Creager, E.B. Butler, R. V. Lewis, J.L. Yarger, G.P. Holland, Solid-state NMR evidence for elastin-like β-turn structure in spider dragline silk, Chem. Commun. 46 (2010) 6714–6716.

[50] H. Berg, K. Augsten, E. Bauer, W. Förster, H.E. Jacob, P. Mühlig, H. Weber, Possibilities of cell fusion and transformation by electrostimulation, Bioelectrochemistry Bioenerg. 12 (1984) 119–133.

[51] A. Rising, H. Nimmervoll, S. Grip, A. Fernandez-Arias, E. Storckenfeldt, D.P. Knight, F. Vollrath, W. Engström, Spider Silk Proteins – Mechanical Property and Gene Sequence, Zoolog. Sci. 22 (2005) 273–281.

[52] R.F. Foelix, Structure and function of tarsal sensilla in the spiderAraneus diadematus, J. Exp. Zool. 175 (1970) 99–123.

[53] J.M. Gosline, C.C. Pollak, P.A. Guerette, A. Cheng, M.E. DeMont, M.W. Denny, Elastomeric Network Models for the Frame and Viscid Silks from the Orb Web of the Spider *Araneus diadematus*, in: 1993: pp. 328–341.

[54] D. Huemmerich, C.W. Helsen, S. Quedzuweit, J. Oschmann, R. Rudolph, T. Scheibel, Primary Structure Elements of Spider Dragline Silks and Their Contribution to Protein Solubility †, Biochemistry. 43 (2004) 13604–13612.

[55] J.D. Van Beek, S. Hesst, F. Vollrath, B.H. Meier, The molecular structure of spider dragline silk: Folding and orientation of the protein backbone, Proc. Natl. Acad. Sci. U. S. A. 99 (2002) 10266–10271.

[56] L. Eisoldt, A. Smith, T. Scheibel, Decoding the secrets of spider silk, Mater. Today. 14 (2011) 80–86.

[57] F. Vollrath, D.P. Knight, Liquid crystalline spinning of spider silk, Nature. 410 (2001) 541–548.

[58] D.P. Knight, M.M. Knight, F. Vollrath, Beta transition and stress-induced phase separation in the spinning of spider dragline silk, Int. J. Biol. Macromol. 27 (2000) 205–210.

[59] M. Andersson, J. Johansson, A. Rising, Silk Spinning in Silkworms and Spiders, Int. J. Mol. Sci. 17 (2016) 1290.

[60] D.T. Grubb, G. Ji, Molecular chain orientation in supercontracted and re-extended spider silk, in: Int. J. Biol. Macromol., 1999: pp. 203–210.

[61] Z. Shao, F. Vollrath, J. Sirichaisit, R.J. Young, Analysis of spider silk in native and supercontracted states using Raman spectroscopy, Polymer (Guildf). 40 (1999) 2493–2500.

[62] R.W. Work, A COMPARATIVE STUDY OF THE SUPERCONTRACTIO N OF MAJOR AMPULLATE SILK FIBERS OF ORB-WEB-BUILDING SPIDERS (ARANEAE) t, n.d.

[63] T.A. Blackledge, C. Boutry, S.C. Wong, A. Baji, A. Dhinojwala, V. Sahni, I. Agnarsson, How super is supercontraction? Persistent versus cyclic responses to humidity in spider dragline silk, J. Exp. Biol. 212 (2009) 1981–1989.

[64] H. Chung, T.Y. Kim, S.Y. Lee, Recent advances in production of recombinant spider silk proteins, Curr. Opin. Biotechnol. 23 (2012) 957–964.

[65] X.X. Xia, Z.G. Qian, C.S. Ki, Y.H. Park, D.L. Kaplan, S.Y. Lee, Native-sized recombinant spider silk protein produced in metabolically engineered Escherichia

coli results in a strong fiber, Proc. Natl. Acad. Sci. U. S. A. 107 (2010) 14059–14063.

[66] S.R. Fahnestock, S.L. Irwin, Synthetic spider dragline silk proteins and their production in Escherichia coli, Appl. Microbiol. Biotechnol. 47 (1997) 23–32.

[67] D.M. Widmaier, D. Tullman-Ercek, E.A. Mirsky, R. Hill, S. Govindarajan, J. Minshull, C.A. Voigt, Engineering the *Salmonella* type III secretion system to export spider silk monomers, Mol. Syst. Biol. 5 (2009) 309.

[68] C.Y. Hayashi, R. V. Lewis, Molecular architecture and evolution of a modular spider silk protein gene, Science (80-.). 287 (2000) 1477–1479.

[69] S.R. Fahnestock, L.A. Bedzyk, Production of synthetic spider dragline silk protein in Pichia pastoris, Appl. Microbiol. Biotechnol. 47 (1997) 33–39.

[70] A. Lazaris, S. Arcidiacono, Y. Huang, J.F. Zhou, F. Duguay, N. Chretien, E.A. Welsh, J.W. Soares, C.N. Karatzas, Spider silk fibers spun from soluble recombinant silk produced in mammalian cells, Science (80-.). 295 (2002) 472–476.

[71] J. Scheller, K.H. Gührs, F. Grosse, U. Conrad, Production of spider silk proteins in tobacco and potato, Nat. Biotechnol. 19 (2001) 573–577.

[72] R. Menassa, H. Zhu, C.N. Karatzas, A. Lazaris, A. Richman, J. Brandle, Spider dragline silk proteins in transgenic tobacco leaves: accumulation and field production, Plant Biotechnol. J. 2 (2004) 431–438.

[73] R.F. Service, MATERIALS SCIENCE: Mammalian Cells Spin a Spidery New Yarn, Science (80-.). 295 (2002) 419b – 421.

[74] H.-T. Xu, B.-L. Fan, S.-Y. Yu, Y.-H. Huang, Z.-H. Zhao, Z.-X. Lian, Y.-P. Dai, L.-L. Wang, Z.-L. Liu, J. Fei, N. Li, Construct Synthetic Gene Encoding

Artificial Spider Dragline Silk Protein and its Expression in Milk of Transgenic Mice, Anim. Biotechnol. 18 (2007) 1–12.

[75] Y. Zhang, J. Hu, Y. Miao, A. Zhao, T. Zhao, D. Wu, L. Liang, A. Miikura, K. Shiomi, Z. Kajiura, M. Nakagaki, Expression of EGFP-spider dragline silk fusion protein in BmN cells and larvae of silkworm showed the solubility is primary limit for dragline proteins yield, Mol. Biol. Rep. 35 (2008) 329–335.

[76] H. Wen, X. Lan, Y. Zhang, T. Zhao, Y. Wang, Z. Kajiura, M. Nakagaki, Transgenic silkworms (Bombyx mori) produce recombinant spider dragline silk in cocoons, Mol. Biol. Rep. 37 (2010) 1815–1821.

[77] F. Teulé, Y.G. Miao, B.H. Sohn, Y.S. Kim, J.J. Hull, M.J. Fraser, R. V. Lewis, D.L. Jarvis, Silkworms transformed with chimeric silkworm/spider silk genes spin composite silk fibers with improved mechanical properties, Proc. Natl. Acad. Sci. U. S. A. 109 (2012) 923–928.

[78] S. Grip, J. Johansson, M. Hedhammar, Engineered disulfides improve mechanical properties of recombinant spider silk, Protein Sci. 18 (2009) 1012–1022.

[79] S. Arcidiacono, C. Mello, D. Kaplan, S. Cheley, H. Bayley, Purification and characterization of recombinant sTRAIL expressed in Escherichia coli, Acta Biochim. Biophys. Sin. (Shanghai). 36 (2004) 118–122.

[80] B. Singh, N. Sharma, Mechanistic implications of plastic degradation, Polym. Degrad. Stab. 93 (2008) 561–584.

[81] P. Bracco, L. Costa, M.P. Luda, N. Billingham, A review of experimental studies of the role of free-radicals in polyethylene oxidation, Polym. Degrad. Stab. 155 (2018) 67–83.

[82] E. Richaud, O. Okamba Diogo, B. Fayolle, J. Verdu, J. Guilment, F. Fernagut, Review: Auto-oxidation of aliphatic polyamides, Polym. Degrad. Stab. 98 (2013) 1929–1939.

[83] F. Szőcs, M. Klimová, J. Bartoš, ESR study of the pressure and temperature dependence of free radical decay in γ-irradiated polyvinylpyrrolidone, Polym. Degrad. Stab. 14 (1986) 231–240.

[84] F. Szocs, M. Klimová, J. Bartoš, An ESR study of the influence of fatigue on the decay of free radicals in gamma irradiated polycarbonate, Polym. Degrad. Stab. 55 (1997) 233–235.

[85] B. Lecouvet, S. Bourbigot, M. Sclavons, C. Bailly, Kinetics of the thermal and thermo-oxidative degradation of polypropylene/halloysite nanocomposites, Polym. Degrad. Stab. 97 (2012) 1745–1754.

[86] M. Day, J.D. Cooney, M. MacKinnon, Degradation of contaminated plastics: a kinetic study, Polym. Degrad. Stab. 48 (1995) 341–349.

[87] N.G.N. Milton, Role of Hydrogen Peroxide in the Aetiology of Alzheimer's Disease: Implications for Treatment, Drugs and Aging. 21 (2004) 81–100.

[88] H. Mohmmad Abdul, R. Sultana, J.N. Keller, D.K. St. Clair, W.R. Markesbery, D.A. Butterfield, Mutations in amyloid precursor protein and presenilin-1 genes increase the basal oxidative stress in murine neuronal cells and lead to increased sensitivity to oxidative stress mediated by amyloid β-peptide (1-42), H2O2 and kainic acid: implications for A, J. Neurochem. 96 (2006) 1322–1335.

[89] T. Parman, M.J. Wiley, P.G. Wells, Free radical-mediated oxidative dna damage in the mechanism of thalidomide teratogenicity, Nat. Med. 5 (1999) 582–585.

[90] M.A. Koperska, T. Łojewski, J. Łojewska, Evaluating degradation of silk's

fibroin by attenuated total reflectance infrared spectroscopy: Case study of ancient banners from Polish collections, Spectrochim. Acta - Part A Mol. Biomol. Spectrosc. 135 (2015) 576–582.

[91] M.A. Koperska, D. Pawcenis, J. Bagniuk, M.M. Zaitz, M. Missori, T. Łojewski, J. Łojewska, Degradation markers of fibroin in silk through infrared spectroscopy, Polym. Degrad. Stab. 105 (2014) 185–196.

[92] M.A. Koperska, D. Pawcenis, J.M. Milczarek, A. Blachecki, T. Łojewski, J. Łojewska, Fibroin degradation - Critical evaluation of conventional analytical methods, Polym. Degrad. Stab. 120 (2015) 357–367.

[93] V. Vassileva, S. Baltova, S. Handjieva, Photochemical behaviour of natural silk - III. Photofading of silk dyed with acid azo dyes, Polym. Degrad. Stab. 61 (1998) 367–373.

[94] S. Baltova, V. Vassileva, Photochemical behaviour of natural silk - II. Mechanism of fibroin photodestruction, Polym. Degrad. Stab. 60 (1998) 61–65.

[95] S. Baltova, V. Vassileva, E. Valtcheva, Photochemical behaviour of natural silk - I. Kinetic investigation of photoyellowing, Polym. Degrad. Stab. 60 (1998) 53–60.

[96] R.. Feynman, There's Plenty of Room at the Bottom: An Invitation to Enter a New Field of Physics, (1959).

[97] P. Wang, J. Sun, Z. Lou, F. Fan, K. Hu, Y. Sun, N. Gu, Assembly-Induced Thermogenesis of Gold Nanoparticles in the Presence of Alternating Magnetic Field for Controllable Drug Release of Hydrogel, Adv. Mater. 28 (2016) 10801–10808.

[98] K. Hu, J. Sun, Z. Guo, P. Wang, Q. Chen, M. Ma, N. Gu, A Novel Magnetic

Hydrogel with Aligned Magnetic Colloidal Assemblies Showing Controllable Enhancement of Magnetothermal Effect in the Presence of Alternating Magnetic Field, Adv. Mater. 27 (2015) 2507–2514.

[99] M. Antman-Passig, O. Shefi, Remote Magnetic Orientation of 3D Collagen Hydrogels for Directed Neuronal Regeneration, Nano Lett. 16 (2016) 2567–2573.

[100] L. Maggini, M. Liu, Y. Ishida, D. Bonifazi, Anisotropically Luminescent Hydrogels Containing Magnetically-Aligned MWCNTs-Eu(III) Hybrids, Adv. Mater. 25 (2013) 2462–2467.

[101] M. Abdalla, D. Dean, D. Adibempe, E. Nyairo, P. Robinson, G. Thompson, The effect of interfacial chemistry on molecular mobility and morphology of multiwalled carbon nanotubes epoxy nanocomposite, Polymer (Guildf). 48 (2007) 5662–5670.

[102] M. Abdalla, D. Dean, M. Theodore, J. Fielding, E. Nyairo, G. Price, Magnetically processed carbon nanotube/epoxy nanocomposites: Morphology, thermal, and mechanical properties, Polymer (Guildf). 51 (2010) 1614–1620.

[103] Y.S. Kim, M. Liu, Y. Ishida, Y. Ebina, M. Osada, T. Sasaki, T. Hikima, M. Takata, T. Aida, Thermoresponsive actuation enabled by permittivity switching in an electrostatically anisotropic hydrogel, Nat. Mater. 14 (2015) 1002–1007.

[104] M. Liu, Y. Ishida, Y. Ebina, T. Sasaki, T. Hikima, M. Takata, T. Aida, An anisotropic hydrogel with electrostatic repulsion between cofacially aligned nanosheets, Nature. 517 (2015) 68–72.

[105] H. Le Ferrand, S. Bolisetty, A.F. Demirörs, R. Libanori, A.R. Studart, R. Mezzenga, Magnetic assembly of transparent and conducting graphene-based

functional composites, Nat. Commun. 7 (2016).

[106] F. Du, R.C. Scogna, W. Zhou, S. Brand, J.E. Fischer, K.I. Winey, Nanotube Networks in Polymer Nanocomposites: Rheology and Electrical Conductivity, Macromolecules. 37 (2004) 9048–9055.

[107] S. Sánchez-Valdes, H. Ortega-Ortiz, L.F. Ramos-de Valle, F.J. Medellín-Rodríguez, R. Guedea-Miranda, Mechanical and antimicrobial properties of multilayer films with a polyethylene/silver nanocomposite layer, J. Appl. Polym. Sci. (2008) NA-NA.

[108] M.L. Cerrada, C. Serrano, M. Sánchez-Chaves, M. Fernández-García, F. Fernández-Martín, A. de Andrés, R.J.J. Riobóo, A. Kubacka, M. Ferrer, M. Fernández-García, Self-Sterilized EVOH-TiO $_2$ Nanocomposites: Interface Effects on Biocidal Properties, Adv. Funct. Mater. 18 (2008) 1949–1960.

[109] Y. Kojima, A. Usuki, M. Kawasumi, A. Okada, Y. Fukushima, T. Kurauchi, O. Kamigaito, Mechanical properties of nylon 6-clay hybrid, J. Mater. Res. 8 (1993) 1185–1189.

[110] A. Usuki, Y. Kojima, M. Kawasumi, A. Okada, Y. Fukushima, T. Kurauchi, O. Kamigaito, Synthesis of nylon 6-clay hybrid, J. Mater. Res. 8 (1993) 1179–1184.

[111] A. Okada, A. Usuki, Twenty Years of Polymer-Clay Nanocomposites, Macromol. Mater. Eng. 291 (2006) 1449–1476.

[112] N. Herrera, A.P. Mathew, K. Oksman, Plasticized polylactic acid/cellulose nanocomposites prepared using melt-extrusion and liquid feeding: Mechanical, thermal and optical properties, Compos. Sci. Technol. 106 (2015) 149–155.

[113] D. Wang, C.A. Wilkie, Preparation of PVC-clay nanocomposites by solution blending, J. Vinyl Addit. Technol. 8 (2002) 238–245.

[114] A. Bansal, H. Yang, C. Li, B.C. Benicewicz, S.K. Kumar, L.S. Schadler, Controlling the thermomechanical properties of polymer nanocomposites by tailoring the polymer–particle interface, J. Polym. Sci. Part B Polym. Phys. 44 (2006) 2944–2950.

[115] A. Fina, D. Tabuani, A. Frache, G. Camino, Polypropylene-polyhedral oligomeric silsesquioxanes (POSS) nanocomposites, Polymer (Guildf). 46 (2005) 7855–7866.

[116] H. Zou, S. Wu, J. Shen, Polymer/Silica Nanocomposites: Preparation, Characterization, Properties, and Applications, Chem. Rev. 108 (2008) 3893–3957.

[117] R. Verdejo, M.M. Bernal, L.J. Romasanta, M.A. Lopez-Manchado, Graphene filled polymer nanocomposites, J. Mater. Chem. 21 (2011) 3301–3310.

[118] C. Manzi-Nshuti, P. Songtipya, E. Manias, M.M. Jimenez-Gasco, J.M. Hossenlopp, C.A. Wilkie, Polymer nanocomposites using zinc aluminum and magnesium aluminum oleate layered double hydroxides: Effects of LDH divalent metals on dispersion, thermal, mechanical and fire performance in various polymers, Polymer (Guildf). 50 (2009) 3564–3574.

[119] J.E. Gardolinski, L.C.M. Carrera, M.P. Cantão, F. Wypych, Layered polymer-kaolinite nanocomposites, J. Mater. Sci. 35 (2000) 3113–3119.

[120] X. Fu, S. Qutubuddin, Polymer-clay nanocomposites: Exfoliation of organophilic montmorillonite nanolayers in polystyrene, Polymer (Guildf). 42 (2001) 807–813.

[121] R.A. Hule, D.J. Pochan, Polymer nanocomposites for biomedical applications, MRS Bull. 32 (2007) 354–358.

Chapter 2

Elucidation of Thermo-Oxidative and Photo Degradation Mechanism of Recombinant Spider Silk

Abstract

In this chapter, the thermo and photo-oxidative degradation of recombinant spider silk were investigated under the oxidizing atmosphere. Thermogravimetric analysis (TGA), chemiluminescence (CL), nuclear magnetic resonance (NMR), infrared (IR) and UV-visible spectroscopy were employed for multilateral analysis. It was concluded that the oxidative degradation of the recombinant spider silk initiates mainly through the hydroperoxide formation at the Cα position of amino acid residues, and its unimolecular decomposition produces imide or α-keto amide groups together with the CL emission.

2.1 Introduction

Recombinant spider silk has been provided in sufficient materials for industrial application [1–5] as well as the major researches of spinning process, and structure-properties correlation for advanced applications are rapidly accelerated [2,6,7]. However, the inherent instability in the application against several factors such as the high temperature, humidity, and ultraviolet light, are recognized to be the most severe obstacle to the service lifetime in industrial manufacturing. As mentioned above, the lifetime design of the material is one of the essential factors for every application. For example, organic polymer materials, which particularly undergo various physicochemical modification, in which the inappropriate subsequent processing steps can be degraded their properties. Many factors such as heat, light, atmospheric oxygen, moisture, and metal residues, etc., may accelerate the degradation through different mechanisms based on the nature of polymer/chemical structure.

Understanding the primary degradation mode and its suppression is a prerequisite for the lifetime design. For instance, oxidative degradation is controlled by using 0.01-0.1 wt % stabilizer such as hindered phenol, phosphoric acid/thioether, or hindered amine etc., in order to control the photodegradation [8,9]. In the case of synthetic polymers, i.e. recombinant spider silk, it cannot be practically used without the elucidation of degradation mechanism and the control of appropriate stabilization strategy. Many efforts have been devoted to understanding the inactivation of proteins and polypeptides for medical purposes of the recombinant spider silk. The degradation can be conducted under mild conditions through the side or terminal functional groups such as deamidation, β elimination, and disulfide formation. However, the degradation of proteins as structural materials, especially silk fibroin, has been hardly studied. Koperska *et al.*

studied silkworm silk under different sever conditions using infrared spectroscopy [10–12]. They assumed that the vying of oxidative degradation and hydrolysis occurred over 150 °C. Baltova *et al.* reported the photodegradation under ultraviolet and quantified the α-keto amide by a titration method [13]. In general, degradation is complicated phenomenon. Various chemical reactions parallelly occur through many kinds of intermediate and chemical compounds, which change polymer structure. Therefore, comprehensive and multilateral analyses for elucidation of degradation mechanism of recombinant spider silk is required. To the best of our knowledge, such systematic research has not been conducted on the degradation of protein materials.

In this chapter, the thermo and photo-oxidative degradation of recombinant spider silk were investigated under the oxidizing atmosphere. Thermogravimetric analysis (TGA), chemiluminescence (CL), nuclear magnetic resonance (NMR), infrared (IR) and UV-visible spectroscopy were employed for multilateral analyses. The development of the physicochemical structure of spider silk was followed during degradation using a statistical approach based on the spectral representation of correlation coefficients. Multilateral and statistical analysis revealed that spider silk pyrolysis was mainly caused by oxidation, leading to carbonyl formation and amide degradation in the amorphous phase.

2.2 Experimental

Materials

Recombinant spider silk was provided by Spiber Inc. in a powder form. The amino acid sequence of the recombinant spider silk mimicked that of Araneus diadematus, consisting of Alanine (19.5%), Asparagine (0.5%), Glutamine (17.1%), Glycine (30.9%), Histidine (1.0%), Methionine (0.2%), Proline (14.1%), Serine (9.7%), and Tyrosine (7.0%) at amino acid purity of 95–100%. The average particle size measured by light scattering (Partica LA-950V2, Horiba) was 25.4 μm in the median diameter. The powder was stored in a refrigerator at 4◦C. Potassium bromide (KBr) was purchased from Wako Pure Chemical Industries, Ltd. for infrared spectroscopy. Tetrakis(trimethylsilyl)silane (TKS) (~98.0%) was purchased from Tokyo Chemical Industry Co., Ltd., which is used as a standard chemical-shift for solid-state NMR spectroscopy. The gases used in all experiments were dry air (78% of N_2, 21% of O_2 and 1% of Ar) and N_2 (≥ 99.99%).

Aging Test

Thermal degradation of the recombinant spider silk powder was implemented at 200 ◦C under a dry air flow at 200 mL/min in a thermostatic oven (FVO–10, TGK, Tokyo, JAPAN). The powder (ca. 0.5–1.0 g) was placed on a glass petri dish and heated in an oven for 24 hours, in which the sampling was done in every 2 hours. Before further measurements and characterizations, all the degraded samples were stored in a refrigerator at 4◦C.

Characterization

A solid-state ^{13}C NMR spectra (125.8 MHz) were recorded on an AVANCE III 400 FT-NMR spectrometer (Bruker BioSpin). Chemical shifts were referred to

tetrakis(trimethylsilyl)silane (TKS ^{13}C δ=3.54, internal standard) or glycine (^{13}C δ = 3.54, external standards). The magic angle spinning (MAS) frequency was fi xed at 8 kHz. The contact time for each cross-polarization (CP) experiment was 2 ms, and the acquisition and relaxation times were set to 27 ms and 5 s, respectively. The Fourier transform was performed using TOPSPIN software, version 3.2 (Bruker). Attenuated total reflection (ATR)-Infrared (IR) spectra were collected on a PerkinElmer Spectrum 100 ATR-IR spectrometer (PerkinElmer, Waltham, USA) equipped with a diamond crystal. The spectra were recorded at room temperature with the resolution of 4 cm^{-1} in the range of 4000–400 cm^{-1}. All the spectra were background- and baseline-corrected using Spectrum software version 6.3, and then normalized by the total area from 1900 to 1100 cm^{-1} for analysis. A thermo- gravimetric analysis (TGA) of spider silk was conducted using ThermoPlus EVO II (Rigaku), where an aluminum pan containing ca. 10 mg of powder was loaded into the instrument at room temperature, followed by heating at a rate of 20 ◦C/min up to 80 ◦C and 5 ◦C/min up to 110 ◦C. The temperature was maintained at 110 ◦C for 2 hours to remove free water. After that, the temperature was increased up to 180 ◦C at a heating rate of 20 ◦C/min, and then up to 200 ◦C at 5 ◦C/min. The temperature was maintained at 200 ◦C for 24 hours. The measurements were performed in dry air and N_2 respectively at a flow rate of 100 mL/min. The chemiluminescence from spider silk under degradation condition was observed on a chemiluminescence analyzer (CLA-ID2-HS, Tohoku Electronic Industrial Co., Ltd.). An aluminum pan with 10 mg of powder was placed into a chamber that was pre-heated at 200 ◦C under 100 mL/min of dry air or N_2 flow. The chemiluminescence was detected by a photon multiplier loaded on top of the chamber at the gate time of 60 s. A chemiluminescence analyzer (CLA-FS4, Tohoku Electronic Industrial Co., Ltd.) was used to detect the thermo-oxidative degradation of a

sample at an isothermal condition. A 10 mg of a sample contained in an aluminum pan (5 mm diameter, 40 µl) was loaded in a sample chamber (CLS-ST3) that was pre-heated to a desired temperature. A chemiluminescence (CL) curve was acquired as photon counts integrated over a period of 1 s by a photomultiplier. The measurements were performed in a range of temperature (120–200 ◦C) under dry air flow of 100 mL/min or at 200 ◦C under nitrogen flow of 100 mL/min. The background intensity was obtained through a measurement with a blank aluminum pan at the corresponding temperatures.

Correlation Coefficient Approach

Similar to other proteins, spider silk has a complex structure composed by many amino acids organized in four levels of morphologies and its degradation invites further complication. Thus, it is difficult to capture the entire picture of degradation of spider silk if one looks at each piece of spectral data independently. We have employed a comprehensive approach which correlates the development of each spectral component with the degradation time in a series of spectra and builds a spectral expression of correlation coefficients. Correlation coefficients are commonly used as a simple indicator in general statistical analysis but have not yet been utilized in the study of protein degradation. Hereafter, the basic idea of our approach is described together with a typical procedure: i) Step 1: Data acquisition: Spider silk powder was aged at 200 ◦C under dry air and sampled at each 2 hours until 24 hours. A series of degraded samples were then characterized by ^{13}C CP/MAS NMR, ATR-IR, and transmission IR. Characterization protocols were preliminarily standardized using pristine powder in order to maximize quantitative reproduction as well as spectrum quality. The aging and characterization were repeated twice for the dataset robustness. ii) Step 2: Normalization All the spectra were baseline corrected by appropriate methods for each measurement principle. Briefly,

IR spectra were background corrected, then baseline subtracted by a straight line to approximate an absorption-free region. The background-corrected spectra were then normalized by the total area of each selected region in order to minimize inconsistency in the signal level, which mostly originated from the quality of sample preparation and the optimization of optical alignment. We can calculate the normalized intensity as follows

$$I(x) = \frac{I^{\circ}(x)}{\int I^{\circ}(x)dx} \quad (1)$$

where I(x) and $I^{\circ}(x)$ are the normalized and raw intensity of a spectrum at position x. The spectroscopic variable x was the chemical shift for NMR and, the wavenumber for IR.

iii) Step 3: Spectral expression of correlation coefficients After the normalization, any change in a series of spectra could be directly linked to the physicochemical variation of spider silk along the degradation. However, it is not a trifling matter to interpret full details of variation from complicated spectra in a hypothesis-free manner. An assumption for the degradation mechanism would facilitate an easier interpretation of spectra by restricting a range of interests, but we consider that the thermal degradation of proteins has not been sufficiently understood for a specific assumption. Under the explained situation, the present study thoroughly employed a specific approach based on the correlation coefficient, which is defined as

$$r(I(x), t) = \frac{\sum_{j=1}^{m} \frac{\left(I_j(x) - \bar{I}(x)\right) - \left(t_j - \bar{t}\right)}{m}}{\sqrt{\sum_{j=1}^{m} \frac{\left(I_j(x) - \bar{I}(x)\right)^2}{m} \sum_{j=1}^{m} \frac{\left(t_j - \bar{t}\right)^2}{m}}} \quad (2)$$

where $I_j(x)$ is the normalized intensity of a spectrum measured at the degradation time of t_j , and I and t are the average value of the intensity and time from j = 1 to m. A correlation coefficient, r(I(x), t), was calculated from the variation of the intensity at x along the

degradation time t, and thus obtained r(I(x), t) was plotted as a spectrum. Direct comparison between normalized spectra and the spectral expression of the corresponding coefficient enables us to list up all systematic changes in the spectra along the degradation time, which include increase/decrease in the peak intensity, peak shift, peak narrowing/broadening, and so on. Specifically, a correlation coefficient reaching to +1 indicates a linear increment of specific chemical species along the degradation, and vice versa. We found that a non-linearity of a change along the degradation (most typically convergent) did not largely alter the characteristics of correlation coefficient spectra. Rather, the most important in acquiring accurate correlation coefficient spectra is the number of samples (m). An insufficient sample number tends to enlarge the magnitude of correlation coefficients that easily fluctuate upon the sample addition/removal. Here, stable correlation coefficients were obtained from 24 samples by duplicating sampling at each 2 hours of the aging time from 0 to 24 hours. A correlation coefficient approach realizes a hypothesis-free interpretation of complicated variation of spider silk upon thermal degradation. Different measurement principles mutually validate and augment respective conclusions. That was how we tackled the problem in the most objective and comprehensive manner.

2.3 Results and Discussion

The thermal behavior of fibrous biomaterials such as silkworm silk, collagen and cellulose have been studied based on TGA and DSC [14,15]. These measurements were typically performed under a nitrogen atmosphere using a linear temperature ramping program, while there have been few reports of measurements under an oxidative atmosphere, especially at an isothermal condition. In the ramping mode under nitrogen, the thermal decomposition of the recombinant spider silk exhibited mass losses in two steps (**Figure 2.1**), similar to that of silkworm silk: i) Water vaporization at 100–120 °C, and ii) the degradation of side chains of amino acid residues as well as the scission of peptide bonds in the backbone at 250–350 °C [16,17]. **Figure 2.2** compares the thermogravimetric behavior of recombinant spider silk under nitrogen and dry air, in which the temperature was first kept at 110 °C, subsequently ramped up to 200 °C, and finally kept at the same temperature. The temperature of 200 °C is one of the most standard temperatures for the isothermal degradation of polymeric materials and is above the glass transition temperature of fibroin [18–21]. In the course of temperature ramping to 110 °C, the weight loss of approximately 5 wt% was observed irrespective of the atmosphere, corresponding to the vaporization of free water. When the temperature was kept at 110 °C, a noticeable difference was observed between the 2 atm in a fairly reproducible manner: The mass gain of ca. 0.5 wt% was detected only under dry air. In the field of polymer degradation, this mass increment is well known as the sign of oxidation [22]. Even though the mass increment at 110 °C was quite small in the absolute value, this led to a huge deviation in the subsequent decomposition at 200 °C: The mass loss after 24 hours amounted to 13.5 wt% under dry air in contrast to 6.7 wt% under nitrogen. The observed thermogravimetric behavior of the recombinant spider silk (i.e.

the mass increment followed by the accelerated decomposition) implied an analogy to the auto-oxidation mechanism, in which the radical formation and spontaneous oxidation accelerates the oxidative degradation and chain scission.

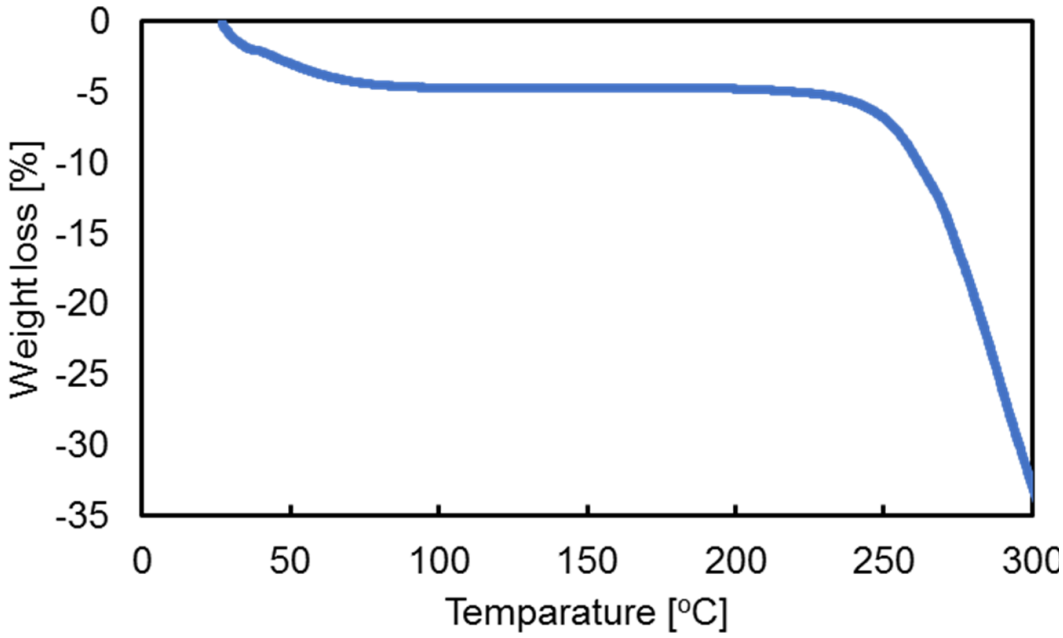

Figure 2.1. TG curve of recombinant spider silk under nitrogen in a temperature ramping mode.

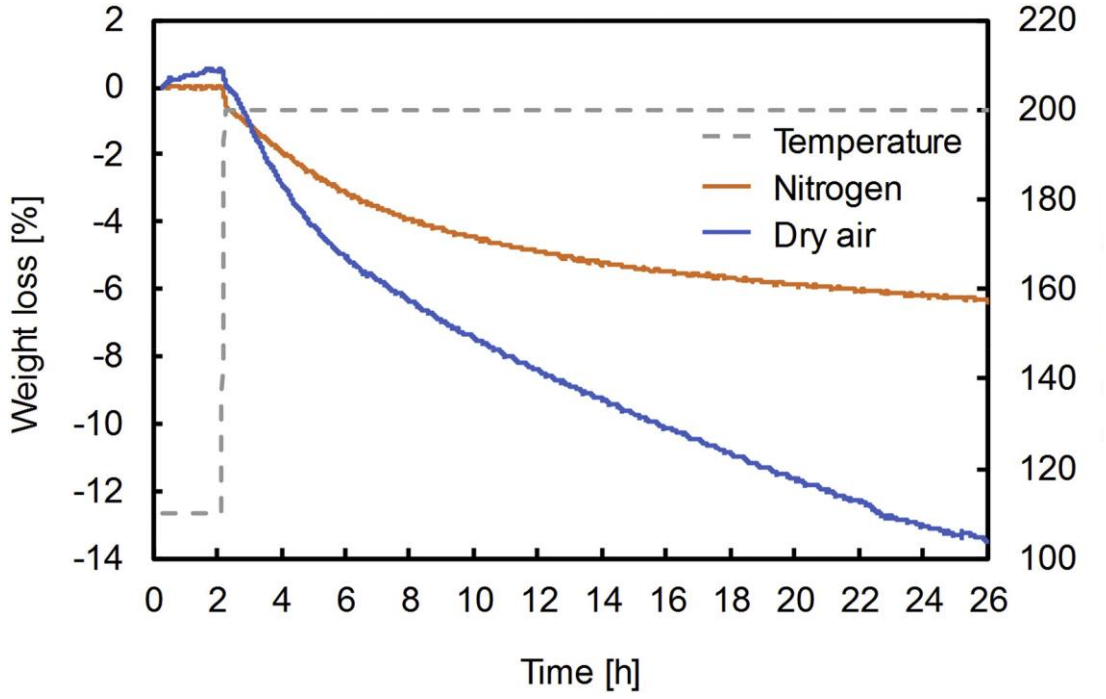

Figure 2.2. TG curves of recombinant spider silk under different atmospheres. The temperature was first kept at 110 °C to remove water, and then at 200 °C.

In oxidative degradation of organic molecules, several reaction mechanisms are known to accompany the CL emission, which includes i) bimolecular decomposition of alkyl peroxide radicals (called the Russell mechanism) [23], ii) decomposition of hydroperoxide [24], iii) metathesis reaction of alkoxy or peroxide radicals [25,26] and iv) unimolecular or bimolecular quenching of $^1O_2$ [27]. CLA has been also applied to study the oxidative denaturation of proteins and amino acids with the aid of radical initiators [28–30]. **Figure 2.3** shows the CL curves of recombinant spider silk acquired at 200 °C under nitrogen or dry air. As expected, the heating of recombinant spider silk under nitrogen never emitted CL. In contrast, relatively intense CL was observed under dry air, proving the occurrence of radical-aided oxidation. The emission initiated immediately after inserting the powder sample in the oven, and reached the maximum after 54 min, followed by slow decay over hours. The time scale of the CL emission was not far from

that of the mass loss at 200 °C even though these two principles observe different aspects of degradation. In this way, we have successfully identified the occurrence of the oxidation and its potential key role for the degradation of recombinant spider silk under an oxidative atmosphere. Hereafter, the CL behavior of recombinant spider silk was studied in comparison with other synthetic polymers whose CL mechanisms are known.

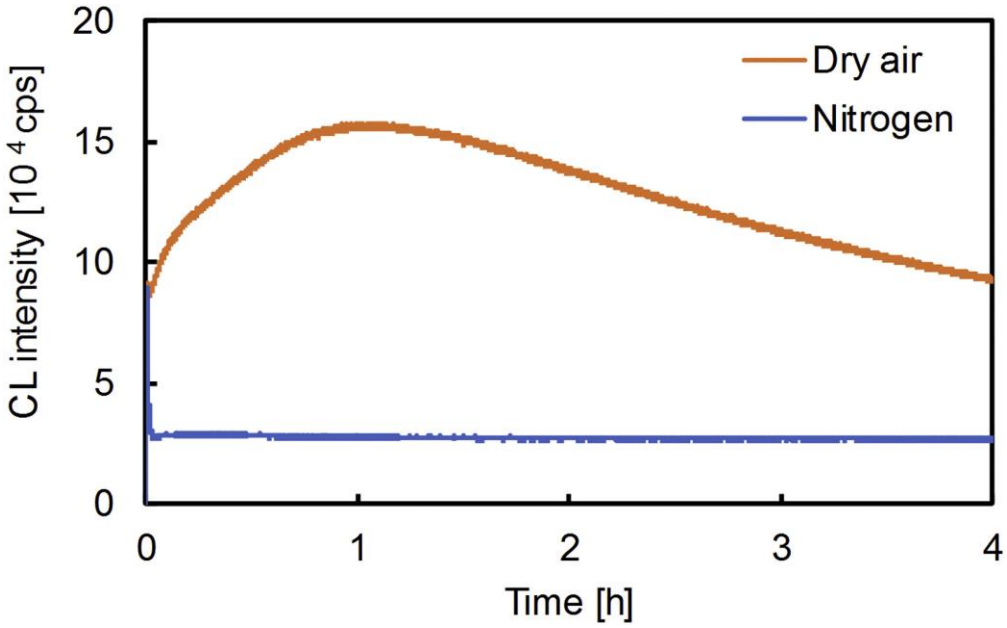

Figure 2.3. CL curves of recombinant spider silk at 200 °C under different atmospheres.

Figure 2.4 represents the CL curves of PP, PA 6, recombinant spider silk and silkworm silk at different temperatures. The CL curves of PP accompanied an induction time (OIT) before initiating rapid emission. When the temperature was decreased, the CL emission was delayed and weakened as a result of slower oxidation, leading to longer OIT. In the case of PA 6, the CL emission immediately started without any induction time, followed by a peak maximum and subsequent decay. By decreasing the degradation temperature, the CL emission became much weaker and dull, but the induction time was hardly observed. It was found that the CL behavior of recombinant spider silk and silkworm silk at different temperatures resembled that of PA 6. The activation energy of the oxidative degradation was estimated from the CL curves taken at different temperatures. An Arrhenius plot of the peak-top time led to 101, 145, and 132 kJ/mol of the activation energy for PA 6, recombinant spider silk, and silkwormsilk, respectively. Millington et al. provided similar activation energies for PA 6 and silkworm silk based on temperature-ramping CL measurements [29]. Richaud et al. reported that the presence or absence of OIT is mainly ascribed by the stability of hydroperoxide [31]. In the case of PP, the bimolecular decomposition of hydroperoxide is kinetically much more facile than the unimolecular pathway (ca. 100 kJ mol^{-1} vs. 50 kJ mol^{-1} in the activation energy), so that the duration till accumulating a sufficient concentration of hydroperoxide for the bimolecular decomposition results in an induction time. On the other hand, hydroperoxde created at the α-methylene of the amide bond of polyamide is unstable to allow the unimolecular decomposition without an induction period. The lack of OIT strongly suggested that the CL emission in recombinant spider silk and silkworm silk was mainly attributed to the unimolecular decomposition of hydroperoxide.

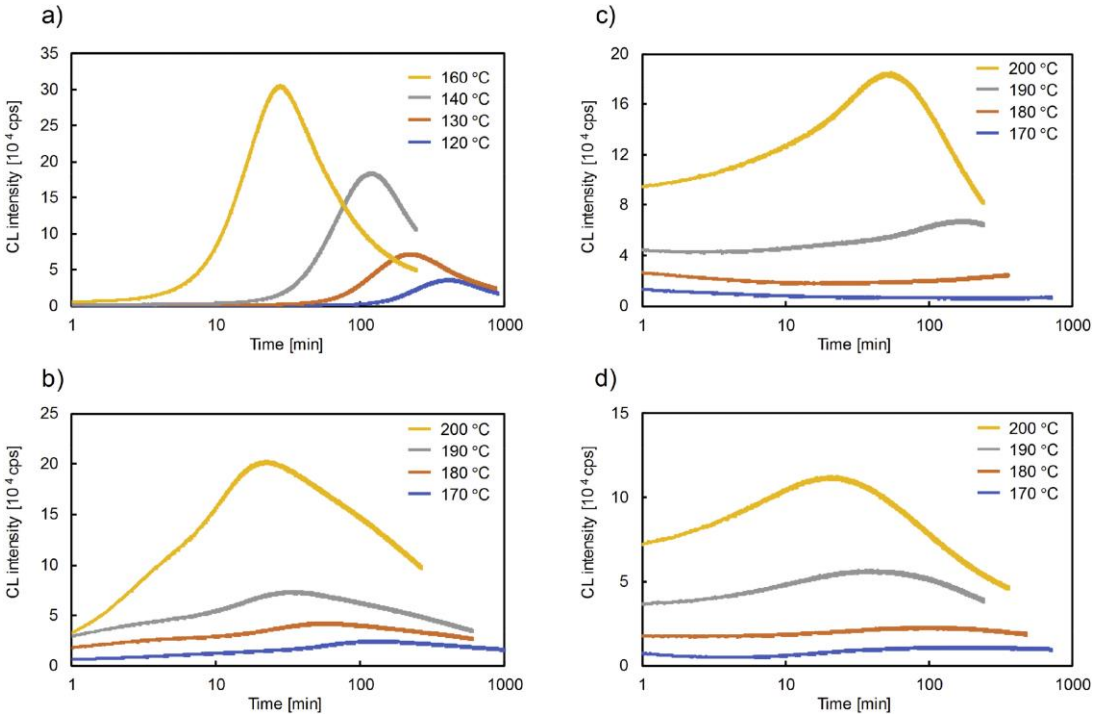

Figure 2.4. CL curves of a) PP, b) PA 6, c) recombinant spider silk, and d) silkworm silk under dry air at different temperatures.

To further understand the mechanism of the CL emission from recombinant spider silk, the CL spectra were compared among four different polymers. The spectra were acquired during the aging time of 1–2.5 min at 200 °C for PA 6, recombinant spider silk and silkworm silk. On the other hand, 13.5–15 min at 160 °C was selected for PP, which was soon after the completion of OIT. Thus, the spectra plausibly reflected luminescent species generated in the beginning of the oxidation, while suppressing the contribution from secondary oxidation. **Figure 2.5** compares the CL spectra of PP, PA 6, recombinant spider silk, and silkworm silk. The CL spectrum of PP was relatively sharp, and its maximum was observed at 380 nm. This band was associated with the formation of isolated carbonyl species at the tertiary carbon [25–27]. The spectrum of PA 6 showed the peak top in the range of 480–520 nm, ca. 100 nm bathochromically shifted as compared

with that of PP. This wavelength was associated with the emission from conjugated carbonyl groups [31,32], which were formed by the oxidation of α-methylene groups adjacent to the amide groups and subsequent unimolecular decomposition of hydroperoxide. The CL spectra of recombinant spider silk and silkworm silk were similar to that of PA 6. These results and the absence of OIT dictated that the CL mechanism for the recombinant spider silk closely resembles that of polyamide, that is, the oxidation of α-carbon of amino acid residues, followed by the unimolecular decomposition of hydroperoxide.

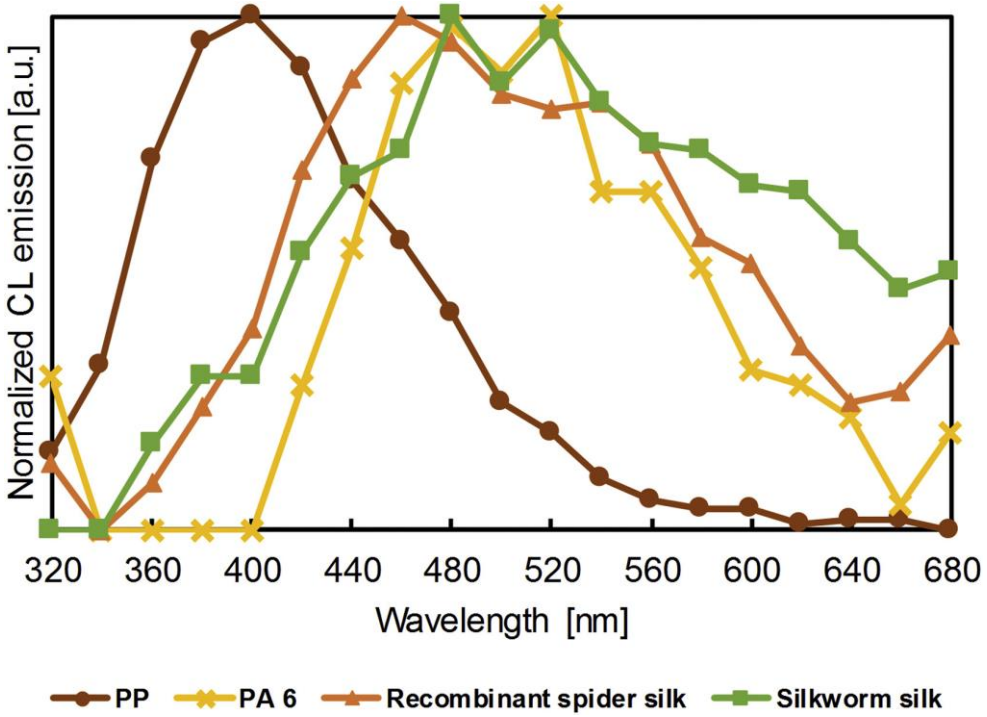

Figure 2.5. CL spectra of PP, PA 6, recombinant spider silk, and silkworm silk under dry air at 200 °C at an early stage of oxidation. The spectra were normalized by the total CL intensity.

Chemical reactions during oxidative degradation were intensively investigated using spectroscopy technique with the combination of correlation coefficient along the aging time. Solid-state ^{13}C CP-MAS NMR and ATR-IR are very useful tools to examine the conformational information of protein in both crystalline and amorphous regions on the bulk and surface, respectively [33–40]. A typical ^{13}C CP/MAS NMR spectrum of pristine spider silk is shown in **Figure 2.6** nad **Table 2.1**, in which the band assignments are summarized based on previous studies using NMR for spider silk.

Due to the conformational and compositional difference depending upon the type of spider silk, some of the observed chemical shifts can be slightly shifted out of the normal range from literature. However, all of the characteristic peaks could be assigned in a compatible way as can be referred from the previous studies. In the aliphatic area, ^{13}C CP/MAS NMR detected Gly Cα (43.2 ppm); Gln Cα (54.6 ppm), Cβ (25.4 ppm) and Cγ (30.7 ppm); Ser Cα (53.2 ppm) and Cβ (61.6 ppm); Pro Cα (61.6 ppm), Cβ (30.7 ppm), Cγ (24.6 ppm) and Cδ (49.8 ppm). Aromatic carbons mainly arose from Tyr C 1 (129.5 ppm), C 2,6 (130.9 ppm), C 3,5 (115.5 ppm), and C 4 (156.2 ppm). Carbonyl carbons in peptide bonds locate in between 172.3 and 176.3 ppm with a single major sharp peak at 173.0 ppm. The secondary structure was also recognized through chemical shifts: e.g. 54.6 and 49.8 ppm for Ala Cα for those of α-helix and β -sheet structures, respectively. Such informative spectra as described would provide a clear view of the transformation of spider silk during degradation in both compositional and conformational aspects.

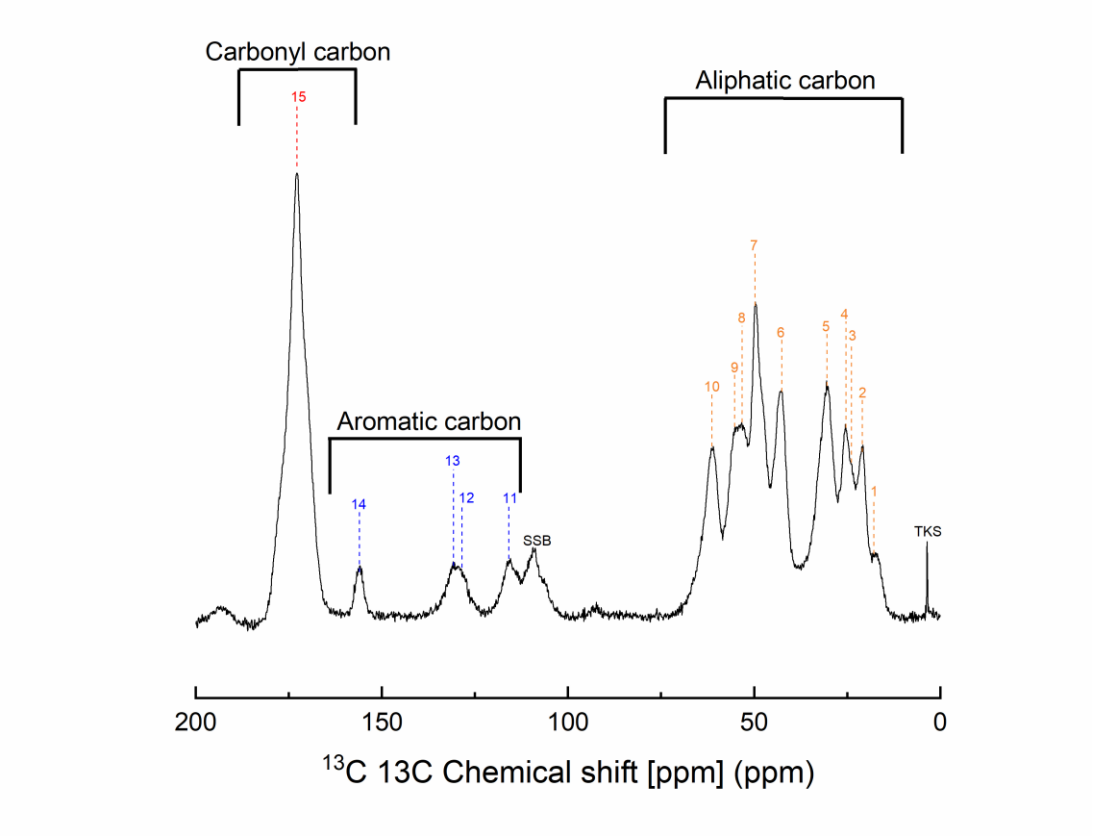

Figure 2.6. Solid-state 13 C CP/MAS NMR spectrum of pristine spider silk powder. The number on each band corresponds to the peak number in **Table 2.1**, and ssb indicates a spinning side band.

Table 2.1. ^{13}C chemical shifts of main amino acid residues for pristine spider silk

Residues	^{13}C	$\delta^{13}C$ [ppm] (Measured) a	$\delta^{13}C$ [ppm] (Reported in literature)	Ref.
Alanine (Ala)	Cα (α-helix)	54.6	54.4 – 56.4	[35,36,39]
	Cα (β-sheet)	49.8	49.6 – 52.1	
	Cβ (α-helix)	17.7	~17.0	
	Cβ (β-sheet)	21.5	19.3 – 23.1	
Glycine (Gly)	Cα (random coil)	43.2	43.5 – 45.3	[36,39]
Glutamine (Gln)	Cα	54.6	55.0 – 55.3	[35,39]
	Cβ	25.4	26.5	
	Cγ	30.7	31.7 – 32.0	
Serine (Ser)	Cα	53.2	~53.0	[35,36,38–40]
	Cβ	61.6	61.4 – 62.1	
Tyrosine (Tyr)	Cα (a-helix)	61.6	60.2 – 62.2	[36,39]
	Cα (β-sheet)	54.6	55.4 – 57.9	
	Cβ	43.2	39.1 – 42.9	
	Aromatic C	129.5 [C_1], 130.9 [$C_{2,6}$], 115.5 [$C_{3,5}$], 156.2 [C_4]	129.0 [C_1], 131.4 [$C_{2,6}$], 116.3 [$C_{3,5}$], 155.9 [C_4]	
Proline (Pro)	Cα	61.6	~62.0	[35,41]
	Cβ	30.7	~30.0	
	Cγ	24.6	~24.0	
	Cδ	49.8	~50.0	

As described above, the entire tendency in complicated spectra can be interpreted with the aid of the correlation coefficient approach. Then, all the obtained conclusions could be individually confirmed by plotting the normalized intensity at a specific position along the aging time, as exemplified in **Figure 2.7**. In **Figure 2.6**, solid-state ^{13}C CP/MAS NMR spectrum is shown, corresponding to correlation coefficient along the aging time. **Table 2.2** lists up the correspondence between the major peaks and the correlation coefficients at the peak-maxima positions, which describes the tendency of an increment/decrement of a specific peak during the aging. The first noticeable descriptor in the correlation coefficient spectrum is the peak of amide (N–C–O) at 173.0 ppm with a highly negative correlation coefficient ($r = -0.901$), which meant that peptide bonds were lost or transformed during the aging. A close look at the correlation coefficient spectrum around the amide peak identified the value inversion from negative to greatly positive at ca. 170.0 ppm. Such a behavior indicates the intensity loss at the higher chemical shift side and gain at the lower side. The former is attributed to the preferential loss of amide residues such as Gln and Pro. The latter is mainly related to the formation of new species around 163–169 ppm. Auto-oxidative degradation of polymer initiates from the generation of carbon-centered radicals with the removal of a hydrogen atom, immediately followed by the attachment of O_2. Thus, formed peroxy radicals undergo a series of reactions classified as propagation, chain branching and termination through key intermediates such as hydroperoxide and alkoxy radicals. Major products are carbonyl groups including ketone and aldehyde, hydroxyl groups, and so on. In the case of aliphatic polyamide, it is known that the first oxidation occurs preferentially at CH or CH 2 directly bonded to amide groups, resulting in either α-keto amide or imide species. A similar situation could be assumed for the oxidative degradation of spider silk: Oxidation tends

to happen close to amide groups, generating similar but more heavily conjugated carbonyl species due to the much higher density of amide bonds. These carbonyl groups can plausibly explain the new species around 163–169 ppm.

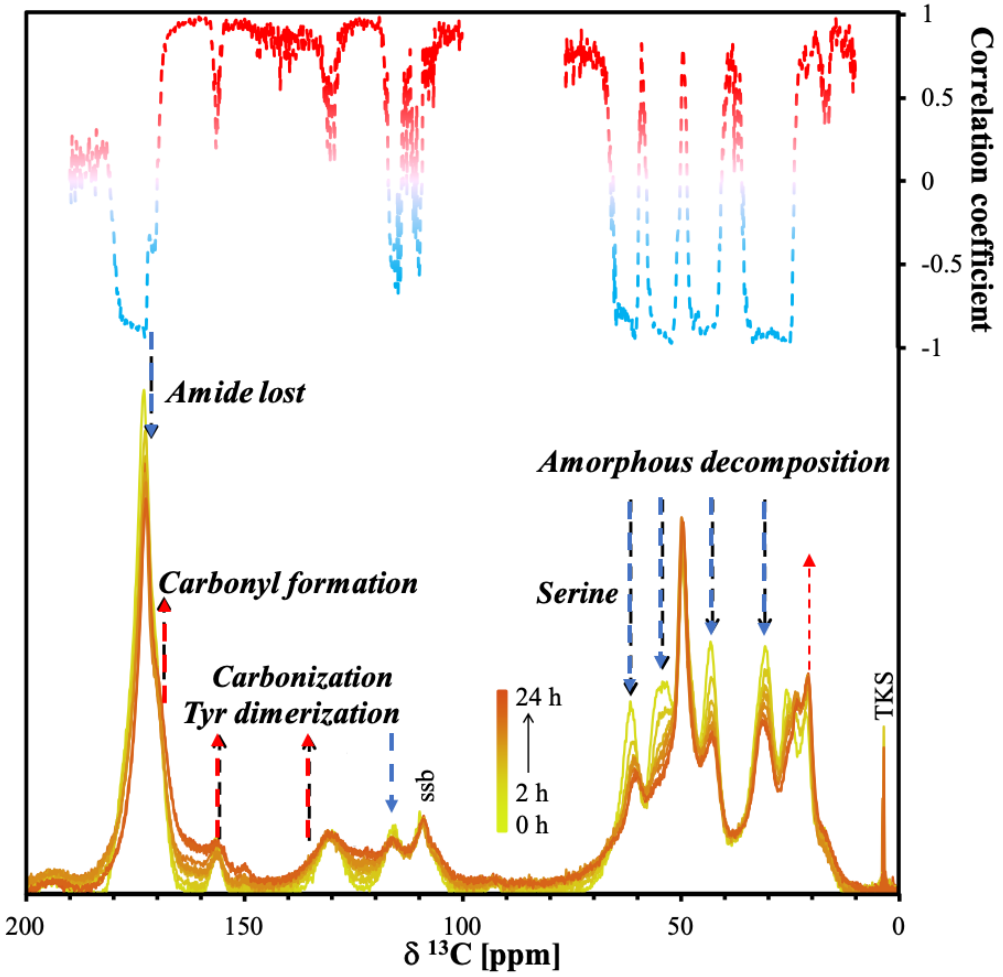

Figure 2.7. NMR spectra for spider silk degraded at 200 °C under dry air, corresponding to the peak number in **Table 2.2**. The color code and sign correspond to the correlation coefficients of the variables with each of the characteristics. The positive color explained the increment of intensity on spectra along the aging time.

Table 2.2. List of major peaks in ^{13}C CP/MAS NMR and their correlation coefficients with the degradation time

Peak number	δ ^{13}C [ppm]	Correlation coefficient (r)	Amino acid residues
1	17.7	0.50	Ala Cβ
2	21.5	0.80	Ala Cβ (β-sheet)
3	24.6	−0.87	Pro Cγ
4	25.4	−0.98	Gln Cβ
5	30.7	−0.93	Gln Cγ, Pro Cβ
6	43.2	−0.89	Gly Cα (random coil), Tyr Cβ
7	49.8	0.46	Ala Cα (β-sheet), Pro Cδ
8	53.2	−0.92	Ser Cα
9	54.6	−0.92	Ala Cα (α-helix), Gln Cα, Tyr Cα (β-sheet)
10	61.6	−0.85	Ser Cβ, Tyr Cα (α-helix), Pro Cα
11	115.5	−0.60	Tyr [C 3,5]
12	129.5	0.42	Tyr [C 1]
13	130.9	0.20	Tyr [C 2,6]
14	156.2	0.39	Tyr [C 4]
15	173.0	−0.90	C—O (amide)

ATR-IR and transmission IR spectra are shown along the aging time together with the corresponding correlation coefficient spectra in **Figure 2.8**. The assignments for typical absorption peaks in pristine spider silk are summarized in **Table 2.3**. Briefly, the ATR-IR spectrum of pristine spider silk shows the amide I band (mainly based on the C–O stretching vibration) in 1590–1700 cm^{-1} region, the amide II band (based on the C–N stretching vibration) in 1460–1590 cm^{-1} region, the amide III band (arising from the N–H bending and the N–H stretching vibration) in the range of 1400–1200 cm^{-1}. From a series of spectra, it is clear that the amide I–III regions went through major changes during

aging. The absorbance intensities of amide I, II dramatically decreased, and the amide III band mostly vanished with the corresponding correlation coefficients highly negative (r= −0.701). Contrary, a left tail of the amide I band developed into a shoulder along the aging, and a highly positive correlation coefficient (r = 0.797) was observed over 1800–1700 cm^{-1}. The position of the shoulder was centered at ca. 1760 cm^{-1}, which is reasonably assigned to carbonyl species as one of the most plausible oxidation products and in line with the solid NMR analyses. This carbonyl band is most frequently observed in the oxidative degradation of synthetic polymers and has been used as a degradation marker (carbonyl index). Importantly, the present result clarified that the thermal degradation of spider silk exhibits the formation of a similar oxidation product, and the development of the said band can be a facile and accurate marker to track the degradation of spider silk, as shown in **Table 2.3**. A clear increase of the intensity at ca. 1173 cm^{-1} must be ascribed to C–O stretching vibration of ester groups, which might be formed via reactions between hydroxyl groups of degradation products or side chains in Ser and Tyr and carboxylic acids. The series of transmission IR spectra (**Table 2.3**) led to basically similar observations to ATR-IR: A dramatic decrease in the absorbance intensities of amide I-III peaks together with highly negative correlation coefficients, and developments of carbonyl and C–O peaks with highly positive coefficients. However, systematic variation in the compositional and conformational structures became much slower for transmission IR compared with ATR-IR. Obviously, the degradation and oxidation promoted faster on surfaces. A modification in the secondary structure of spider silk was also confirmed: In the amide I region, the overall intensity decreased and the remaining band clarified the two peaks located at 1667 and 1632 cm^{-1} for the β- sheet structure. These facts answer that the crystallinity enhancement observed in the solid-state NMR originates from the

preferential degradation of the amorphous region rather than crystallization at an elevated temperature.

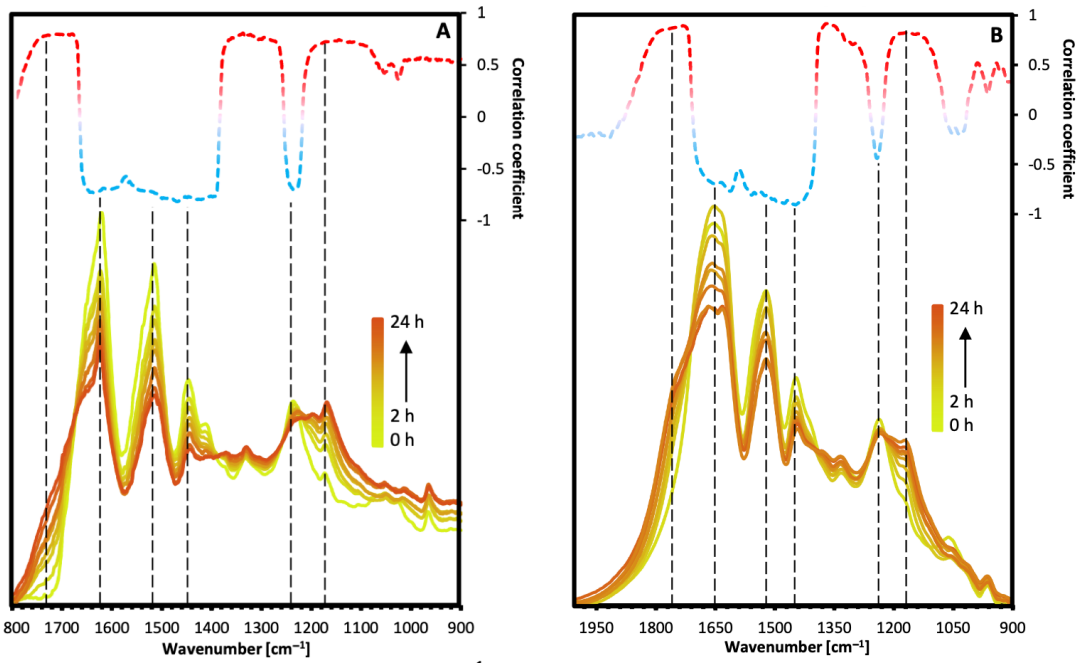

Figure 2.8. Series of ATR-IR (A) and transmission IR (B) spectra for spider silk degraded at 200 ◦C under dry air and the corresponding correlation coefficient spectra.

Table 2.3. Overview of absorption bands in IR for pristine spider silk

Wavenumber [cm^{-1}][a]		Wavenumber [cm^{-1}][b]	Assignment	Ref.
ATR	Trans.			
965	963	963	Ala (CH_3 rock, N–C_α stretch)	[42,43]
1051	–	1055	Ala (C_α–C_β stretch)	[42]
1061	1063	1065	CH_3 rock, C–N stretch	[11,42]
1173	1170	1164–1170	Tyr (C–N stretch), Ala (H^α bend, CH_3 symmetric bend)	[11,42]
1236	1237	1230–1240	Amide III (random coil and α-helical)	[11,42,44]
1256	1262	1260–1270	Amide III (β-sheet)	[11,42,44]
1333	1331	1315–1350	C–H bend	[11]
1412	1413	1410	Gln (C–N stretch)	[45]
1515	1523	1510–1520	Amide II (β-sheet)	[11,43,45]
1539	1543	1535–1542	Amide II (random coil and α-helical)	[11,43,45]
1622	1632	1610–1630	Amide I (β-sheet)	[11,43,45]
	1653	1648–1660	Amide I (random coil and α-helical)	[11,43,45]
1662	1667	1665	Amide I (anti-parallel pleated sheets)	[11,43,45]

The increase of the carbonyl region was in agreement to the thermo-oxidative degradation process (also see **Figure 2.9** and **Table 2.4**). The decrease in intensities was also observed in amide I, II, and III regions. However, amide I showed much weaker decomposition in photo-degradation than those in thermal degradation. From this observation, there is some difference in the correlation coefficient value between a photo- and thermal- degradation. Since the changes in these peaks are referred to amino, the differences in the values of the correlation coefficient can be negligible. In both cases, peak at 1174 cm^{-1} (C–O stretching vibration derived from ether or ester) has a highly positive correlation coefficient. However, this development was observed to be much

stronger in thermal oxidation.

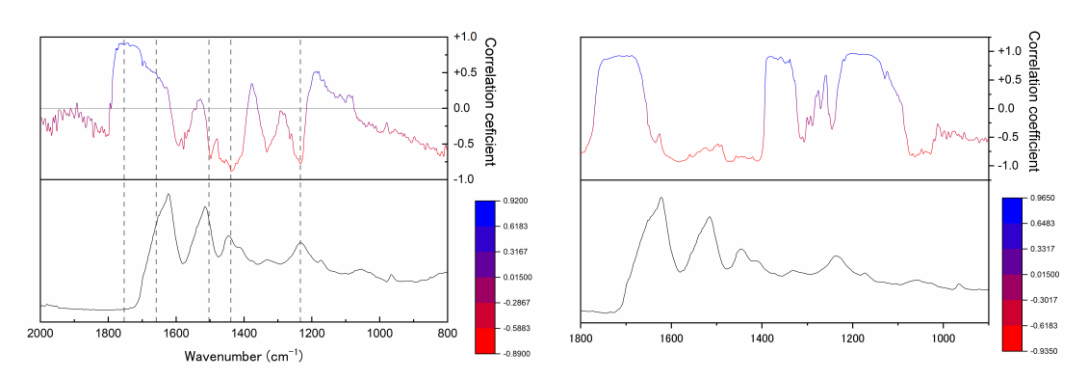

Figure 2.9. ATR-IR spectra of spider silk through (left) photo-degradation, (right) thermo-oxidative degradation at 170 °C and corresponding correlation coefficient spectra.

Table 2.4. Assignments of the main changes in vibrational function in **Figure 2.9**.

	Wavenumber [cm^{-1}]	Correlation coefficient (r)		Assignments
		Photo	Thermal	
(1)	1725–1760	0.96	0.97	C=O stretching vibration
(2)	1610–1670	**–0.47**	**–0.96**	Amide I C=O stretching vibration (random coil and α-helical)
(3)	1490–1550	–0.79	–0.93	Amide II (N–H deformation and C–N stretching vibration)
(4)	1445	–0.93	–0.94	Ala (CH_2 bend, CH_3 asymmetric bend)
(5)	1330	–0.43	0.44	CH bend
(6)	1238	–0.75	–0.34	Amide III (random coil and α-helical)
(7)	1174	**0.73**	**0.98**	C–O stretching vibration

The FTIR results show the absorbance of Amide I–III bands decreased when the irradiation dose was increased. This effect is probably observed due to the weakening and/or breaking of the peptide bond in polypeptides. However, the ratio of the area of Amide I and Amide II spectra, which indicates the relationship between the crystalline

and amorphous phases in the silk did not change significantly with the increasing time of irradiation. Thus, this result showed that UV radiation did not affect the primary structure of polypeptide arrangement.

The UV–vis absorption spectra of the recombinant spider silk are shown in **Figure 2.10**. The changes of absorbance with increasing dose of UV-irradiation are listed in **Table 2.5**. It can be seen from the figure that the absorption spectra of the recombinant spider silk in solution showed a wide peak in the region 200–300 nm. The main chromophores absorbing in the UV region are probably the aromatic amino acids, which is mainly tyrosine in the silk chain. After UV-irradiation of the recombinant spider silk, we observed a minor increase in the overall absorption in the region 250–400 nm, with wide peaks between 250 and 280 nm and between 290 and 340 nm was observed. For the recombinant spider silk before irradiation, only one peak was observed with a maximum at 275 nm. After UV-irradiation, a wide peak emerged with a maximum at about 305 nm. A comparison of the changes in the absorbance with increasing UV-irradiation dose has been shown in **Figure 2.10**. The new peak between 290 nm and 310 nm is probably due to the new photoproducts formed during UV-irradiation. These new photoproducts may be new cross-links and/or oxidized form of aromatic amino acids which can appear after UV- irradiation in recombinant spider silk.

Table 2.5. Changes of absorbance $\Delta A = (A_t - A_0)/A_0$ of recombinant spider silk (A_0– absorbance before irradiation, and A_t – after irradiation).

Wavelength (nm)	48 hours	72 hours	96 hours	120 hours
280	0.11	0.13	0.16	0.17
350	0.70	0.82	0.94	0.97
450	0.25	0.25	0.44	0.56

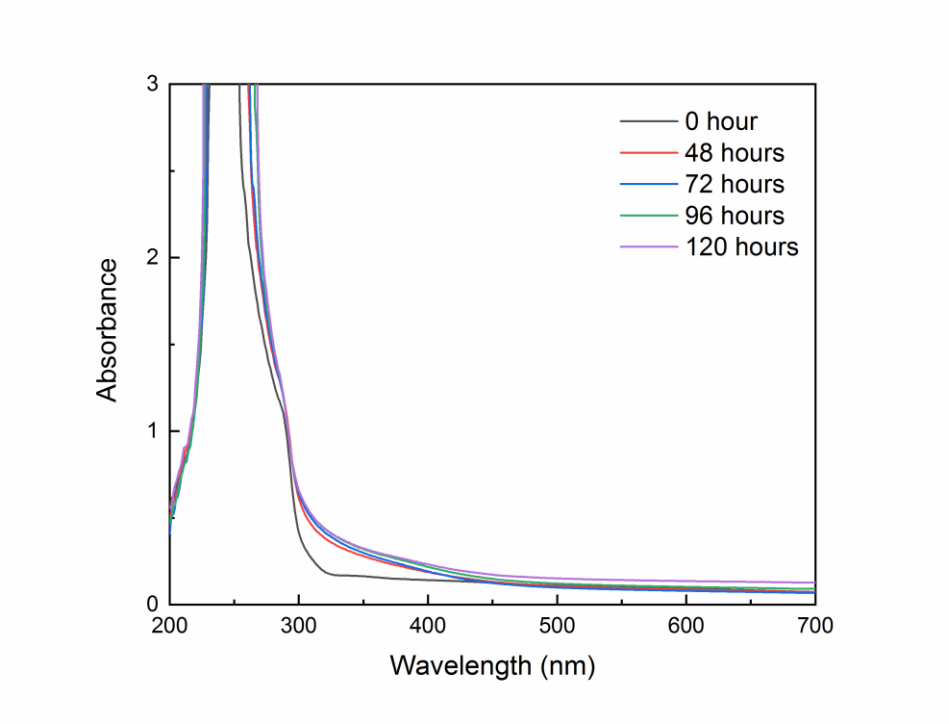

Figure 2.10. UV-DRS spectra of spider silk powder along the aging time.

2.4 Conclusions

Recombinant spider silk has arisen as one of the most promising nature-derived building blocks owing to its excellent mechanical properties, while its inherent instability against harsh environments has not been addressed. Here, the thermal- and photo-oxidation of unstabilized recombinant spider silk was investigated by means of combination of multilateral measurement and statistical analyses. The CL behavior of recombinant spider silk resembled that of PA 6 in terms of the absence of the induction time and the wavenumber of the maximum CL emission. Thus, obtained results reliably indicated a dominant role of oxidation in the thermal degradation process of spider silk, together with the identification of main degradation products such as carbonyl species conjugated with amide groups. It was suggested that the oxidation of recombinant spider silk initiates from the formation of hydroperoxide at the Cα position of amino acid residues and its unimolecular decomposition into imide or α-keto amide species causes the CL emission.

In addition, UV-irradiation of recombinant spider silk leads to the new photoproducts formed during UV exposure. These new photoproducts contain chromophores which cause alterations of absorption and fluorescence spectra of recombinant spider silk. Partial degradation of recombinant spider silk has been recorded by FTIR spectroscopy. Further studies are required to explain the photodegradation pathways in regenerated silk fibroin. In addition, UV-vis absorption at 450 nm can be detected for degradation earlier than ATR-IR.

References

[1] X.X. Xia, Z.G. Qian, C.S. Ki, Y.H. Park, D.L. Kaplan, S.Y. Lee, Native-sized recombinant spider silk protein produced in metabolically engineered Escherichia coli results in a strong fiber, Proc. Natl. Acad. Sci. U. S. A. 107 (2010) 14059–14063.

[2] F. Teulé, A.R. Cooper, W.A. Furin, D. Bittencourt, E.L. Rech, A. Brooks, R. V. Lewis, A protocol for the production of recombinant spider silk-like proteins for artificial fiber spinning, Nat. Protoc. 4 (2009) 341–355.

[3] F. Teulé, Y.G. Miao, B.H. Sohn, Y.S. Kim, J.J. Hull, M.J. Fraser, R. V. Lewis, D.L. Jarvis, Silkworms transformed with chimeric silkworm/spider silk genes spin composite silk fibers with improved mechanical properties, Proc. Natl. Acad. Sci. U. S. A. 109 (2012) 923–928.

[4] D.M. Widmaier, D. Tullman-Ercek, E.A. Mirsky, R. Hill, S. Govindarajan, J. Minshull, C.A. Voigt, Engineering the *Salmonella* type III secretion system to export spider silk monomers, Mol. Syst. Biol. 5 (2009) 309.

[5] C. Vendrely, T. Scheibel, Biotechnological Production of Spider-Silk Proteins Enables New Applications, Macromol. Biosci. 7 (2007) 401–409.

[6] S. Arcidiacono, C.M. Mello, M. Butler, E. Welsh, J.W. Soares, A. Allen, D. Ziegler, T. Laue, S. Chase, Aqueous Processing and Fiber Spinning of Recombinant Spider Silks, Macromolecules. 35 (2002) 1262–1266.

[7] S. Rammensee, U. Slotta, T. Scheibel, A.R. Bausch, Assembly mechanism of recombinant spider silk proteins, Proc. Natl. Acad. Sci. U. S. A. 105 (2008) 6590–6595.

[8] R. Pfaendner, How will additives shape the future of plastics?, Polym. Degrad.

Stab. 91 (2006) 2249–2256.

[9] J. Pospíšil, S. Nešpůrek, Chain-breaking stabilizers in polymers: the current status, Polym. Degrad. Stab. 49 (1995) 99–110.

[10] M.A. Koperska, D. Pawcenis, J.M. Milczarek, A. Blachecki, T. Łojewski, J. Łojewska, Fibroin degradation - Critical evaluation of conventional analytical methods, Polym. Degrad. Stab. 120 (2015) 357–367.

[11] M.A. Koperska, D. Pawcenis, J. Bagniuk, M.M. Zaitz, M. Missori, T. Łojewski, J. Łojewska, Degradation markers of fibroin in silk through infrared spectroscopy, Polym. Degrad. Stab. 105 (2014) 185–196.

[12] M.A. Koperska, T. Łojewski, J. Łojewska, Evaluating degradation of silk's fibroin by attenuated total reflectance infrared spectroscopy: Case study of ancient banners from Polish collections, Spectrochim. Acta - Part A Mol. Biomol. Spectrosc. 135 (2015) 576–582.

[13] S. Baltova, V. Vassileva, Photochemical behaviour of natural silk - II. Mechanism of fibroin photodestruction, Polym. Degrad. Stab. 60 (1998) 61–65.

[14] L.F. Drummy, D.M. Phillips, M.O. Stone, B.L. Farmer, R.R. Naik, Thermally Induced α-Helix to β-Sheet Transition in Regenerated Silk Fibers and Films, Biomacromolecules. 6 (2005) 3328–3333.

[15] M. Li, W. Tao, S. Kuga, Y. Nishiyama, Controlling molecular conformation of regenerated wild silk fibroin by aqueous ethanol treatment, Polym. Adv. Technol. 14 (2003) 694–698.

[16] S.Y. Cho, Y.S. Yun, S. Lee, D. Jang, K.Y. Park, J.K. Kim, B.H. Kim, K. Kang, D.L. Kaplan, H.J. Jin, Carbonization of a stable β-sheet-rich silk protein into a pseudographitic pyroprotein, Nat. Commun. 6 (2015).

[17] V. Müller, M. Cestari, S.M. Palácio, S.D. de Campos, E.C. Muniz, E.A. de Campos, Silk fibroin nanofibers electrospun on glass fiber as a potential device for solid phase microextraction, J. Appl. Polym. Sci. 132 (2015) n/a-n/a.

[18] X. Hu, D. Kaplan, P. Cebe, Dynamic Protein−Water Relationships during β-Sheet Formation, Macromolecules. 41 (2008) 3939–3948.

[19] X. Hu, D. Kaplan, P. Cebe, Determining Beta-Sheet Crystallinity in Fibrous Proteins by Thermal Analysis and Infrared Spectroscopy, Macromolecules. 39 (2006) 6161–6170.

[20] A. Motta, L. Fambri, C. Migliaresi, Regenerated silk fibroin films: Thermal and dynamic mechanical analysis, Macromol. Chem. Phys. 203 (2002) 1658–1665.

[21] L.F. Drummy, D.M. Phillips, M.O. Stone, B.L. Farmer, R.J. Naik, Thermally induced α-helix to β-sheet transition in renegated silk fibers and films, Biomacromolecules. 6 (2005) 3328–3333.

[22] H. Nakatani, S. Suzuki, T. Tanaka, M. Terano, New kinetic aspects on the mechanism of thermal oxidative degradation of polypropylenes with various tacticities, Polymer (Guildf). 46 (2005) 12366–12371.

[23] G. Russell, Additions and Corrections: Deuterium-isotope Effects in the Autoxidation of Aralkyl Hydrocarbons. Mechanism of the Interaction of Peroxy Radicals., J. Am. Chem. Soc. 80 (1958) 6699–6699.

[24] S.S. Stivala, E.B. Kaplan, L. Reich, . ; S S Stivala, G. Yo, Kinetics of Autoxidation of Atactic Polypropylene in the Presence of Cobalt Salts by Infrared Spectroscopy “Autoxidation of Hydro-carbons of Polyolefins,” This scheme was recently modified by Bawn and Chaudhri6 to account for the kinetics of manganese salts catalyzed autoxidation of atactic polypropylene,

UTC, n.d. https://pubs.acs.org/sharingguidelines (accessed November 17, 2019).

[25] E.M.Y. Quinga, G.D. Mendenhall, Chemiluminescence from hyponitrite esters. Excited triplet states from dismutation of geminate alkoxyl radical pairs, J. Am. Chem. Soc. 105 (1983) 6520–6521.

[26] F. Käser, B. Roduit, Prediction of the ageing of rubber using the chemiluminescence approach and isoconversional kinetics, J. Therm. Anal. Calorim. 93 (2008) 231–237.

[27] W. Adam, D. V. Kazakov, V.P. Kazakov, Singlet-Oxygen Chemiluminescence in Peroxide Reactions, Chem. Rev. 105 (2005) 3371–3387.

[28] K.R. Millington, H. Ishii, G. Maurdev, Chemiluminescence from thermal oxidation of amino acids and proteins, Amino Acids. 38 (2010) 1395–1405.

[29] K.R. Millington, G. Maurdev, M.J. Jones, Thermal chemiluminescence of fibrous proteins, Polym. Degrad. Stab. 92 (2007) 1504–1512.

[30] A. Aspée, E.A. Lissi, Kinetics of the chemiluminescence associated to the reaction between peroxyl radicals and proteins, J. Protein Chem. 20 (2001) 479–485.

[31] E. Richaud, O. Okamba Diogo, B. Fayolle, J. Verdu, J. Guilment, F. Fernagut, Review: Auto-oxidation of aliphatic polyamides, Polym. Degrad. Stab. 98 (2013) 1929–1939.

[32] T. Sago, H. Ishii, H. Hagihara, N. Takada, H. Suda, Analysis of chemiluminescence spectra in oxidative degradation of oleic acid, Chem. Phys. Lett. 565 (2013) 138–142.

[33] N.J.A. Martin, B. List, Highly Enantioselective Transfer Hydrogenation of α,β-Unsaturated Ketones, J. Am. Chem. Soc. 128 (2006) 13368–13369.

[34] Y. Suzuki, S. Kawanishi, T. Yamazaki, A. Aoki, H. Saito, T. Asakura, Structural Determination of the Tandem Repeat Motif in *Samia cynthia ricini* Liquid Silk by Solution NMR, Macromolecules. 48 (2015) 6574–6579.

[35] M.S. Creager, J.E. Jenkins, L.A. Thagard-Yeaman, A.E. Brooks, J.A. Jones, R. V Lewis, G.P. Holland, J.L. Yarger, Solid-state NMR comparison of various spiders' dragline silk fiber., Biomacromolecules. 11 (2010) 2039–43.

[36] M. Hronska, J.D. van Beek, P.T.F. Williamson, F. Vollrath, B.H. Meier, NMR Characterization of Native Liquid Spider Dragline Silk from *Nephila edulis*, Biomacromolecules. 5 (2004) 834–839.

[37] A. Simmons, E. Ray, L.W. Jelinski, Solid-State 13C NMR of Nephila clavipes Dragline Silk Establishes Structure and Identity of Crystalline Regions, Macromolecules. 27 (1994) 5235–5237.

[38] T. Asakura, J. Yao, 13C CP/MAS NMR study on structural heterogeneity in Bombyx mori silk fiber and their generation by stretching, Protein Sci. 11 (2009) 2706–2713.

[39] G.P. Holland, M.S. Creager, J.E. Jenkins, R. V. Lewis, J.L. Yarger, Determining Secondary Structure in Spider Dragline Silk by Carbon−Carbon Correlation Solid-State NMR Spectroscopy, J. Am. Chem. Soc. 130 (2008) 9871–9877.

[40] T. Asakura, Y. Suzuki, Y. Nakazawa, K. Yazawa, G.P. Holland, J.L. Yarger, Silk structure studied with nuclear magnetic resonance, Prog. Nucl. Magn. Reson. Spectrosc. 69 (2013) 23–68.

[41] X. Shi, G.P. Holland, J.L. Yarger, Molecular Dynamics of Spider Dragline Silk Fiber Investigated by ^{2}H MAS NMR, Biomacromolecules. 16 (2015) 852–859.

[42] A. Heidebrecht, L. Eisoldt, J. Diehl, A. Schmidt, M. Geffers, G. Lang, T.

Scheibel, Biomimetic Fibers Made of Recombinant Spidroins with the Same Toughness as Natural Spider Silk, Adv. Mater. 27 (2015) 2189–2194.

[43] P. Papadopoulos, J. Sölter, F. Kremer, Structure-property relationships in major ampullate spider silk as deduced from polarized FTIR spectroscopy, Eur. Phys. J. E. 24 (2007) 193–199.

[44] M.A. de Moraes, C.R. Albrecht Mahl, M. Ferreira Silva, M.M. Beppu, Formation of silk fibroin hydrogel and evaluation of its drug release profile, J. Appl. Polym. Sci. 132 (2015) n/a-n/a.

[45] A. Barth, Infrared spectroscopy of proteins, Biochim. Biophys. Acta - Bioenerg. 1767 (2007) 1073–1101.

Chapter 3

Stabilization of Recombinant Spider Silk in Thermo-Oxidative and Photo Degradation

Abstract

In this chapter, I have implemented the first extensive exploration on the stabilization of recombinant spider silk against the thermo- and photo-oxidative degradation based on HTP-CLI and multiple UV analyses.

3.1 Introduction

Most of the mechanisms can be deteriorated in physical properties during processing and services, which depend on the nature of polymer and environmental conditions. The possible failure mechanism is oxidation, hydrolysis, thermolysis, proteolysis, photolysis, or/and their combination [1–6].

The introduction of appropriate stabilizers is the most widely employed to diminish the degradation of polymers, in which the selection of stabilizers primarily depends on the degradation mechanism [7–9]. In general, the efficiency of stabilizers cannot be preciously ascribed, only the aging tests can be relatively examined under the specific aging condition with specific material. The tests can possibly be affected by several factors, e.g solubility, migratability, and retentionability of the polymeric in nature [10–12]. In addition, the demand in stabilizers exploration has been extensively concerned for a high-throughput methodology.

The machine combines an extreme sensitivity of the chemiluminescence (CL) method to detect the oxidation of polymers (ca. 20 times faster detection was reported in comparison to traditional mechanical tests), and the feasibility of in-situ imaging for parallelization [13]. Recently, we have developed a high-throughput chemiluminescence imaging (HTP- CLI) instrument, which enables simultaneous determination of polymer lifetime for 100 samples in a single measurement for screening antioxidants on thermo-oxidative degradation [14]. The first demonstration on the stabilization of polypropylene using this powerful machine showed the significance of HTP-CLI in acquiring the lifetime data of 3 years within only 1 month. From the results, HTP-CLI is also expected to play an important role for the study on degradation and stabilization for not only the well-known commercial but also the new developed materials. Moreover, the

methodology of this high-throughput screening can expand to give an advantage for the photo-degradation screening in solution cast method and multiple UV-vis. The screening protocols can detect parallel for each degradation from the initial term.

So far, study on the degradation and stabilization on silk-based materials has been primarily focused on silkworm silk due to its natural abundance and common usages in textiles and medicals. In the textile applications, the interesting on stabilizers function is to prevent the photo-degradation and discoloration of silkworm silk whereas in the medical applications, the control of biodegrade-ability of silk and the proliferation of cells for tissue engineering using the stabilizers are focused [15–17]. For example, the recent study from Kaplan group shows the preservation of the natural antioxidants including curcumin and vitamin C inside a silkworm silk film, in which a positive consequence of strong interaction between the antioxidants and the hydrophobic residues of silk via their aromatic moieties is also reported [18].

In the research, we have firstly reported the durability and degradation mechanism of the recombinant spider silk under a harsh condition which aiming to the development of industrial building block materials. The results showed the auto-oxidation mechanism can dominate for the degradation of recombinant spider silk at an elevated temperature. From this, the radical formation is initiated at the C position of amino acid residues where its unimolecular decomposition affords the conjugated carbonyl groups. Not only this discovery, our next big step target is to explore the suitable stabilizers that can effectively inhibit the thermo-oxidative degradation of recombinant spider silk.

In this chapter, I have implemented the first extensive exploration on the stabilization of recombinant spider silk against the thermo- and photo-oxidative degradation based on HTP-CLI and multiple UV analyses. The antioxidants efficiency

was identified as a result of the implementation at a scale of 103 degradation tests by HTP-CLI and subsequent validation using other techniques. A variety of antioxidants including nature-derived antioxidants as well as synthetic hindered phenols, thioethers and phosphates were selectively screened.

A key issue was found at the compatibility of antioxidants with employed processes and effective interaction with recombinant spider silk. The potential antioxidants were identified for powder impregnation.

3.2 Experimental

Materials

Materials Recombinant spider silk was provided by Spiber Inc. in a powder form. The amino acid sequence of the recombinant spider silk mimicked that of *Araneus diadematus*, consisting of Alanine (19.5%), Asparagine (0.5%), Glutamine (17.1%), Glycine (30.9%), Histidine (1.0%), Methionine (0.2%), Proline (14.1%), Serine (9.7%), and Tyrosine (7.0%) at amino acid purity of 95–100%. The average particle size measured by light scattering (Partica LA-950V2, Horiba) was 25.4 μm in the median diameter. The powder was stored in a refrigerator at 4 ◦ C. Potassium bromide (KBr) was purchased from Wako Pure Chemical Industries, Ltd. for infrared spectroscopy. The antioxidants and photo stabilizer used in this study are commercially avail-able grades and their structures are shown in Figure 3.1−3 and Figure 3.4, respectively. Silkworm silk was purchased from KB SEIREN. Polyamide 6 (nylon 6) pellets were purchased from Sigma-Aldrich Co. An additive-free powder of isotactic polypropylene was obtained (Mn = 4.6 × 104, *mmmm* = 98%) by propylene polymerization using a MgCl2-supported Ziegler-Natta catalyst.

Sample Preparation

Stabilization of recombinant spider silk powder was carried out by impregnating the powder in a solvent containing a specified amount of an antioxidant. A mixture of acetone and methanol (1/1 v/v) was chosen as a typical example to dissolve an antioxidant at the concentration of 0.1–0.5 mg/mL 2.0 mL of the antioxidant solution was then added to 200 mg of recombinant spider silk powder. The mixture was kept for 16 h under mild stirring and then naturally dried, affording the stabilized powder containing 0.1–0.3 wt% of an antioxidant. All samples were prepared at room temperature and 20–30% R.H. The

obtained powder was filled into the wells of a multi-cell plate and subjected to the HTP-CLI measurements.

The cast film was prepared in a solvent containing a specific amount of a photo stabilizer. Hexafluoro-2-propanol (HFIP) was chosen to dissolve a photo stabilizer at the concentration of 0.5 wt%. After adding to 4 wt% recombinant spider silk to solvent weight, the dope solution was stirred for 3 hours at 50 ◦C. Then, the dope solution was Casted on glass multiple cell plate, drying for 4 hours at 60 ◦C. Noted that the thickness of cast film was prepared, putting same amount of dope solution.

Characterization

A chemiluminescence analyzer (CLA-FS4, Tohoku Electronic Industrial Co., Ltd.) was used to detect the thermo-oxidative degradation of a sample at an isothermal condition. 10 mg of a sample contained in an aluminum pan (5 mm diameter, 40 μl) was loaded in a sample chamber (CLS-ST3) that was pre-heated to a desired temperature. A CL curve was acquired as photon counts integrated over a period of 1 s by a photomultiplier. The measurements were performed at different temperatures (120–200 °C) under dry air flow of 100 mL/min or at 200 °C under nitrogen flow of 100 mL/min. The background intensity was obtained through a measurement with a blank aluminum pan at the corresponding temperatures. CL spectra were also acquired, in which the total emission was divided into every 20 nm between 320 and 700 nm with the aid of 20 high-pass filters. The high-throughput chemiluminescence imaging (HTP-CLI) instrument was illustrated elsewhere. A multi-cell with 10 × 10 columnar wells was placed in a constant-temperature oven which equipped cartridge heaters and a circulating fan. An Antor iXon EMCCD camera (ANDOR) was loaded at the top of the system. Dry air was supplied at a controlled flow volume to the gas inlets of the multi-cell after heated to a target temperature using

an external heater. The distributed air flow is for ejecting volatile degradation products and thus prohibiting the infectious spreading. The temperature of the degradation was set to 200 °C and the flow volume was 8.0 L/min. CL profiles were acquired by continuously capturing images with an exposure time of 600 s. These continuous images were analyzed by ImageJ software, where CL intensity for each well was tracked along the series of images. Finally, CL curves for 10 × 10 samples were simultaneously acquired and used to evaluate the stability of recombinant spider silk. DSC measurements were conducted on a Mettler Toledo DSC 822 analyzer. The temperature was increased from 40 to 300 °C at a rate of 5 °C/min under dry air flow of 75 mL/min. The oxidation induction temperature was determined as the onset temperature of the oxidative reaction, which was indicated by an abrupt exothermic signal from the specimen. The microplate spectrophotometer Epoch 2 (manufactured by BioTek) was used for photo degradation screening in the wavelength range of 200–800 nm.

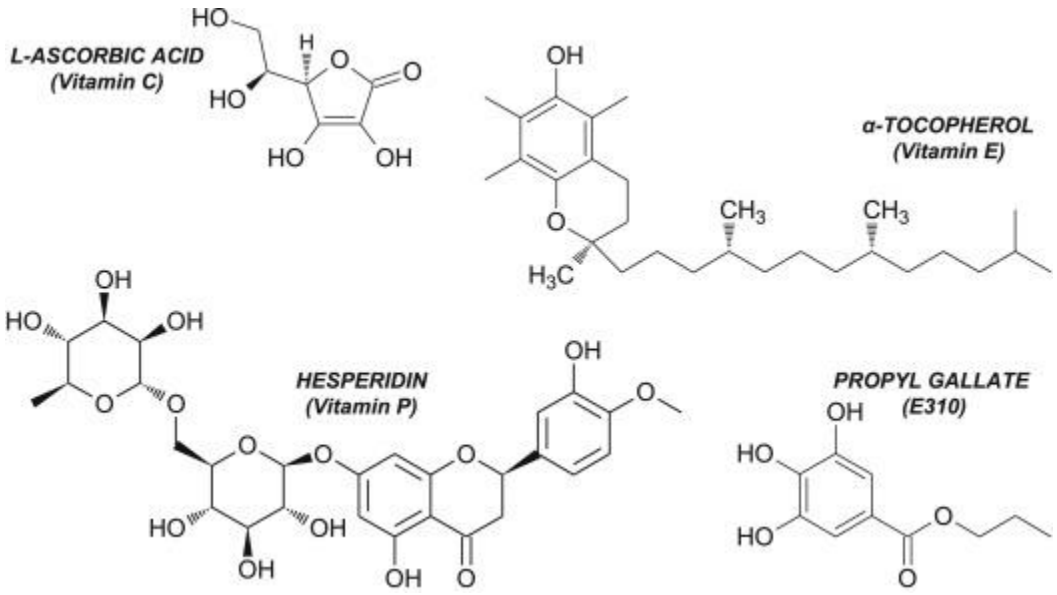

Figure 3.1. Structures of the antioxidants used in this work (nature-derived).

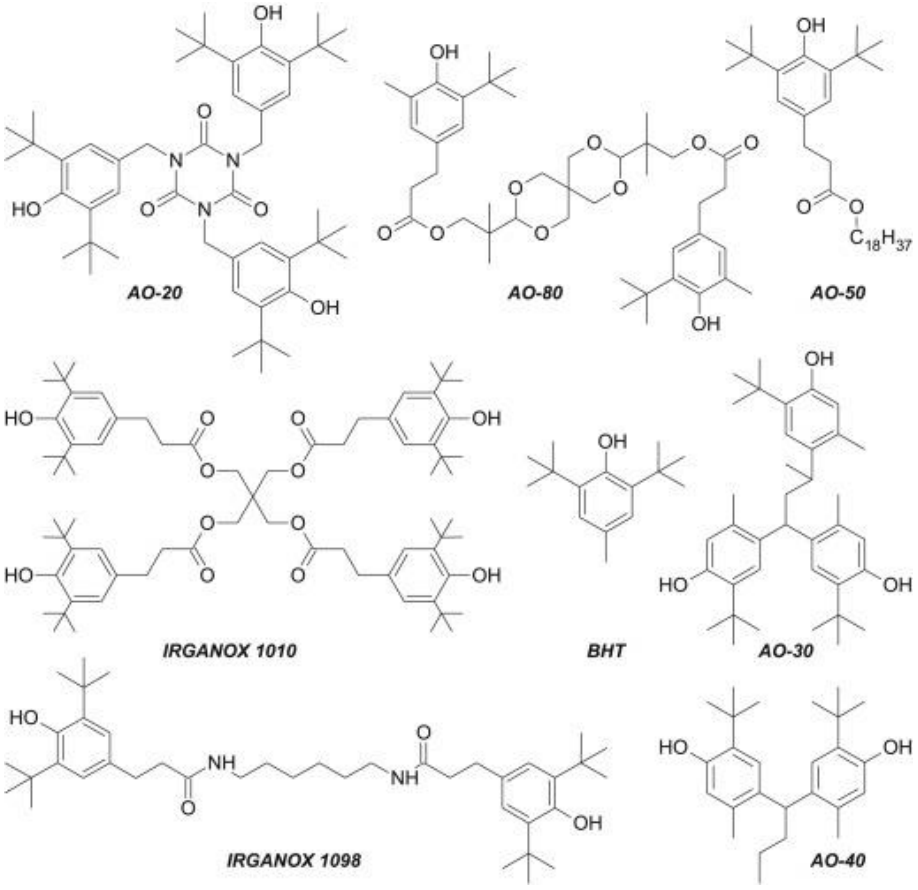

Figure 3.2. Structures of the antioxidants used in this work (hindered phenols).

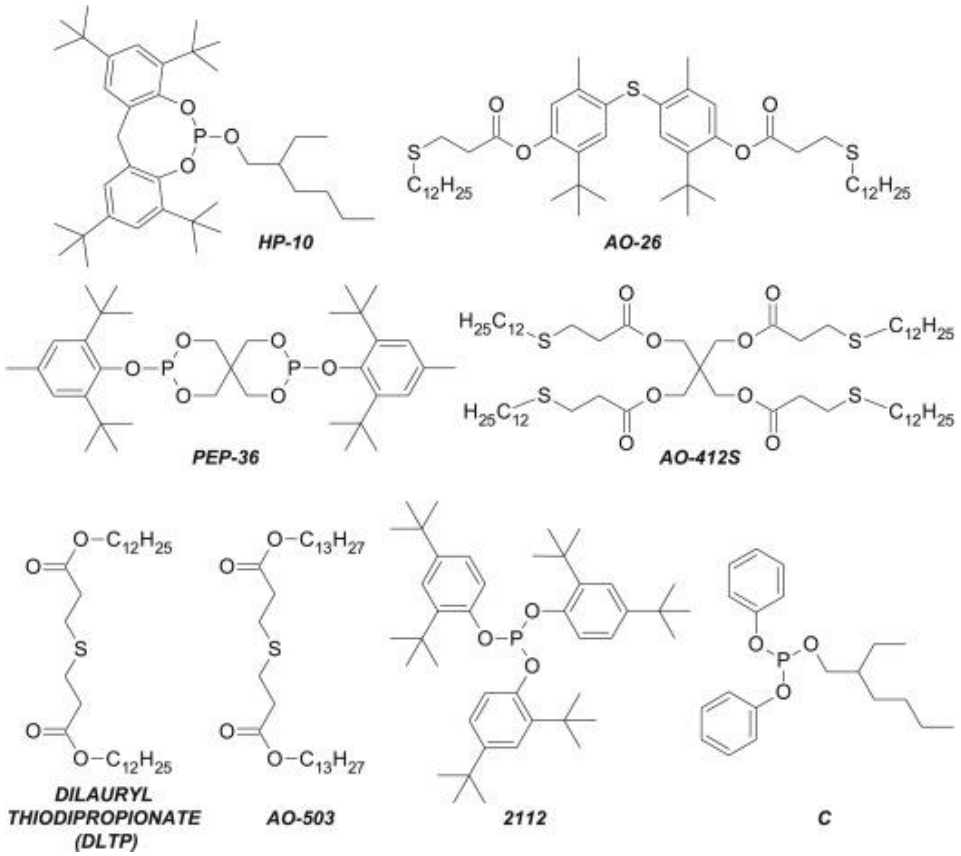

Figure 3.3. Structures of the antioxidants used in this work (thioethers and phosphites).

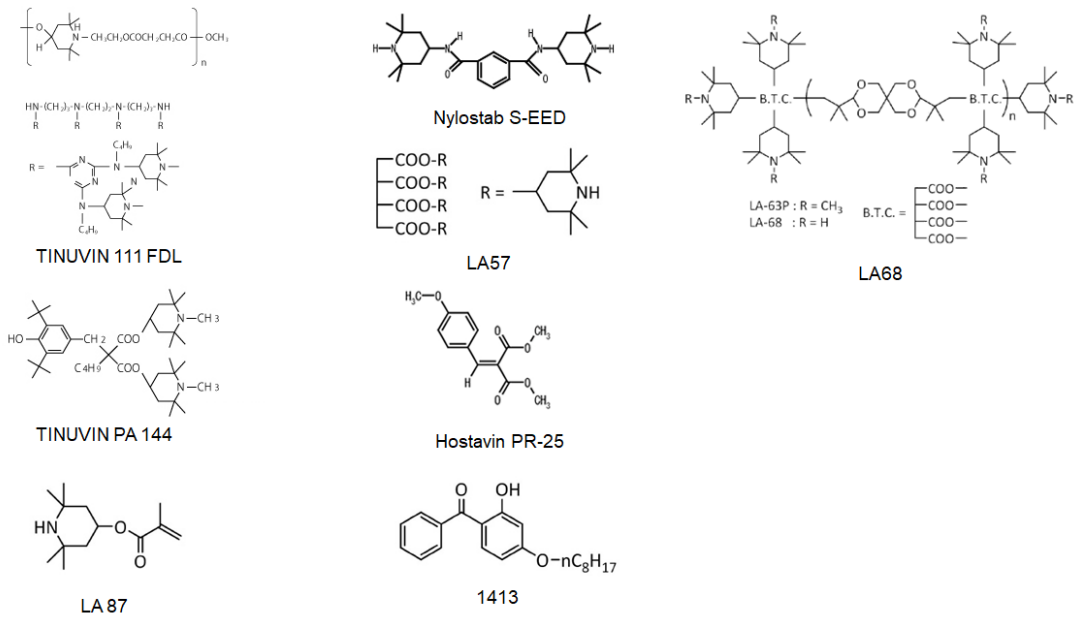

Figure 3.4. Structure of the photo stabilizer used in this work.

3.3 Results and Discussion

Stabilization of Thermo Oxidative Degradation

The CL method is known to be one of the most effective and sensitive detection methods for polymer oxidative degradation. In this sense, HTP-CLI that can screen 100 samples in a single measurement is the very powerful measurement in **Figure 3.5**.

It is expected to further shorten the experiment time with reliable results, in this case, the emissions from 100 samples of powder were clearly observed. The evolution of CL along with aging time has been converted into CL curves for each cell. As illustrated

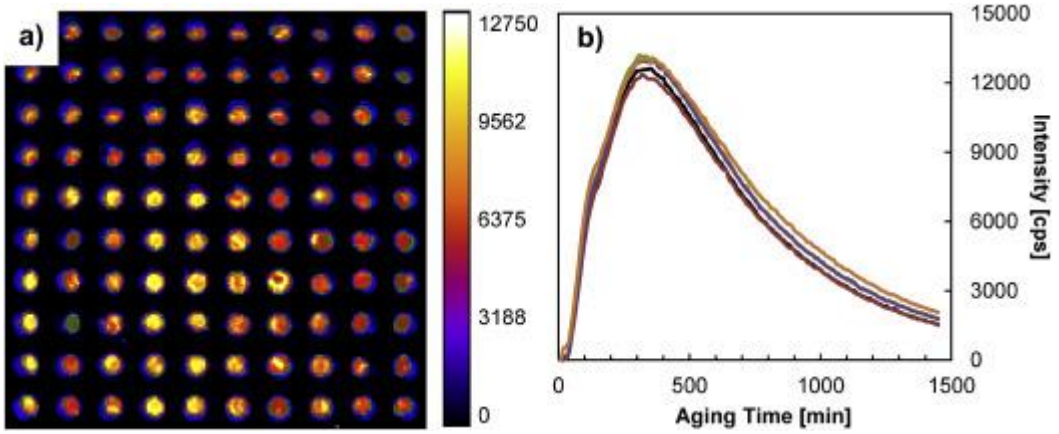

Figure 3.5. (a) A snapshot from a HTP-CLI measurement of unstabilized and stabilized recombinant spider silk powder (N = 10), and (b) CL curves of unstabilized recombinant spider silk obtained from various positions of the multi-cell. Powder samples were degraded at 200 °C under dry air flow. The snapshot corresponds to the image at 200 min. The CL curves confirmed highly reproducible results, where the maximum CL intensity was reached after *ca.* 365 min.

in the **Figure. 3.5b**, unstabilized recombinant spider silk powder showed a highly reproducible profile, reaching maximum strength after aging 365 minutes at 200 °C under dry air flow.

As mentioned above, the CL behavior of recombinant spider silk under oxidative degradation was found to be very similar to that of polyamide (e.g. nylon 6). Simply put, the CL profile of spider silk or nylon 6 shows no oxidation induction time. For oxidative

degradation of polyolefins such as polypropylene, the oxidation induction time or OIT in CL measurements is usually calculated as the start time of the oxidation reaction under isothermal conditions where a dramatic improvement in CL strength begins. When effective antioxidants are added, the release of CL is delayed and weakens due to slower oxidation, resulting in longer OIT (**Figure 3.6a**).

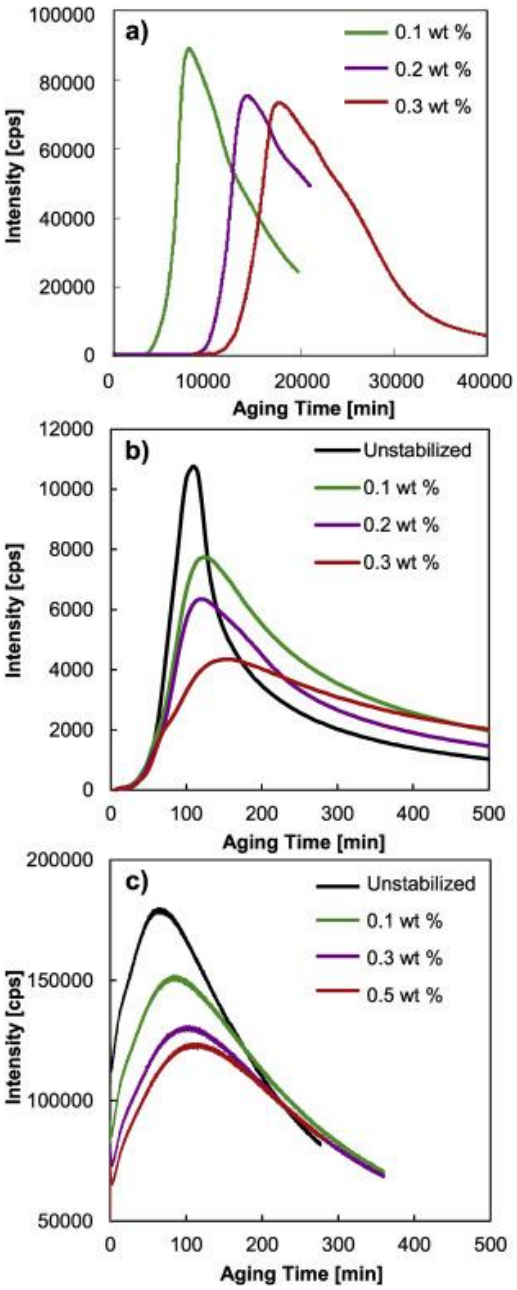

Figure 3.6. CL responses to the stabilization of different materials: (a) polypropylene stabilized by Irganox 1010 (130 °C), (b) nylon 6 stabilized by Irganox 1098 (200 °C) and (c) recombinant spider silk stabilized by E310 (200 °C).

In the case of nylon 6, CL release begins immediately without induction time and is followed by a maximum and subsequent decay (**Figure 3.6b**). Decreasing the decomposition temperature or adding antioxidants slows down the oxidation, which increases the time to reach maximum strength and reduces overall strength. The time scale of oxidation of polymers without induction time, such as nylon 6, can be expressed in terms of time of maximum strength (t_{Imax}). Therefore, it is expected that the effectiveness of antioxidants can be judged based on the extension of t_{Imax} value of recombinant spider silk. In fact, when stabilized with E310, the CL strength of the recombinant spider silk decreased and slowed down (**Figure 3.6c**, Imax value is also possible, so tImax is used rather than CL strength (Imax) to screen the stabilizing effect. It is less reliable) due to light absorption by colored by-products, which may vary with antioxidants.

From HTP-CLI measurements of recombinant spider silk powder with and without antioxidants, CL curves were generated and t_{Imax} values were calculated (**Figure 3.7**). In this case, the recombinant spider silk powder impregnated with nine antioxidants was subjected to oxidative degradation at 200 °C, as was the unstabilized powder. Each sample was inserted into 10 different positions (N = 10) so that the final CL profile was an average of 10 profiles. The results show that E310 effectively slowed down tImax of the recombinant spider silk powder. Specifically, tImax values were extended by 35 and 91 minutes when 0.1 and 0.3 wt% E310 were incorporated into recombinant spider silk, respectively.

Similarly, 20 antioxidants were added individually to the recombinant spider silk powder, and their stabilizing effects were screened by HTP-CLI measurements. The results are summarized in **Figure 3.7**, where effectiveness is quantified based on the elongation of t_{Imax} compared to that of unstabilized recombinant spider silk powder. In

the case of vitamin C, the t_{Imax} value decreased significantly, but in fact, it is known that proteolysis is accelerated at low pH by acidic hydrolysis. When it was impregnated with hydrochloric acid (HCl), it was significantly reduced. On the other hand, other antioxidants are well known to be very effective against other polymers, including nylon 6 (such as Irganox 1098), but do they have any impact on the life of recombinant spider silks showed very little impact. Molecules that penetrate protein aggregates at specific depths, and thus a negligible effect on the stabilizing function of antioxidant molecules, when the solvent for impregnation is changed to ethanol, dichloromethane, residues, etc.

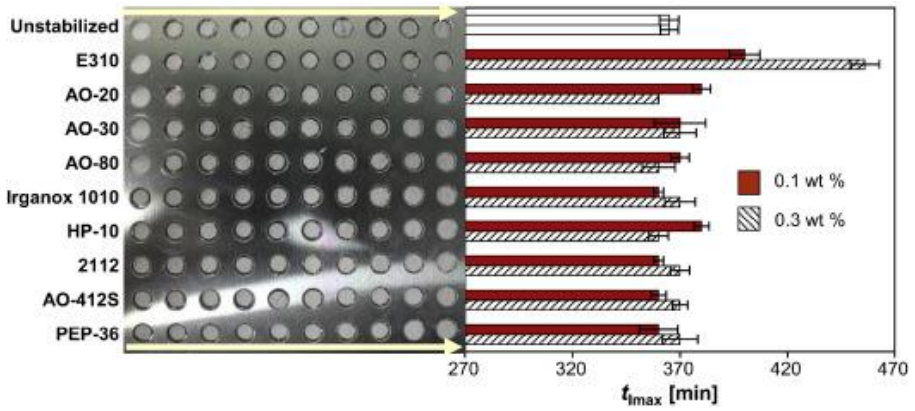

Figure 3.7. (Left) Sample preparation on a multi-cell plate and (right) the time of the maximum CL intensity (t_{Imax}) obtained from HTP-CLI measurements at 200 °C. Recombinant spider silk powder was impregnated with an antioxidant of 0.1 or 0.3 wt %.

The invasion mainly depended on molecules. These results strongly indicate that recombinant spider silk is effectively stabilized by phenolic antioxidants, and more importantly by small molecules. It is worth noting that these antioxidants can further increase the stability of recombinant spider silk by increasing their content. This fact has proven the significance of HTP-CLI in dramatically accelerating a screening study for antioxidants.

Stabilization of recombinant spider silk powder by addition of E310 and BHT was verified by other methods: oxidation induction temperature in DSC measurement and evolution of IR spectrum during oven aging. DSC is an antioxidant for polymers. An alternative option for assessing the effectiveness of the heat flow is recorded along with a constant temperature rise, and a sharp increase in the exothermic heat flow gradient at the oxidation induction temperature corresponds to the onset of oxidation.

Table 3.1 summarizes the oxidation induction temperatures of stabilized and stabilized recombinant spider silks. It was found that the addition of 0.3% by weight of antioxidant improves the oxidation induction temperature by 6 °C for E310 and 5 °C for BHT. Although the exponential dependence of the oxidation rate on temperature resulted in a slight difference in temperature compared to the temperature of t_{Imax}, stabilization was confirmed reliably.

Table 3.1. Oxidation induction temperature for unstabilized and stabilized recombinant spider silk powder.

	Oxidation induction temperature in DSC [°C]	t_{Imax} in CL [min]
Unstabilized	225	365
Stabilized with E310 (0.3 wt %)	225	456
Stabilized with BHT (0.3 wt %)	225	450

Stabilization of Photodegradation

Control and stabilized recombinant spider silk film were exposed to accelerated photo-ageing treatments when increasing the time up to 408 h, in this time, the changes induced by the irradiation were periodically checked using UV-vis. The UV-vis spectra of control (non-irradiated) and irradiated recombinant spider silk standards are displayed in **Figure 3.8** between 0-36 hours. It is important to point out that in order to compensate for small differences in film thickness from sample to sample each spectrum was normalized by the band intensity at 400 nm, taking account of the effects with degradation. Also, considering error, the sample was prepared for eight per experiment.

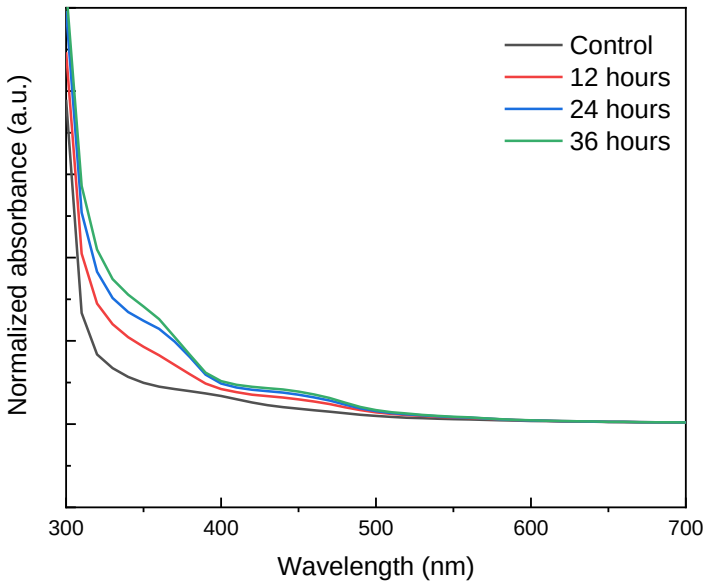

Figure 3.8. UV-spectra of recombinant spider silk standards irradiated at the indicated time interval.

We have observed that the absorbance at 450 nm was growing along irradiation time. The main chromophores absorbances in the UV region are probably the aromatic amino acids tyrosine and this absorption feature can be assigned to a dityrosine in the

photodegradation products. Tyrosine efficiently absorbs for photoconversion and ensuing chemical degradation to dityrosine which is the factor of yellowing. The characteristic absorption at 380 nm was also observed. However, the UV absorber as a photo degradation stabilizer has the absorbance, overlapping at around the region (**Figure 3.9**)

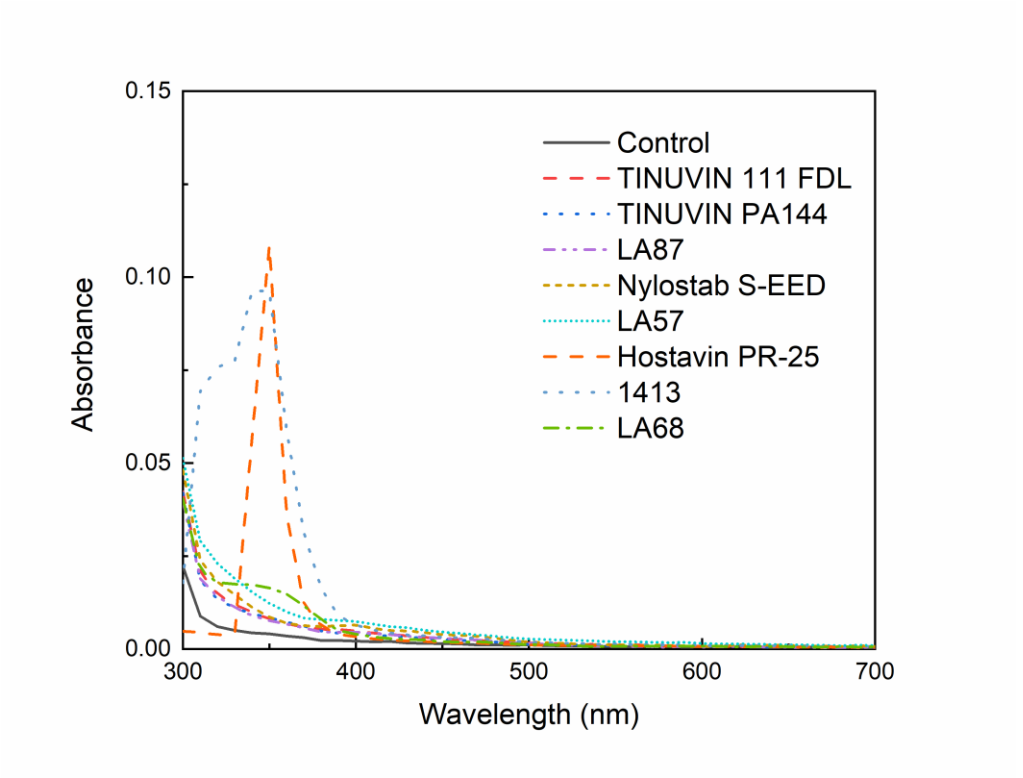

Figure 3.9. UV-spectra of recombinant spider silk standards and its stabilized films.

and we discuss the effect of stabilization using UV-vis at 450 nm below.

Figure 3.10 shows the normalized absorbance based on UV-vis spectra after irradiating for 408 hours. Most stabilizers testing in this time effectively worked on recombinant spider silk as you see under the reference line. The film containing of LA87 stabilizer shows the highest decrease by 63% comparing to the control film. On the contrary, the LA 24 shows the highest increase in absorbance, indicating to the efficiently absorbed UV light due to the change from its initial color. The Nylostab S-EED is

suggested to be immiscible. The hindered amine stabilizers (HALS), widely used for polyolefin stabilization, are based on the inherently basic structure of sterically hindered piperidine. Their basicity decreases with substitution on the piperidine nitrogen in series: >N–H, >N–R, >N–OR.

Therefore, the interaction between recombinant spider silk and nitrogen was satisfied. In addition, when pH of the system is low, the interaction is suggested to much stronger.

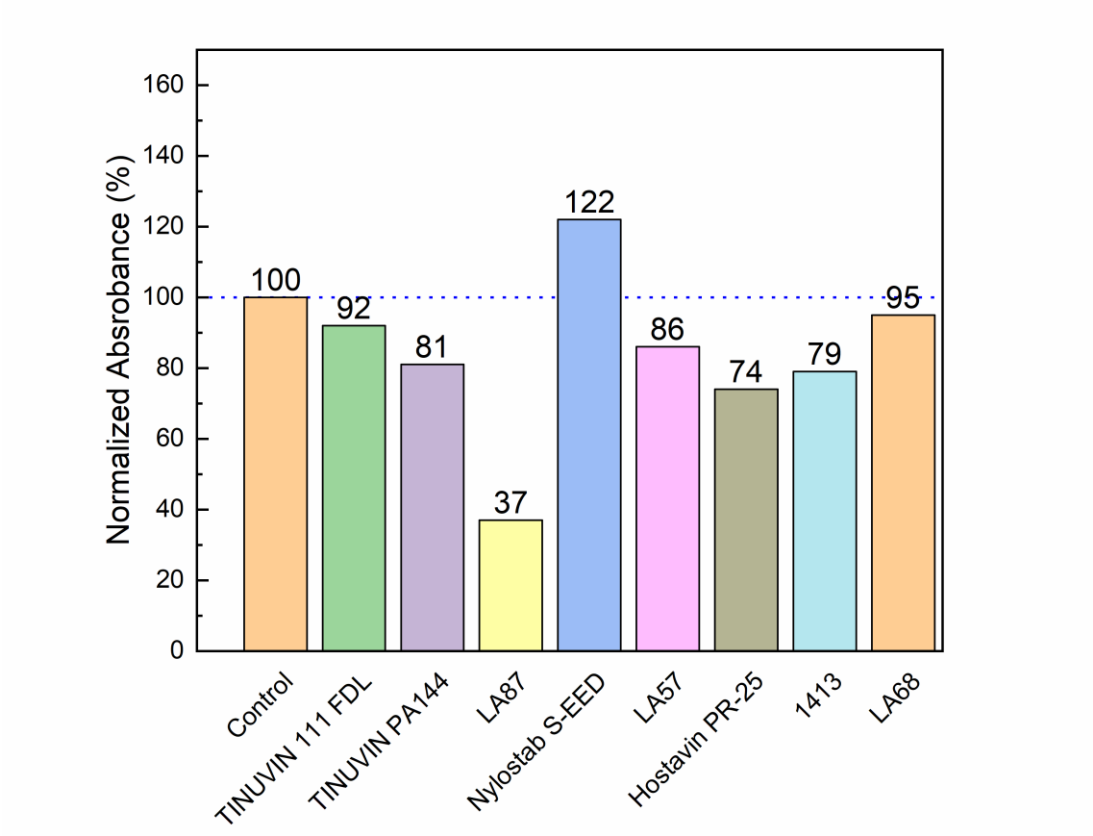

Figure 3.10. Degree of stabilization based on UV-spectra of stabilized recombinant spider silk films with reference line at normalized absorbance of control at 408 hours.

3.4 Conclusions

I have firstly implemented a high-throughput screening of antioxidants in stabilizing recombinant spider silk against thermo-oxidative degradation. The usage of high-throughput chemiluminescence imaging has allowed us to screen various types of antioxidants in a quick and reliable manner. In the powder impregnation process, the penetration of antioxidant molecules into recombinant spider silk is essential, and two substances, E310 and BHT, are found to be effective. The accelerated aging study has proven that these antioxidants suppress the thermo-oxidation of recombinant spider silk through scavenging the formed radical species and slowing down the formation of carbonyl groups as oxidation products.

Screening system of photo degradation on recombinant spider silk film was efficiently worked. Most of stabilizer stabilized recombinant spider silk against UV irradiation. Specific, LA 87 give enormous stabilization to recombinant spider silk films.

References

[1] M.C. Celina, Review of polymer oxidation and its relationship with materials performance and lifetime prediction, in: Polym. Degrad. Stab., 2013: pp. 2419–2429.

[2] A.A. Shah, F. Hasan, A. Hameed, S. Ahmed, Biological degradation of plastics: A comprehensive review, Biotechnol. Adv. 26 (2008) 246–265.

[3] Q. Lu, B. Zhang, M. Li, B. Zuo, D.L. Kaplan, Y. Huang, H. Zhu, Degradation Mechanism and Control of Silk Fibroin, Biomacromolecules. 12 (2011) 1080–1086.

[4] A.Y. Snegirev, V.A. Talalov, V. V. Stepanov, O.P. Korobeinichev, I.E. Gerasimov, A.G. Shmakov, Autocatalysis in thermal decomposition of polymers, Polym. Degrad. Stab. 137 (2017) 151–161.

[5] G. Scott, Developments in the photo-oxidation and photo-stabilisation of polymers, Polym. Degrad. Stab. 10 (1985) 97–125.

[6] E. Richaud, O. Okamba Diogo, B. Fayolle, J. Verdu, J. Guilment, F. Fernagut, Review: Auto-oxidation of aliphatic polyamides, Polym. Degrad. Stab. 98 (2013) 1929–1939.

[7] A. Gregorová, Z. Cibulková, B. Košíková, P. Šimon, Stabilization effect of lignin in polypropylene and recycled polypropylene, Polym. Degrad. Stab. 89 (2005) 553–558.

[8] C. Latocha, M. Uhniat, The kinetics of oxidative induction of LDPE stabilized with commercial antioxidants, Polym. Degrad. Stab. 35 (1992) 17–22.

[9] F. Gugumus, Advances in the stabilization of polyolefins, Polym.

Degrad. Stab. 24 (1989) 289–301.

[10] L. Matisová-Rychlá, J. Rychlý, Thermal oxidation of nonstabilized and stabilized polymers and chemiluminescence, J. Polym. Sci. Part A Polym. Chem. 42 (2004) 648–660.

[11] M. Celina, J.M. Skutnik Elliott, S.T. Winters, R.A. Assink, L.M. Minier, Correlation of antioxidant depletion and mechanical performance during thermal degradation of an HTPB elastomer, Polym. Degrad. Stab. 91 (2006) 1870–1879.

[12] N.C. Billingham, P.D. Calvert, I.W. Okopi, A. Uzuner, The solubility of stabilizing additives in polypropylene, Polym. Degrad. Stab. 31 (1991) 23–36.

[13] D.R. Kohler, C. Kröhnke, Chemiluminescence as an industrial test method for antioxidant effectiveness in polyolefins: II. Versatile application aspects, Polym. Degrad. Stab. 63 (1999) 165–173.

[14] N. Aratani, I. Katada, K. Nakayama, M. Terano, T. Taniike, Development of high-throughput chemiluminescence imaging instrument for parallel evaluation of polymer lifetime, Polym. Degrad. Stab. 121 (2015) 340–347.

[15] V. Vassileva, S. Baltova, S. Handjieva, Photochemical behaviour of natural silk - III. Photofading of silk dyed with acid azo dyes, Polym. Degrad. Stab. 61 (1998) 367–373.

[16] S. Baltova, V. Vassileva, Photochemical behaviour of natural silk - II. Mechanism of fibroin photodestruction, Polym. Degrad. Stab. 60 (1998) 61–65.

[17] S. Baltova, V. Vassileva, E. Valtcheva, Photochemical behaviour of natural silk - I. Kinetic investigation of photoyellowing, Polym. Degrad. Stab. 60 (1998) 53–60.

[18] T. Luo, L. Yang, J. Wu, Z. Zheng, G. Li, X. Wang, D.L. Kaplan, Stabilization of Natural Antioxidants by Silk Biomaterials, ACS Appl. Mater. Interfaces. 8 (2016) 13573–13582.

Chapter 4

Development of Recombinant Spider Silk/Clay Nanocomposites

Abstract

In this chapter, I reported that the development of novel biomaterial recombinant spider silk-clay nanocomposites. Compounding of recombinant spider silk with nano clay through a solution casting method was found to be appealing. The elastic modulus of the nanocomposites was found to increase with increasing the content of clay.

4.1 Introduction

Nature has many materials, which possess sophisticated structures and properties, and provides a sort of inspiration to material scientists. For instance, wood, bone, nacre, and silk represent attractive strength, toughness, and biocompatibility. Especially, a spider silk dragline—possesses its remarkable mechanical properties [1,2] (Surprisingly, the combination with strength and ductility [3])—has long been targeted for obtaining a mass product in biomimetics. But it was difficult because the spider is a territorial and carnivorous animal. Quite recently, mass production of recombinant spider silk has been realized mass product as an industrial material using a heterologous host such as *Escherichia coli* and transgenic silkworms (*Bombyx mori*) [4].

The recombinant protein can be modified and optimized in the amino acid sequences and recombinant spider silk is a tailor-made polymeric material possessing advantages that synthetic polymers do not have. One important shortfall for limiting the use of recombinant spider silk is its unsatisfactory resistance to humidity due to the existence of hydrophilic peptide bonds or functional groups [5–7]. The water sensitivity ins represented by supercontraction effect, which makes spider silk fiber shortened when the spider silk is submerged into water or exposure to high humidity. During supercontraction, water is considered to plasticize silk fibers by breaking hydrogen bonds between proteins, thereby allowing re-orientation of silk molecules to lower energy levels. Recent studies have focused on the importance of disrupting secondary structure in the glycine-rich blocks for mobilization of proteins within the amorphous network [8]. This allows the random-coil regions to move rapidly to more disordered, higher entropy configurations, driving the contraction of the silk. Eles et al. suggested that a molecular mechanism for silk's mechanical properties based on entropic springs that were drawn in

preformed extended structures, stabilized by interchain hydrogen bonding, and collapsed by hydration [9,10]. Plaza et al. quantified supercontraction stress to be ~ 60 MPa by raising the humidity up to 100% under constant length [6]. They then observed that humidity can be linked to the glass transition in silk. Considering the usage of recombinant spider silk, to overcome this disadvantage may open the gateway to producing multifunctional silk materials.

It has been suggested that the inherent shortcoming of spider silk could be overcome by nanocomposites. Nanocomposite materials introduce improvement in the barrier [11,12], mechanical properties [13,14] and heat resistance [15,16] compared to the pristine polymer and conventional composite materials. The most extensively studied polymer nanocomposites are based on nano clay as a reinforcing phase due to their mass availability, potential functionality (high aspect ratio and surface area) and low cost. Although nano clay composites with petroleum-based polymers have also been developed, I focus on nano clay composites with biopolymers because of their attractiveness from a sustainability perspective and potentially mass applications. One of the obstacles in obtaining an excellent clay nanocomposite is the dispersion of the clay sheets in polymer matrix. Proteins are natural copolymers containing both hydrophobic and hydrophilic domains, which could interact with clay surfaces. In addition, interaction between clay and protein is the key to understand and design the particular properties of bionanocomposites. For improving humidity resistance, crystallization, confinement, and barrier effects by plates impermeable are expected positive.

In this work, I reported that the development of novel biomaterial recombinant spider silk-clay nanocomposites.

4.2 Experimental

Materials

A recombinant spider silk was synthesized and provided in an unprocessed powder form by Spiber Inc. The amino acid sequence of the recombinant spider silk mimicked that of *Araneus diadematus*, consisting of Alanine (19.5%), Asparagine (0.5%), Glutamine (17.1%), Glycine (30.9%), Histidine (1.0%), Methionine (0.2%), Proline (14.1%), Serine (9.7%), and Tyrosine (7.0%) at amino acid purity of 95–100%. The particle size of the powder measured by light scattering (Partica LA-950V2, Horiba) was 15.7 μm in the median diameter. The powder was stored in a refrigerator at 4 °C. Dimethyl sulfoxide (DMSO) was purchased from Kanto Chemical Co., Inc. Clays were provided from KUNIMINE INDUSTRIES CO., LTD. Kunipia-F™ is a pristine montmorillonite (MMT), Sumecton SAN™ is modified with dimethyl distearyl ammonium hectorite, and Sumecton SEN™ is modified with dipolyoxyethylene coconut alkyl methyl ammonium chloride. They are named as MMT, C_{18}-mMMT, PEG-mMMT in this chapter, respectively. C_{18}-mMMT and PEG-mMMT were derived from Kunipia-F by corresponding organic modification. Since a unit layer is up to 2 μm in length and about 1 nm in thickness, the aspect ratio can be as high as 2000. Nano silica with an average diameter of 7 nm (Aerosil 300), was purchased from Evonik Resource Efficiency GmbH. Graphite powder (particle size > 45 μm, purity > 98%) was supplied by Wako Pure Chemical Industries, Ltd. Graphene oxide (GO) was prepared based on a modified Hummer's method. The dispersibility of these fillers in DMSO used as a solvent for recombinant spider silk was examined by a sedimentation test. Classification of the surface state of fillers and their interaction with polymers in advance is important for developing nanocomposite materials. **Figure 4.1** and **Table 4.1** summarizes the

sedimentation test for observing the suspension state in the recombinant spider silk dope solution. The suspension state was classified to transparent, turbid, and sedimentation. 3 wt% filler in dope solution were placed at r. t. overnight. After mechanically stirring dispersion, precipitates were observed at the bottom of test tube except for dope solution with PEG-mMMT or silica.

Table 4.1. Sedimentation test of fillers

Filler	Suspension state
Kunipia F (MMT)	Sedimented
PEG-mMMT	Transparent
C_{18}-mMMT	Turbid
Graphene oxide (GO)	Turbid/partly Sedimented
Silica	Transparent

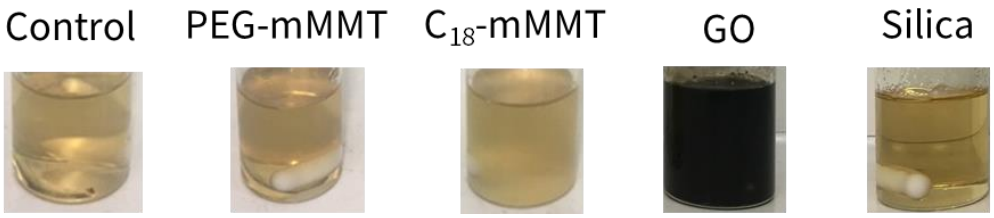

Figure 4.1. Optical image of recombinant spider silk dope solution with different fillers for a sedimentation test.

Film Preparation

Recombinant spider silk films can be obtained by evaporation of solvent at an evaluated temperature. A dope solution of recombinant spider silk was prepared by dissolving 9.5－10.0 wt% into DMSO. Nano filler was added into the dope solution to meet the final concertation of 0.5 and 3.0 wt% recombinant spider silk. After stirring for 6 hours at 80 °C, the dope solution was casted on a PET substrate and held at 70 °C for 12 hours. This provided a film with the thickness of 50 μm. The film was washed three times with water. The obtained film was stored in a constant temperature and humidity oven before a mechanical test.

Fiber Preparation

DMSO/LiCl (96: 4 w / w) was selected as a solvent, and a recombinant spider silk dope solution of a 20 wt% concentration was prepared. The silk powder was completely dissolved and kept stirred at 60 °C overnight. The dope solution was wet-spun using a spinning instrument (**Figure 4.2.**). As a potential coagulant, water, methanol and acetone were tested. As a result, methanol was employed due to the fastest rate of coagulation. The spinning condition was determined at 0.3 MPa of discharging pressure and 4 times of draw ratio using the spinning instrument. The drawing process was conduct in water as well as the fiber was washing during the process (**Figure 4.2.b**). The filler content was valid from 0.5 to 3.0 wt% with respect to the weight of recombinant spider silk in the dope solution.

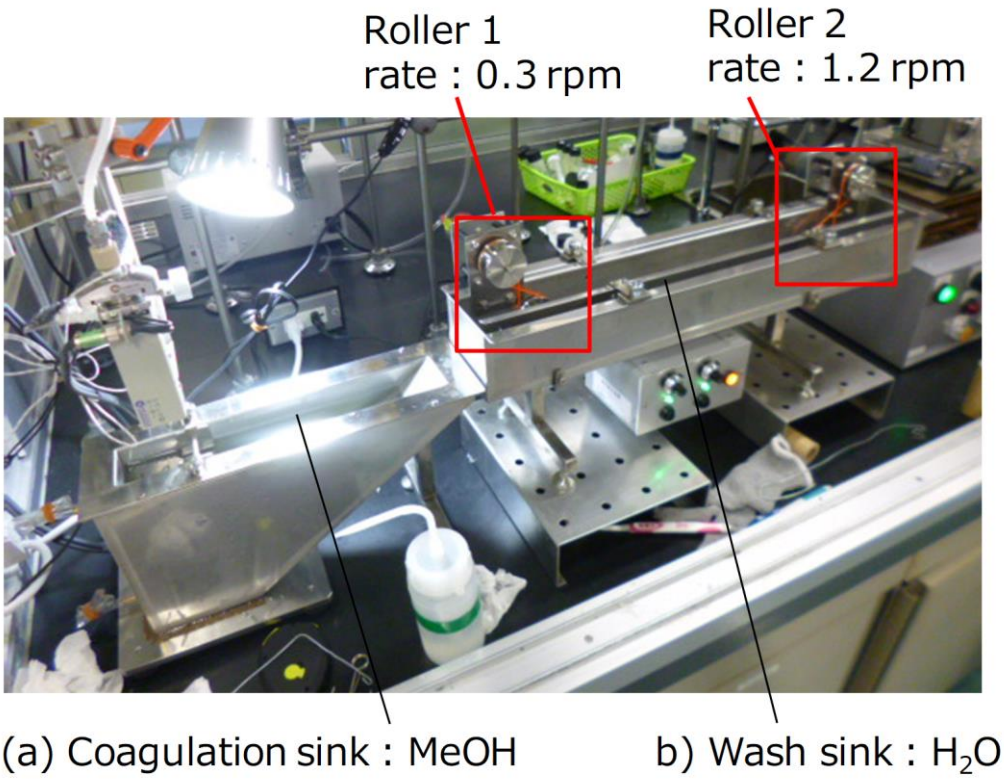

Figure 4.2. The spinning device that we developed. a) was methanol sink for coagulation, b) was water sink for washing and stretching (draw ratio was set to 4 times).

Characterization

The X-ray diffraction (XRD) patterns were collected in a reflection geometry using a Rigaku SmartLab X-ray diffractometer at room temperature with CuKα radiation (wavelength 1.542 Å, 40 kV, 30 mA) at a scan speed of 2000 s per degree over the 2θ range from 5 to 45 degrees. Spider silk powder was filled into a well of the quartz substrate with dimensions of 25 × 15 mm and then was flattened with a glass slide. The dispersion and distribution of filler particles in a matrix was monitored by a transmission electron microscope (TEM, H-7100 Hitachi), operated at an acceleration voltage of 100 kV. A sample thickness was prepared by an ultra-microtome Reichent Ultracut FCS (Reica) equipped with multi knife such as a glass and diamond. To smoothen the cross

section of a film, a film was cut to 1 μm–500 nm with a glass knife which is durability before using a diamond knife. A TEM specimens with thickness of 100 nm were prepared with a diamond knife. A specimen was floated on ethylene glycol and prepared on a copper grid. Dynamic mechanical analysis (DMA) was performed by DMTA Q800 (TA instrument) equipped with a humidity controlling accessory. The resolution of temperature is 1 °C, and that of the relative humidity is 2%. Uniaxial tensile tests were conducted at a force-ramping rate of 0.05 N/min (comparable to a strain rate of 1%/s) at 30 °C and 40 RH% in films or 30 °C and 25 RH% after being equilibrated in the chamber for 1 hour under nitrogen purge. Dynamic mechanical test was performed at 50 MPa static stress, ~0.1% dynamic strain, and 1 Hz frequency. The relative humidity was ramped from 40 to 90 in films or 25 to 90 RH% at the rate of 2%/min, while keeping the temperature at 30 °C. In addition, typical temperature-ramping DMA without the humidity accessory was employed from 50 °C to 250 °C at the ramping rate of 5 °C /min with 50 MPa static stress and 1 Hz frequency. A solid-state ^{13}C NMR spectra (125.8 MHz) were recorded on an AVANCE III 400 FT-NMR spectrometer (Bruker BioSpin). Chemical shifts were referred to glycine. The magic angle spinning (MAS) frequency was fixed at 8 kHz. The contact time for each cross-polarization (CP) experiment was 2 ms, and the acquisition and relaxation times were set to 27 ms and 5 s, respectively. The Fourier transform was performed using TOPSPIN software, version 3.2 (Bruker). Attenuated total reflection (ATR)-Infrared (IR) spectra were collected on a PerkinElmer Spectrum 100 ATR-IR spectrometer (PerkinElmer, Waltham, USA) equipped with a diamond crystal. The spectra were recorded at room temperature with the resolution of 4 cm^{-1} in the range of 4000–400 cm^{-1}.

4.3 Results and Discussion

Recombinant spider silk film nanocomposite

There are three categories of descriptor using XRD to analyze a polymer clay nanocomposite: immiscible, intercalation and exfoliation. Noted that these definitions are based on XRD results and are for ideal cases, assuming that dispersion state falls into only one of three categories. **Figure 4.3.** shows the degree of dispersion of clay in recombinant spider silk nanocomposite film and the selected clays. Here, the content was increased to 10 wt% for clearer observation. The XRD pattern of recombinant spider silk/MMT nanocomposite film shows the interlayer distance is 19.4 Å and a difference of 5.2 Å from the corresponding 14.2 Å for a hydrous MMT framework. Whereas, there is no characteristic peak of (100) on XRD pattern of recombinant spider silk/PEG-mMMT nanocomposite film, suggesting exfoliation of montmorillonite layers in the recombinant

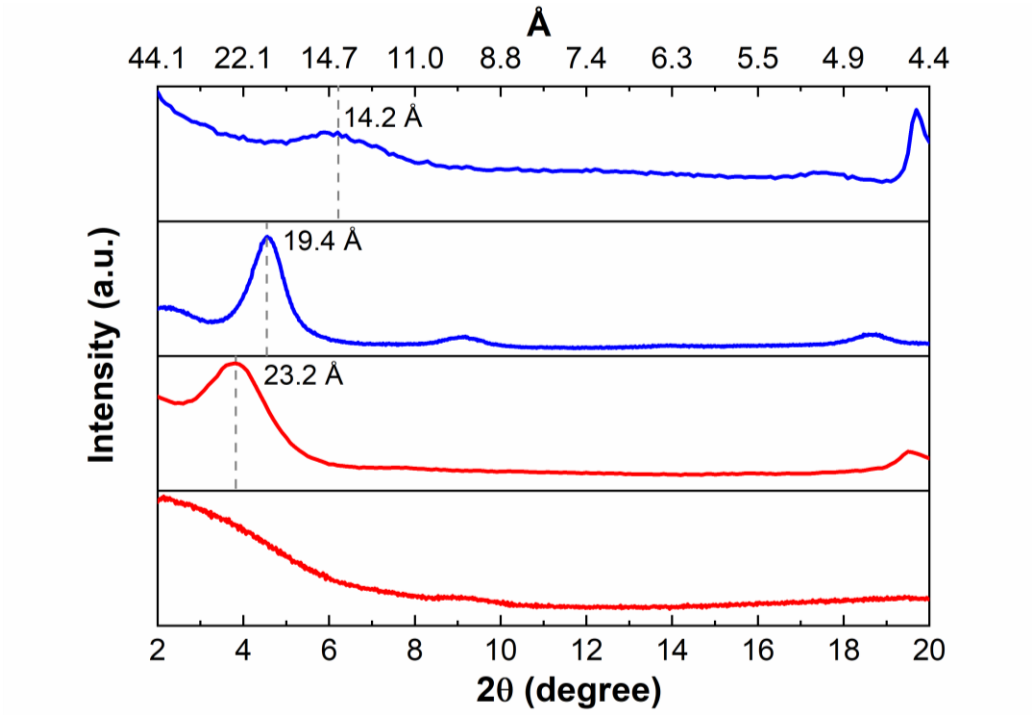

Figure 4. 3. XRD pattern of a) clay and b) recombinant spider silk films containing 10 wt% of clay.

spider silk matrix.

The dispersion of the filler in the recombinant spider silk/ PEG-mMMT nanocomposite film, which were transparent film, is investigated. Transmission electron microscopy (TEM) micrographs of the film are reported in **Figure 4.4**. A closer observation of the micrograph at high magnification reveals that each dark line often corresponds to an exfoliated clay layers. This interesting detail in the nanostructure demonstrates. The average distance between the stacks of layers evaluated from the overall picture is 18 nm. It was supposed that PEG-mMMT as a filler be good dispersion in recombinant spider silk matrix.

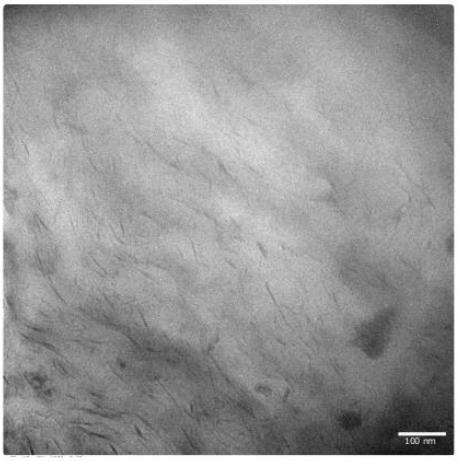

Figure 4.4. TEM images of a 5.0 wt% recombinant spider silk/PEG-mMMT nanocomposite cast film.

The mechanical properties of the recombinant spider silk nanocomposites were studied based on uniaxial tensile test at 30 °C and 40 RH%. The relatively high aspect ratio and high elastic modulus of filler would provide a reinforcing effect on the mechanical properties of recombinant spider silk. The obtained stress–strain (s-s) curves are presented in **Figure 4.5.** The elastic modulus (Young's modulus), tensile strength and elongation at break of the films are summarized in **Table 4.2**. It can be obviously seen from the **Figure** and table that the tensile properties of prepared nanocomposite films

were affected by the addition of different types of filler and their contents. The control film exhibited mechanical properties, i.e., the elastic modulus of 2.2 GPa, tensile strength of 54 MPa, and elongation at break of 4.05%. In case of MMT nanocomposite film, all parameters decreased due to the agglomeration. When the recombinant spider silk nanocomposite films were prepared, the Young's modulus in most of nanocomposite film was increased comparing to the control film. With comparison to organomodifed clay and GO (plate shape filler)/silica (spherical filler), tensile properties of GO and silica nanocomposite film were decreased. This is because the dispersion of fillers in matrix or the adhesion at the filler–matrix interfaces was not sufficient. However, when increasing the content up to 3.0 wt% of the organomodified clay of, in this case are PEG-mMMT and C_{18}-mMMT, the elastic modulus and elongation at break were decreased to 49, 29% and 32, 4%, respectively.

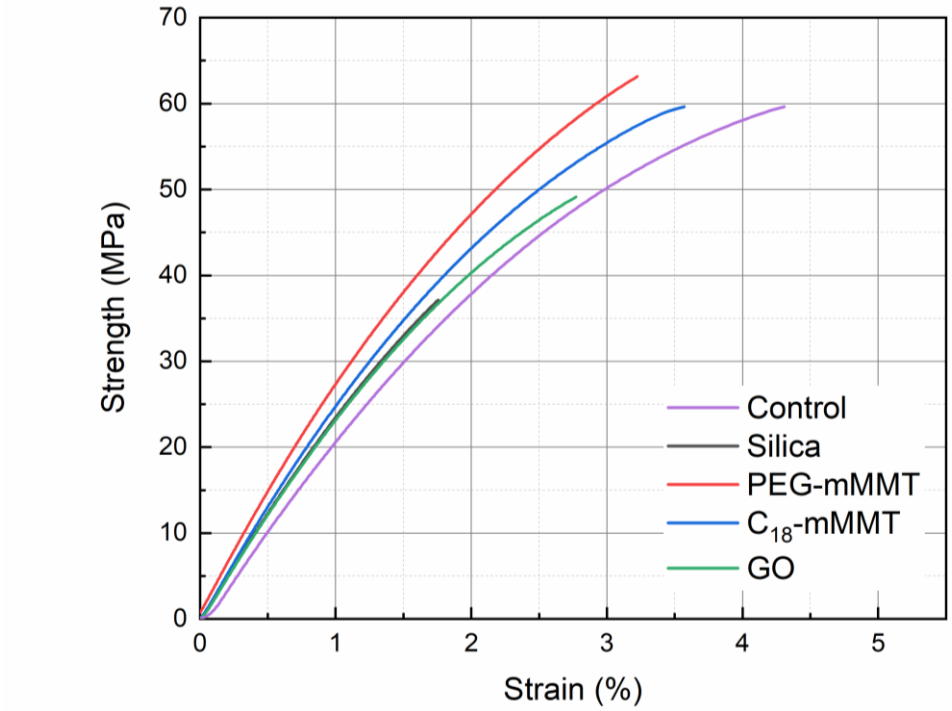

Figure 4.5. Stress-strain curves for recombinant spider silk and its nanocomposite films with 3wt% different fillers. This tests at the rate of 0.05 N/min was conducted at 30 °C and 40 RH%.

Table 4.2. Summary of tensile properties in recombinant spider silk and its nanocomposite films.

Sample	Young's modulus [GPa]	Tensile strength [MPa]	Elongation at break [%]
Control	2.2 ± 0.2	54 ± 7	4.05 ± 0.81
MMT	2.0 ± 0.4	44 ± 14	2.77 ± 0.75
PEG-mMMT	2.9 ± 0.2	55 ± 5	2.75 ± 0.46
C_{18}-mMMT	2.5 ± 0.1	56 ± 4	3.89 ± 0.24
Silica	2.4 ± 0.4	37 ± 7	1.82 ± 0.46
GO	2.4 ± 0.1	40 ± 10	2.14 ± 0.66

A further study was performed by investigating the extent of reinforcement as a function of the filler content for selected fillers. **Figure 4.6.** summarized the tensile mechanical properties of recombinant spider silk nanocomposites. The addition of the organomodified clay to an improvement in the modulus and strength of recombinant spider silk. An improvement of about 23% is observed with an addition of 0.5 wt% of PEG-mMMT, whereas a maximum of 33% improvement is observed with the addition of 3.0 wt% of PEG-mMMT. In the case of C_{18}-mMMT, 29% improvement is observed with an addition of 0.5% and then it continuously decreased to 15% improvement. This deterioration was plausibly attributed to the promotion of aggregation when the loading was increased. When the amount added is taken into account, even the strength is improved. Though the error range was large, the addition of clays tended to slightly deteriorate the elongation at break, the improvement in elastic modulus was likely related to the exfoliation and good dispersion of nono sized clay sheets that restricts the mobility of polymer chains. As well, good interfacial adhesion between the particles and the recombinant spider silk matrix must be important. The average strength of clay nanocomposites increased compared to control recombinant spider silk film. The

compounding of organomodified clay in a recombinant spider silk matrix with a solution casting method produces the higher viscosity. As a result, the mixture becomes highly viscous with time and may hinder the complete degassing before casting. It was interred that under tensile loading, cracks can initiate from these tiny voids and cause specimen failure at relatively low strains.

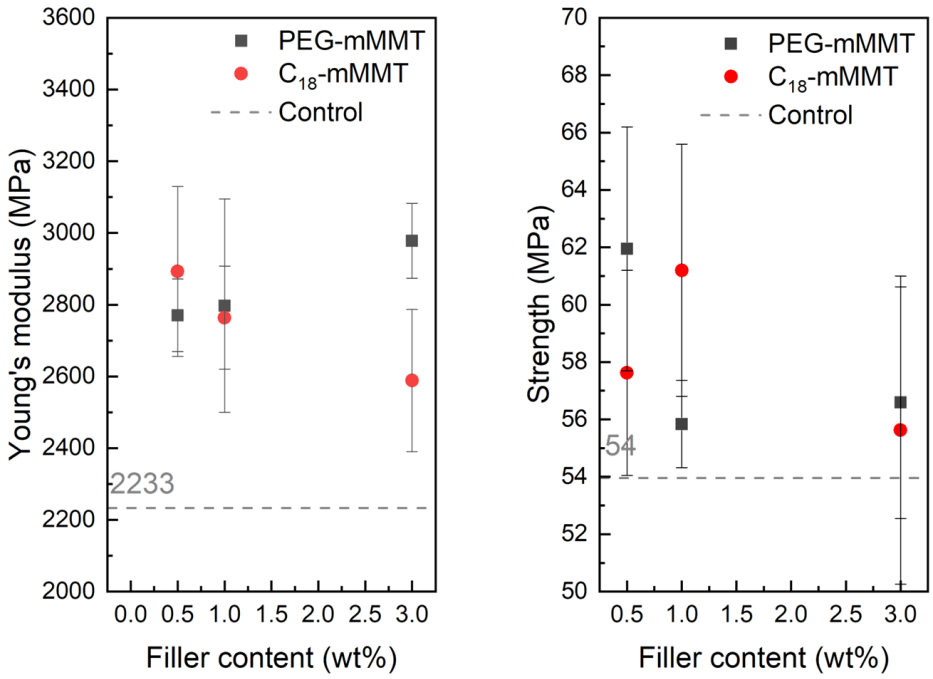

Figure 4.6. Mechanical properties of recombinant spider silk/clay nanocomposite films with different fillers.

Figure 4.7. shows dynamic mechanical properties of recombinant spider silk cast film in response to humidity at the controlled temperature of 40 °C. As the humidity increased, the storage modulus dropped slowly at first and then more rapidly when the humidity went above 75.5%. The loss tangent increased as the modulus decreased, showing a peak at 92 RH %. The glass transition temperature of dried silk proteins is usually observed at about 200 °C, while the glass transition of silk fibroin sensitively depends on the bound water contents. It was reported that the glass transition temperature of silk fibroin is

around 70 °C in DSC when bound water is included. Plaza et al. investigated the glass transition condition for spider silk using a tensile test with an environmental chamber. The reduction of glass transition temperature was shown in the ramping relative humidity. Thus, the DMA data were consistent with these past reports when the humidity was ramped, the glass transition happened even at 40 °C. To qualify the glass transition as critical humidity, I took the onset of the reduction in modulus by extrapolating the linear parts of the modulus-humidity curves below and above the main region of curvature as shown in **Figure 4.7**.

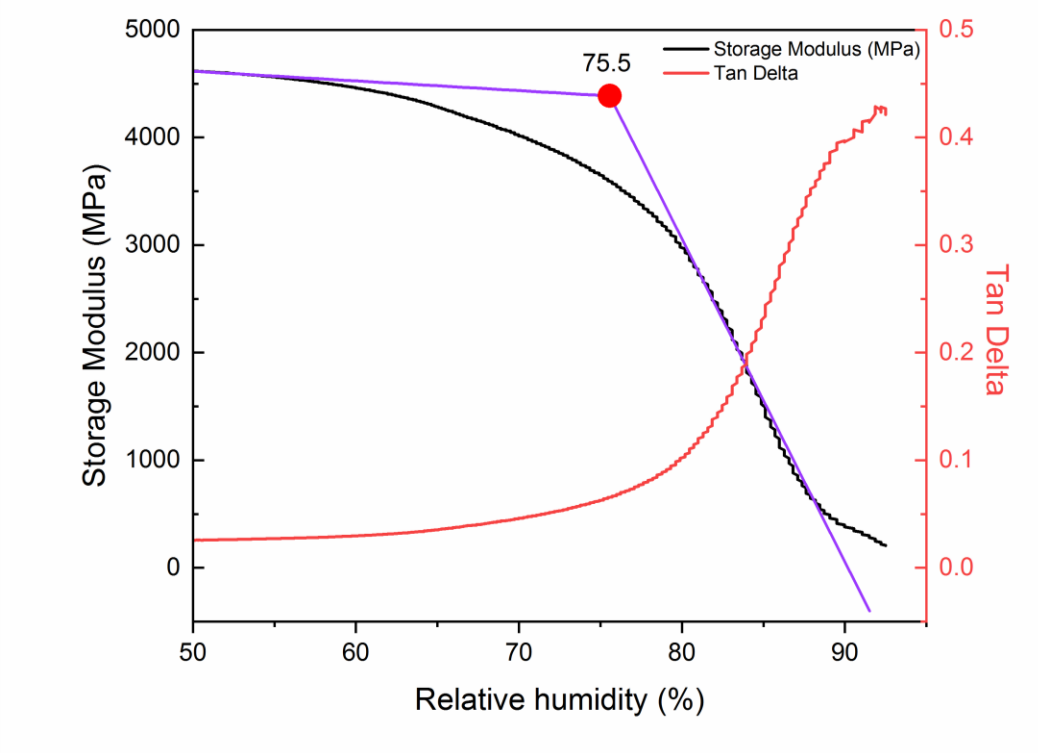

Figure 4.7. Storage modulus and loss tangent as a function of relative humidity at 40 °C and 50 MPa stress.

This is consistent with the approach of Fu in the analogy of heat distortion temperature in storage modulus versus temperature and is correlated with shrinkage measurements. I discuss a resistance of humidity using the intersection of two lines (hereinafter, this is called the distortion humidity). The effects of the clay content on the distortion humidity of recombinant spider silk nanocomposite films are shown in **Figure 4.8**.

The distortion humidity increased rapidly with an increasing clay content from 0 to 1 wt%. The storage modulus of the nanocomposites increased dramatically up to 1wt%, while

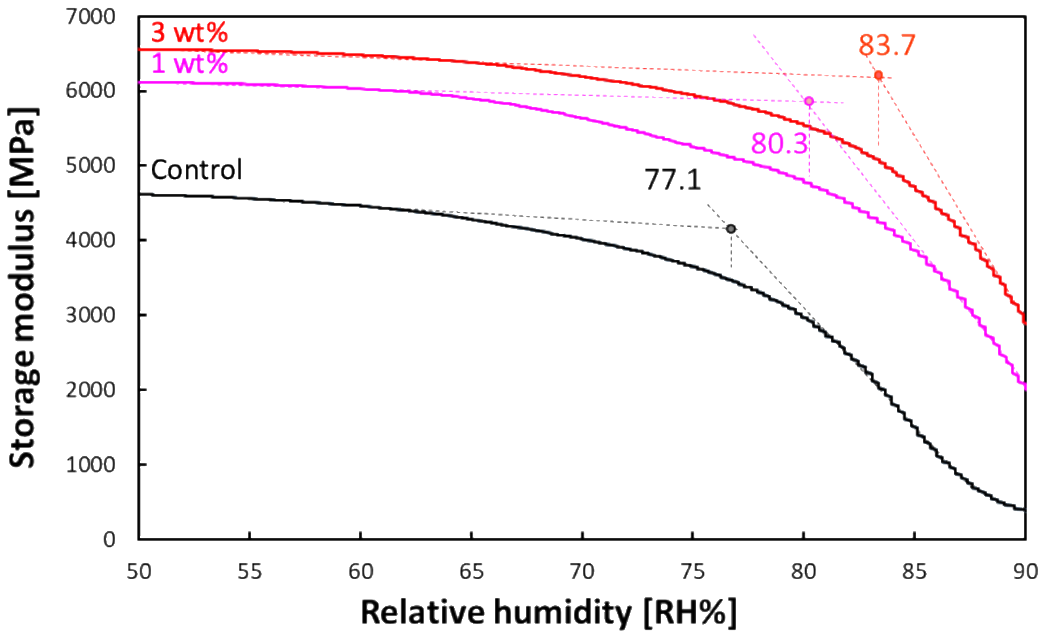

Figure 4.8. Distortion humidity of recombinant spider silk/PEG-mMMT nanocomposites based on DMA results at 40 °C.

the increment became milder beyond 1 wt%. In isothermal DMA with ramping humidity, the clay was clearly effective to improve the humidity resistance on nanocomposites film.

With respect to the improvement of dispersion mechanical properties and humidity resistance, ATR-IR and NMR was employed to detect the interaction between clay and recombinant spider silk. **Figure 4.9.** shows the ATR-IR of recombinant spider silk and its

nanocomposite. In this nanocomposite material, the filler content is set up to 20 wt%. The peak at 1060 cm^{-1} in recombinant spider silk/PEG-mMMT nanocomposites was clearly shifted to a long wave number side. This peak is assigned to Si-O and the shifting peak is based on the increase of the number of the exposed clay surface due to the high dispersibility. Therefore, it is considered that the peak top shifted where it was apparent only in PEG-mMMT with good dispersibility.

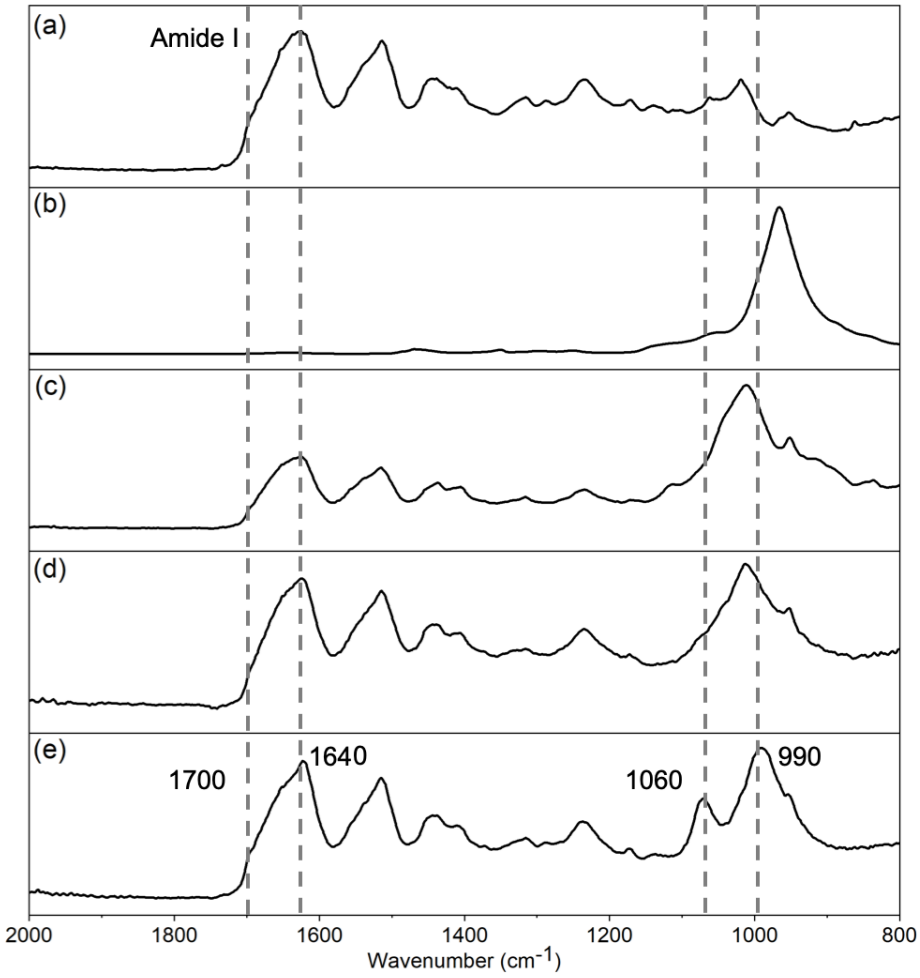

Figure 4.9. ATR-IR of a) recombinant spider silk control film, b) PEG-mMMT powder, c) recombinant spider silk/MMT nanocomposite, d) recombinant spider silk/C_{18}-mMMT nanocomposite, e) recombinant spider silk/PEG-mMMT nanocomposite films between 2000-800 cm^{-1}.

Figure 4.10. shows that the ^{13}C solid-state NMR spectra of recombinant spider silk and its nanocomposites. There is a remarkable change at around 20 ppm assigned to secondary structure of alanine in the spectra between nanocomposites. After the addition of PEG-mMMT, the peak intensity of Ala based on random coil decreased at 17 ppm as well as that of β-sheet at 20 ppm increased and it is indicated that the content of β-sheet increased. To explain why PEG-mMMT has an effect on the secondary structure of recombinant spider silk in its nanocomposite, I ascribe it to the interactions between clay and recombinant spider silk and the existence of clay layers acting as efficient nucleating agent.

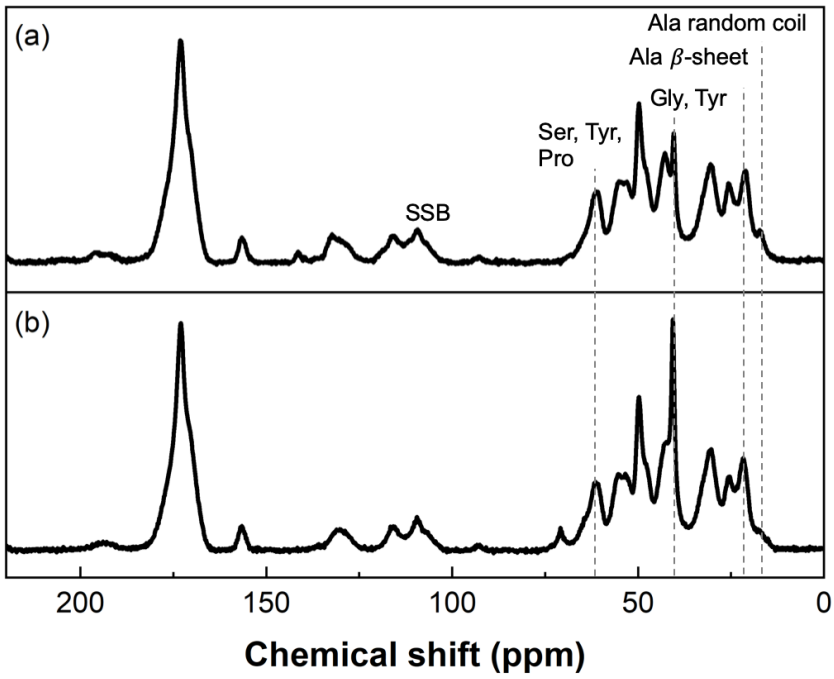

Figure 4.10. ^{13}C solid-state NMR of a) recombinant spider silk and b) its 20 wt% PEG-mMMT nanocomposite, which was produced by reprecipitation.

Recombinant spider silk fiber nanocomposite

Given the results in nanocomposite films, recombinant spider silk nanocomposite fiber was developed with wet spinning at room temperature using the spinning instrument that we developed. The mechanical properties of the recombinant spider silk nanocomposite fiber were studied based on uniaxial tensile test at 30 °C and 25 RH%. The obtained s–s curves are presented in **Figure 4.11**, as adding PEG-mMMT, the tensile strength of the fiber also increased. The 0.5 wt% of nanocomposite fibers showed the maximum increment by 30% and 8% in the Young's modulus and tensile strength, respectively, when compared with that of control fiber. However, the ductility dropped gradually starting from 0.5 wt% and drastically by around 90% for 1.0 wt% nanocomposite fiber, when compared with that of control fiber. The elastic modulus (Young's modulus), tensile strength and elongation at break of the films are summarized in **Table 4.3**. The addition of 3.0 wt% was too fragile to measure tensile test. Maybe because that the agglomeration of filler was occurred in matrix.

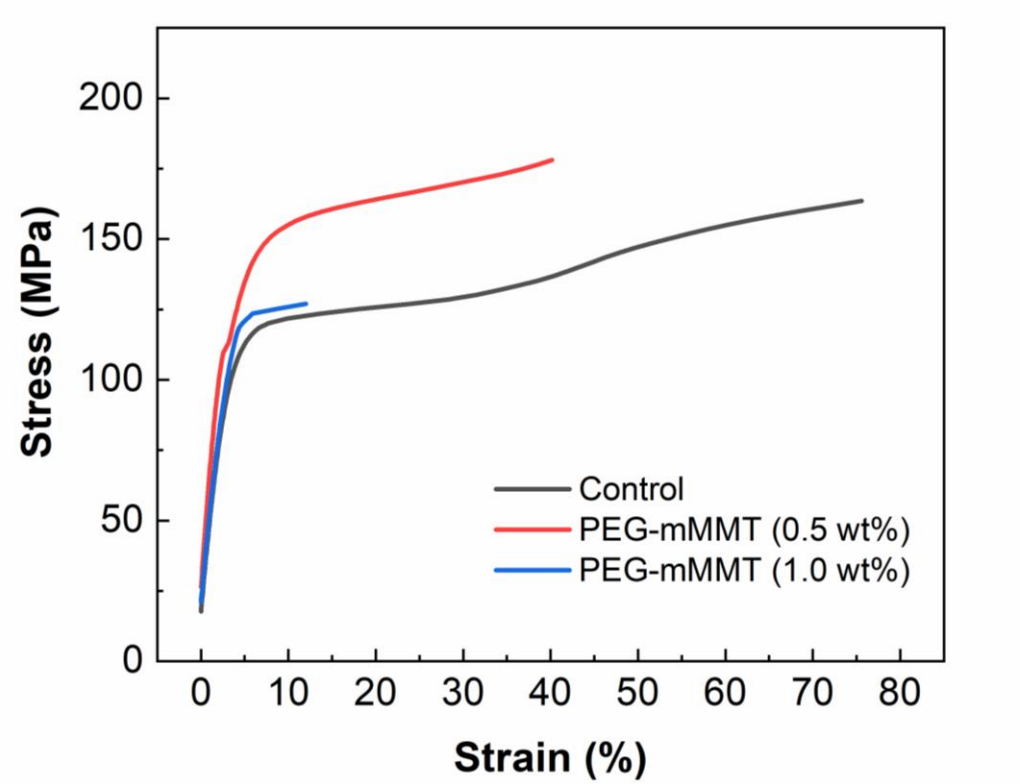

Figure 4.11. S-S curves of recombinant spider silk and its PEG-mMMT nanocomposite fiber at 30 °C and 25 RH%.

Table 4.3. The summary of tensile properties of recombinant spider silk fiber and its nanocomposites

Sample	Young's modulus [GPa]	Tensile strength [MPa]	Elongation at break [%]
Control	3.8 ± 0.5	171±17	61±7
PEG-mMMT (0.5 wt%)	4.9 ± 0.5	185±14	43±7
PEG-mMMT (1.0 wt%)	4.0 ± 0.6	124±13	7±4

Figure 4.12. shows the DMA of recombinant spider silk and its nanocomposites fiber under humidity-ramping mode from 25 RH%. As well as the method of films, the distortion humidity of fiber was examined from storage modulus. The results of recombinant spider silk control and clay nanocomposites fiber were 69.3 and 79.3 RH%, respectively. The fiber even by addition of 0.5 wt% of organically modified clay (PEG-mMMT) was recognized for improving humidity resistance. In the peak top of loss modulus, the position was clearly shifted to higher humidity while addition nanofillers. Consequently, the nanocomposite technology can be applied to film, fiber and other materials as a structure.

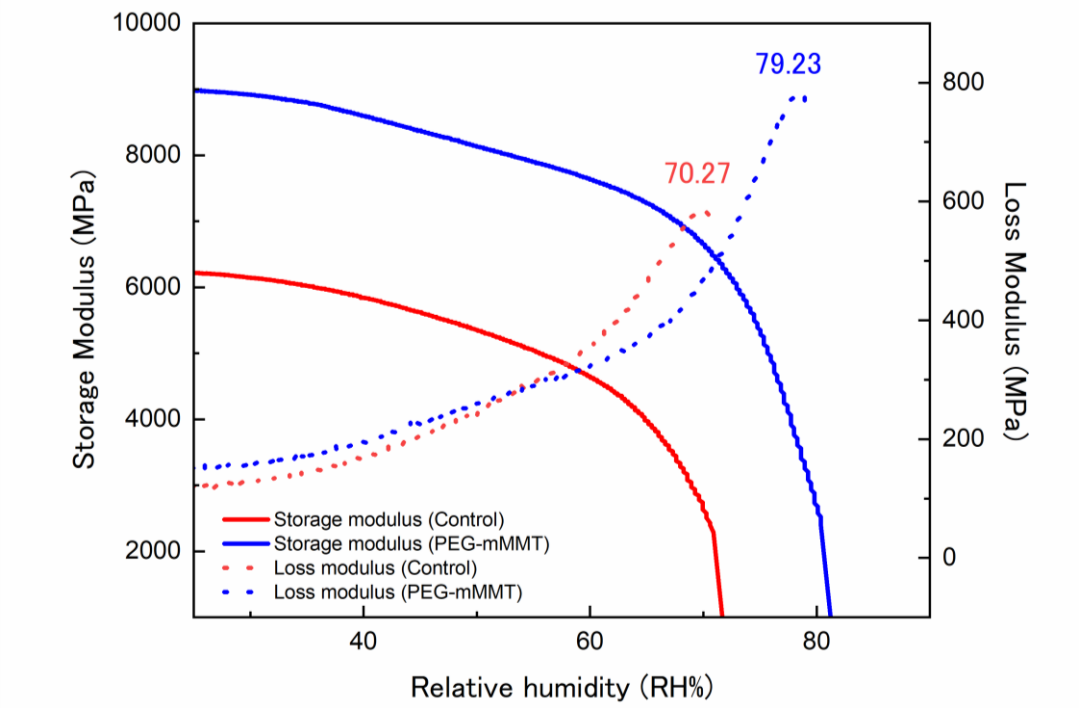

Figure 4.12. DMA of recombinant spider silk and its 0.5 wt% PEG-mMMT nanocomposite fiber with ramping-humidity.

4.4 Conclusions

Compounding of recombinant spider silk with nano clay through a solution casting method was found to be appealing. The elastic modulus of the nanocomposites was found to increase with increasing the content of clay and a maximum of 49% improvement was observed for an addition of 3 wt% of organomodified clay. The barrier effect of nanocomposite may be found to improve with higher content of clay is observed.

Additionally, the technology was applied for the recombinant spider silk nanocomposite fiber. The mechanical properties and humidity resistance of recombinant spider silk fibers were improved.

References

[1] W. Huang, D. Ebrahimi, N. Dinjaski, A. Tarakanova, M.J. Buehler, J.Y. Wong, D.L. Kaplan, Synergistic Integration of Experimental and Simulation Approaches for the de Novo Design of Silk-Based Materials, Acc. Chem. Res. 50 (2017) 866–876.

[2] R. V. Lewis, Spider Silk: Ancient Ideas for New Biomaterials, Chem. Rev. 106 (2006) 3762–3774.

[3] R.O. Ritchie, The conflicts between strength and toughness, Nat. Mater. 10 (2011) 817–822.

[4] H. Chung, T.Y. Kim, S.Y. Lee, Recent advances in production of recombinant spider silk proteins, Curr. Opin. Biotechnol. 23 (2012) 957–964.

[5] M. Elices, G.R. Plaza, J. Pérez-Rigueiro, G. V. Guinea, The hidden link between supercontraction and mechanical behavior of spider silks, J. Mech. Behav. Biomed. Mater. 4 (2011) 658–669.

[6] G.R. Plaza, G. V. Guinea, J. Pérez-Rigueiro, M. Elices, Thermo-hygro-mechanical behavior of spider dragline silk: Glassy and rubbery states, J. Polym. Sci. Part B Polym. Phys. 44 (2006) 994–999.

[7] J. Guan, F. Vollrath, D. Porter, Two Mechanisms for Supercontraction in *Nephila* Spider Dragline Silk, Biomacromolecules. 12 (2011) 4030–4035.

[8] K.N. Savage, J.M. Gosline, The role of proline in the elastic mechanism of hydrated spider silks, J. Exp. Biol. 211 (2008) 1948–1957.

[9] P.T. Eles, C.A. Michal, Strain Dependent Local Phase Transitions Observed during Controlled Supercontraction Reveal Mechanisms in Spider Silk, Macromolecules. 37 (2004) 1342–1345.

[10] P.T. Eles, C.A. Michal, A DECODER NMR Study of Backbone Orientation in *Nephila c lavipes* Dragline Silk under Varying Strain and Draw Rate, Biomacromolecules. 5 (2004) 661–665.

[11] O. Ozcalik, F. Tihminlioglu, Barrier properties of corn zein nanocomposite coated polypropylene films for food packaging applications, J. Food Eng. 114 (2013) 505–513.

[12] P.B. Messersmith, E.P. Giannelis, Synthesis and barrier properties of poly(ε-caprolactone)-layered silicate nanocomposites, J. Polym. Sci. Part A Polym. Chem. 33 (1995) 1047–1057.

[13] S.C. Tjong, Structural and mechanical properties of polymer nanocomposites, Mater. Sci. Eng. R Reports. 53 (2006) 73–197.

[14] M.A. Rafiee, J. Rafiee, Z. Wang, H. Song, Z.-Z. Yu, N. Koratkar, Enhanced Mechanical Properties of Nanocomposites at Low Graphene Content, ACS Nano. 3 (2009) 3884–3890.

[15] E.P. Giannelis, Polymer Layered Silicate Nanocomposites, Adv. Mater. 8 (1996) 29–35.

[16] S. Bourbigot, E. Devaux, X. Flambard, Flammability of polyamide-6/clay hybrid nanocomposite textiles, Polym. Degrad. Stab. 75 (2002) 397–402.

Chapter 5

General Conclusion

This dissertation discussed applied polymer science from the elucidation of the degradation mechanism of recombinant spider silk to the establishment of stabilization.

In Chapter 1, general introductions introduced the recent advance of biopolymer, importance of polymer degradation and its stability, nanocomposite technique and the objectives of this dissertation.

In Chapter 2, the thermal- and photo-oxidation of unstabilized recombinant spider silk was investigated by means of combination of multilateral measurement and statistical analyses. UV-irradiation of recombinant spider silk leads to the new photoproducts formed during UV exposure. These new photoproducts contain chromophores which cause alterations of absorption and fluorescence spectra of recombinant spider silk. Partial degradation of recombinant spider silk has been recorded by FTIR spectroscopy. Further studies are required to explain the photodegradation pathways in regenerated silk fibroin. In addition, UV-vis absorption at 450 nm can be detected for degradation earlier than ATR-IR.

In Chapter 3, I have firstly implemented a high-throughput screening of antioxidants in stabilizing recombinant spider silk against thermo-oxidative degradation. The usage of high-throughput chemiluminescence imaging has allowed us to screen various types of antioxidants in a quick and reliable manner. E310 and BHT, are found to be effective. The accelerated aging study has proven that these antioxidants suppress the thermo-oxidation of recombinant spider silk through scavenging the formed radical species and slowing down the formation of carbonyl groups as oxidation products.Screening system of photo degradation on recombinant spider silk film was efficiently worked. Most of stabilizer stabilized recombinant spider silk against UV irradiation. Specific, LA 87 give enormous stabilization to recombinant spider silk films.

In Chapter 4, Compounding of recombinant spider silk with nano clay through a solution casting method was found to be appealing. The elastic modulus of the nanocomposites was found to increase with increasing the content of clay and a maximum of 49% improvement was observed for an addition of 3 wt% of organomodified clay. Additionally, this nanocomposite technology was applied to the fiber formation of recombinant spider silk. The mechanical properties (tensile strength and Young's modulus) of nanocomposite fiber increased with the addition of 0.5 wt% of PEG-mMMT. The barrier effect of nanocomposite may be found to improve with higher content of clay is observed.

Acknowledgement

I would like to express my sincere gratitude to Associate Professor Dr. Toshiaki Taniike. This work would never have been achieved without his kind helps. I am deeply grateful to Research Assistant Professor Dr. Toru Wada and Research Assistant Professor Dr. Ashutosh Thakur for many helpful discussion and advices. I am deeply grateful to Dr. Kengo Takeuchi, and Jun'ichi Shimokata, Kojima Press Industry Co., for for their suggestions. I deeply appreciate Associate Professor Dr. Shinohara Ken-ichi, Associate Professor Dr. Kazuaki Matsumura, Associate Professor Dr. Ejiro Miyako for valuable advices and comments. Finally, I wish to express my gratitude to all the laboratory members for their kind encouragements.

I highly appreciate my wife for her understanding my work and supporting my success.

Koyuru Nakayama